"Identification and characterization of genes that modify tubulogenesis defects caused by over-expression of *Imaginal Disc Growth Factor-3* using the *Drosophila* dorsal appendage model, a partial genomic expedition"

by

Claudia Y Espinoza

A dissertation submitted as partial fulfillment of the requirements for the degree of:

Doctor in Philosophy

University of Washington

2020

Reading Committee:

Celeste Berg, Chair

Barbara Wakimoto

Young Kwon

Program Authorized to Offer Degree:

Genome Sciences

University of Washington

## Abstract

"Identification and characterization of genes that modify tubulogenesis defects caused by over-expression of *Imaginal Disc Growth Factor-3* using the *Drosophila* dorsal appendage model, a partial genomic expedition"

Claudia Y Espinoza

Chair of the Supervisory Committee:

Professor Celeste A. Berg

Biological tube formation underlies organ development, and when disrupted, can cause severe birth defects. To investigate the genetic basis of tubulogenesis, I study the formation of Drosophila melanogaster eggshell structures, called dorsal appendages, which are produced by epithelial tubes. Previously in my lab we found that precise levels of Drosophila Chitinase-like proteins (CLPs), encoded by the *Imaginal disc growth factor (Idgf)* gene family, are needed to regulate dorsal-appendage tube closure and tube migration. To identify factors that act in the *Idgf* pathway, I developed a genetic modifier screen based on the finding that overexpressing *Idgf3* causes dorsal appendage defects with ~50% frequency. Using a library of partially overlapping heterozygous deficiencies, I scanned chromosome 3L and found regions that enhanced or suppressed the *Idgf3*-overexpression phenotype. Using smaller deletions, RNAi, and mutant alleles, I further mapped five regions and refined the interactions to 58 candidate

genes. Importantly, mutant alleles identified combover (*cmb*), a substrate of Rho-kinase (Rok) and a component of the Planar Cell Polarity (PCP) pathway, as an *Idgf3*-interacting gene: loss of function enhanced while gain of function suppressed the dorsal appendage defects. Since PCP drives cell intercalation in other systems, I asked if *cmb/+* affected cell intercalation in my model, but I found no evidence of its involvement in this step. Instead, I found that loss of *cmb* dominantly enhanced tube defects associated with *Idgf3*-overexpression by expanding the apical area of dorsal appendage cells. Apical surface area determines tube volume and shape; in this way, *Idgf3* and *cmb* regulate tube morphology. Additionally, I narrowed down the strongest enhancer region to *eIF3e* as a gene candidate. Validation of an interaction between *Idgf3* and *eIF3e* remains to be tested, as a null allele for *eIF3e* is not available. Also, I found that by silencing *eIF3e*, eclosion and egg production fail, preventing me from testing this interaction with the genetic tools available. By testing genes known to interact with *eIF3e*, I looked for indirect evidence that *Idgf3* interacts with *eIF3e* for dorsal appendage formation. *eIF3e* is part of a translation regulatory complex, which plays a role in regulating *Mical* translation. Mical interacts with PlexA for neuronal dendrite pruning. I found evidence that suggests overexpression of *Mical* might suppress the DA phenotypes that result from overexpressing *Idgf3*. Additionally, I found a role for PlexA in DA formation, and that lowering expression of *PlexA* enhances the *Idgf3*-overexpression phenotype. I suggest different experiments that can allow me to verify this interaction, and I hypothesize models that explain how *Idgf3* might interact with the PlexA-Mical pathway, only if PlexA and Mical interact in the dorsal-appendage making cells during DA formation as they interact in neurons during dendrite pruning. Finally, I quickly tested other genes that, in my lab, we have found to play a role in DA formation. In this way I identified other possible *Idgf3*-interacting genes.

## Table of Contents


***Chapter I: Biological tubes are an important feature of nature's design ..... 8***

**Studying tube formation can help us understand neural tube defects ..... 9**

**The *Drosophila* egg and egg chamber serve as models to study tube formation..... 12**

**How do dorsal appendages form? ..... 14**

**What are the *Idgfs?*..... 17**

**Idgfs are related to human Chitinase-like proteins, which underlie human disease..... 21**

**Remaining questions about tube formation, *Idgfs,* and CLPs. ..... 23**

**Dissertation overview..... 24**

***CHAPTER II: Detecting new allies: Modifier screen identifies a genetic interaction between Imaginal disc growth factor 3 and combover, a Rho-kinase substrate, during dorsal appendage tube formation in Drosophila ..... 33***

**RESULTS AND DISCUSSION ..... 37**

Modifier-screen set up ..... 37

Screening for suppressors and enhancers ..... 40

Selecting regions to narrow down ..... 41

Narrowing down the interacting regions ..... 42

Identifying interacting genes ..... 43

*Idgf3* genetically interacts with *combover* ..... 44

*Idgf3* and *cmb* do not affect cell intercalation during dorsal appendage formation ..... 45

*Idgf3* and *cmb* affect apical area of dorsal appendage tubes ..... 47

Role of *Idgf3* and *cmb* during dorsal appendage formation ..... 48

*Chapter III: Does Idgf3 interact with the eukaryotic translation initiation factor 3 subunit e (eIF3e) and the Mical pathway during Drosophila dorsal appendage formation? ..... 63*

**Modifier screen identifies a region that strongly interacts with Idgf3..... 63**

**Tiling deficiencies narrowed down the strongest enhancer to one candidate gene, *eIF3e*..... 64**

**Efforts towards verifying a genetic interaction between *eIF3e* and *Idgf3* lead to additional routes to elucidate a possible interaction..... 65**

***eIF3e* regulates *Mical* translation for dendrite pruning..... 69**

***Mical* constructs combined with the *Idgf3*-overexpression mutant reveal intriguing dorsal-appendage phenotypes..... 69**

**Does eIF3e regulate translation of Mical during dorsal appendage formation? ..... 72**

***PlexA* plays a role in dorsal appendage formation and enhances the *Idgf3*-overexpression phenotype..... 73**

*Chapter IV: Additional implications and future directions ..... 89*

**Modifier screen identifies *Idgf3*-interacting gene candidates but is limited by dosage sensitivity and efficacy of constructs. ..... 89**

**Modifier screen identified *eIF3e* as an interesting *Idgf3*-interacting gene candidate and directed attention towards the *Mical* pathway..... 92**

**Additional investigation of the modifier screen could increase our understanding of the *Idgfs*. .. 98**

**How are *cmb-Idgf3* affecting the apical area of the dorsal-appendage-making cells? - Proposed experiments..... 99**

**What is the earliest stage of egg chamber development that is affected by the *cmb-Idgf3* interaction?..... 101**

**Additional tested deficiencies** ..... **102**

**Final remarks** ..... **105**

***Chapter V: MATERIALS AND METHODS*** ..... ***111***

**Fly Stocks used** ..... **111**

**Modifier-screen crosses** ..... **111**

**Creation of the temperature-sensitive Idgf3 overexpression** ..... **112**

**Dorsal-appendage analyses:** ..... **112**

**Immunostaining** ..... **113**

**Confocal image acquisition** ..... **114**

**Image analysis** ..... **115**

**Statistical analysis** ..... **115**

**Mical translation experimental set up** ..... **116**

***ACKNOWLEDGEMENTS*** ..... ***117***

***Bibliography*** ..... ***119***

***Tables*** ..... ***128***

## Chapter I: Biological tubes are an important feature of nature's design

Biological tubes define the basic structure of organs. For instance, biological tubes make up the architecture of the kidney, the lungs and the vasculature system (Lubarsky and Krasnow, 2003). In other instances, biological tubes are transient structures of organs during development. For example, the mammalian central nervous system starts as a tube and undergoes further morphogenesis to build up more complex structures, which are the spinal cord and the brain (Colas and Schoenwolf, 2001). In nature, the structural diversity of biological tubes ranges from single-cell tubes, like capillaries of the excretory system of worms (Buechner *et al.,* 1999), to multicellular-tubes of more complex design, like the mammalian lung (Schittny, 2017). Regardless of the diversity of tube structure, biological tubes share the basic feature of a single cell or a sheet of cells enclosing or creating a lumen or space (Baer *et al.,* 2009). Additionally, multicellular tubes display distinctive characters, such as cellular apical and basal polarity, in which the apical side of the cell faces the tube lumen; intercellular junctions, which can be adheren junctions, tight junctions in mammalian cells, or septate junctions in the *Drosophila* epithelium; and Extra Cellular Matrix (ECM) or basement membrane, which surrounds the tube cells and influences tube formation (Andrew and Ewald, 2010; Diaz-de-la-Loza *et al*., 2018).

The mechanisms that drive biological tube formation can be broadly categorized into five classes. 1) The wrapping mechanism, which makes the mammalian neural tube, creates a tube from an epithelial sheet by bending and sealing in parallel to the starting plane. 2) The budding mechanism, which forms the lungs and other branching structures, produces a tube by budding perpendicularly out from the plane of an existing monolayer sheet of cells. 3) The cavitation mechanism, which makes the proamniotic cavity of vertebrate embryos, forms by apoptosis and elimination of cells located in the center of a mass of cells. 4) The cord hollowing mechanism,

which forms nascent blood vessels, occurs when single cells come together and build an epithelial sheet de novo in the shape of a tube. This mechanism is also used by the well documented epithelial-cell-model, the Madin-Darby Canine Kidney (MDCK ) cells (Dukes *et al*., 2011), to form epithelial tubular structures when growing in a collagen matrix. 5) The cell hollowing mechanism, which makes the excretory cells in *C. elegans,* uses vesicle coalescence to create a hollow region within the cell's cytoplasm (Lubarsky and Krasnow, 2003) (Figure 1.1).

During development, the accuracy of these mechanisms of tube formation is crucial because tube formation has an effect on the successor organ's function. For instance, during mammalian neural tube development, a process known as primary neurulation, a sheet of epithelial cells undergoes wrapping to give rise to a long tubular structure, which is the spinal cord. One of the main functions of the spinal cord is to connect the brain with distant parts of the body and transport signals through long distances (Smith and Schoenwolf, 1997; Colas and Schoenwolf, 2001).

Another example that shows the correlation between tube formation and function is the development of the lungs. The lungs form through several rounds of the "budding" mechanism of tube formation (Schittny, 2017). This repeated budding forms a network of branched tubes, covering a large surface area for optimal oxygen absorption (Hogan and Kolodziej, 2002). In this way, the mode and accuracy by which biological tubes form is correlated and essential to the tube's function.

**Studying tube formation can help us understand neural tube defects.**

Since biological tubes are the foundation that shape organs, errors during tube formation cause detrimental effects in the developing organism. For example, problems in wrapping

during neural tube formation can disrupt tube closure and thus the development of the spine, a defect known as *spina bifida*. Problems in wrapping during neural tube formation can also interrupt the development of part of the neural tube that gives rise to the brain, resulting in the underdevelopment or lack of development of the brain, a defect known as *anencephaly* (Copp and Greene, 2013). These two types of developmental defects are examples of neural tube defects (NTDs).

NTDs represent a large problem for society. They affect 0.5-2 in 1000 births worldwide (Mitchell, 2005). The range of severity of NTDs varies. The more severe cases of *anencephaly* are lethal before or at birth. Less severe cases of *spina bifida*, while compatible with survival, are accompanied by morbidities or life-threatening conditions that require surgery or costly treatments (Greene and Copp, 2014; Yi *et al*., 2011). Due to advances in technology, NTDs can be diagnosed before birth through ultrasound imaging (Cameron and Moran, 2009). If treatable, like in some less severe cases of *spina bifida*, fetal surgery could ameliorate neurological damage and improve limb functioning during development (Dewan and Wellons III, 2019). Nevertheless, while fetal surgery has greatly helped in alleviating *spina bifida's* health effects, the treatment is highly intrusive and is associated with severe premature labor, maternal pulmonary edema, and maternal need of blood transfusion after labor (Dewan and Wellons III, 2019). Thus, studies that aim to understand the genetic programs underlying tube formation could help develop diagnostic and preventive treatments for NTDs and reduce the number of incidents of NTDs in our society.

The causes of NTDs are multifactorial and include both genetic and environmental factors (Copp and Greene, 2013). Environmentally, low levels of folic acid during pregnancy are linked to NTDs, and consumption of folic acid as a supplement during pregnancy has

lowered the index of NTD cases worldwide (Czeizel and Dudás, 1992; Berry *et al*., 1999; Czeizel *et al*., 2013). Nevertheless, there is still high prevalence of NTD cases regardless of folic acid supplementation. A high index of recurrence for affected siblings, and the high risk for NTDs in families where more than two individuals are affected, point to genetic factors underlying these developmental diseases (Rampersaud *et al*., 2006). Having an understanding of the genes that cause defects during neural tube formation, and of the mechanisms by which those genes function, could aid in the prevention of NTDs.

Elucidating the genetic bases of NTDs in humans has been a challenging goal. One reason for this difficulty is the ethical issue underlying the manipulation of neural tube formation during human embryonic development. Furthermore, GWAS studies intending to find causative mutations of NTDs face the difficulty of obtaining a sufficiently large sample size to draw conclusions with confidence (Molloy *et al*., 2009). Studies of miscarriages of human embryos that had developed NTDs (Lei *et al*., 2010), candidate-gene studies in humans that look at the components of folate metabolism (Boyles *et al.,* 2005), and mice models that develop NTDs (Harris and Juriloff, 2007) have helped overcome research challenges and have pointed to genetic pathways that might play a role in human neural tube formation.

Nevertheless, more extensive research to understand the genetic basis of neural tube defects is needed, for the results from all these lines of research are not always congruent; some mutations that are linked to specific human NTDs cause a different phenotype in the mouse model (Greene *et al.,* 2009). For example, in humans, heterozygous variants of the planar cell polarity (PCP) pathway gene *VANGL2* are associated with anencephaly (interrupted development of the brain) and closed *spina bifida* (also known as *spina bifida occulta*, when the neural tube seals, but the backbone does not fully form) (Lei *et al*., 2010). In contrast, heterozygous

mutations in the *VANGL2* mouse homolog, *vangl2*, do not show any spine defects. It is the homozygous mutations in *vangl2* that cause NTDs, but the defects are open brain and open spinal cord, which are different from what is seen in humans (Chen *et al*., 2013; Torban *et al.,* 2008; Greene *et al*., 2009). These observations could reflect the multifactorial nature of neural tube development and genetic differences between species. This complexity is why studying developmental genetic pathways involved in tube formation and characterizing them at a cellular level using simple models are crucial to understanding more complicated processes.

**The *Drosophila* egg and egg chamber serve as models to study tube formation.**

The *Drosophila melanogaster* egg is a good model system to study tube formation (Osterfield *et al.,* 2017; Berg 2008; Berg 2005). The egg has two appendages located dorsally that, like the neural tube, are made by sheets of cells that use the wrapping mechanism to create two tubes (Dorman *et al.,* 2004) (Figure 1.2). These tube cells secrete chorion protein into their lumens to create the appendages, called dorsal appendages, which facilitate the diffusion of oxygen into the egg (Hinton 1969). The dorsal appendages are not tubes, but cellular tubes mold their shape during oogenesis (Dorman *et al.,* 2004).

Dorsal appendage formation takes place in the developing follicle, also known as an egg chamber, inside the female ovaries. The ovaries are made of multiple assembly lines containing several egg chambers, ranging from stage1 (S1) to stage 14 (S14), with increasingly more mature stages arranged from anterior to posterior (King, 1970) (Figure 1.3A). The presence of multiple egg chambers at different stages of development lets one observe a timeline of events in material from a single female. Additionally, the ovaries of a well-fed female represent one third of her body weight, providing ample material for analysis. Importantly, the cells of interest are located

at the surface of the egg, which facilitates confocal imaging with high resolution. Moreover, studies of the dorsal appendage model system have set a strong foundation of knowledge of both the genetic patterning and morphogenesis aspects of development (reviewed by Osterfield *et al.,* 2017).

In a broader context, *Drosophila melanogaster* is a model that can facilitate studies of otherwise difficult experiments. *Drosophila* has been at the forefront of genetic research since the beginning of the 20$^{th}$ century (Morgan 1910; Bridges 1916). Since then, there has been a great expansion and improvement of tools to study genetic and molecular processes of development (Hales *et al*., 2015).

One biotechnology used extensively for genetic studies is the *GAL4/UAS* system, which lets one control the time and location of gene expression in *Drosophila*. This system consists of the yeast transcription factor Gal4p, and its corresponding binding sequence, the upstream activating sequences (*UAS*), which were introduced into the *Drosophila* genome and were made easily accessible to the *Drosophila* field (Brand and Perrimon, 1993). By placing the *GAL4* yeast gene under the activation of an endogenous fly promoter or under an enhancer of interest, we can control where and when *GAL4* is expressed. By cloning the *UAS* sequence upstream of a gene of interest and by crossing these flies to Gal4p drivers that are expressed in the desired spatial and temporal patterns, we can control the transcription of any gene downstream of the *UAS* sequence. The optimal temperature for the Gal4p protein activity is 30$^{o}$C, allowing us to use temperature as another layer for controlling gene expression (Hales *et al*., 2015).

Another resource that makes *Drosophila* a powerful genetic system is the availability of a suite of overlapping deletion lines that have defined break points and together uncover nearly all regions of the fly genome (Parks, *et al*., 2014; Ryder *et al.,* 2007). These lines were made by

randomly inserting (into *white*$^{-/-}$ mutants) *P* elements carrying complementary *white*$^{+}$ gene fragments located between yeast FLP Recombination Target (FRT) sites of different orientations (another technology borrowed from yeast). The *P*-element insertions were mapped using PCR, and deletions were induced by crosses to the FLP recombinase such that the resulting deletion would be marked with a reconstituted *white*$^{+}$ gene. In this way, each deletion within the kit has specific end points and originated from the same genetic background (Ryder *et al*., 2007).

The above-mentioned characteristics of *Drosophila* and the egg chamber, in addition to reproducibility due to number of egg chambers in one female and the easy husbandry (Hales *et al.,* 2015), make the *Drosophila* egg a great model to study tube formation.

**How do dorsal appendages form?**

The tube formation that shapes the two dorsal appendages (DAs) occurs in the context of the egg chamber. The egg chamber is made of germline cells surrounded by follicle cells. The germline cells include 15 interconnected nurse cells that are connected to the oocyte and that provide nutrients for the future embryo as the egg chamber develops (Mahajan-Miklos and Cooley, 1994). The germline cells are surrounded by ~650 follicle cells. At S10B, when dorsal-appendage tube formation begins, a squamous layer called the "stretch cells" covers the nurse cells, and columnar "main body" follicle cells cover the oocyte (Figure 1.3B). The follicle cells secrete molecules crucial to set up embryonic polarity (Merkle *et al.,* 2020) and to send signals important for egg chamber and eggshell maturation, such as signals for the differentiation and migration of several distinct groups of follicle cells that make specialized structures of the eggshell, and the expression of eggshell-producing genes (Waring, 2000; Horne-Badovinac and

Bilder 2005; Montell *et al.,* 2012; Saadin and Starz-Gaiano 2016; Duhart *et al*., 2017; Osterfield *et al*., 2017.).

Among the follicle cells at S10B, two patches composed of ~63 cells are genetically programed to differentiate and form the two tubes that mold the DAs (Dorman *et al*., 2004). Each of the two patches is made of ~52 columnar follicle cells that become the top part of the DA tubes. These cells are known as roof cells. Each patch is also made of ~11 cells that become the bottom part of the tube and interact with the stretch cells during dorsal appendage tube formation. These cells are known as floor cells (Dorman *et al.,* 2004).

Dorsal appendage formation is a complex process that includes patterning and morphogenetic changes, both of which are not fully understood. From stage 1 to stage 10A, genetic programs are put in place in order to promote the mechanical changes that, after S10B, drive DA tube formation (Berg, 2008). These genetic programs rely on signals such as expression of the bone morphogenetic protein (BMP) Decapentaplegic, which is produced by anterior follicle cells and interacts with a heterodimeric receptor to regulate downstream SMADs (e.g., Yakoby *et al*., 2008), and the transforming growth factor α (TGF- α)-like signaling molecule Gurken, which is secreted by the oocyte and signals to the epidermal growth factor EGF receptor homolog (EGFR) to genetically pattern the cells of the egg chamber that will form the DA tubes (Osterfield *et al.,* 2017; Merkle *et al.,* 2020).

The physical changes that form the DA tubes start at S10B, when roof cells first elongate to form a thickened placode, and then at S11, they constrict their apical side, which faces the oocyte. This latter process is known as apical constriction (Dorman *et al*., 2004). Also starting at S11, the floor cells stretch their lateral sides under the roof cells; their apices come into contact with each other and fuse during late S11 and early S12 (Dorman *et al.,* 2004). These

morphological cell changes result in a sealed DA tube. During this process of tube formation, the apical sides of the roof cells initially face the oocyte, but they finish by facing the lumen of the tube (Osterfield *et al.,* 2013).

Tube elongation happens during S12 and S13. During S12, roof cells intercalate among each other, converging dorsally and extending the tube anteriorly, a process also known as cell intercalation (Figure 1.4). Next, the floor cells physically interact with the stretch cells to migrate anteriorly (Tran and Berg 2003; Berg, 2008). Simultaneously, the roof cells re-expand their constricted apices anteriorly (Peters and Berg 2016A), extending the tube lumen in a process driven by the 69-kD isoform of the Tramtrack zinc finger transcription factor (Ttk69). Disruption of Ttk69 expression during late oogenesis results in two small appendages (French *et al*., 2003; Boyle and Berg, 2009) (Figure 1.2C). Further tube elongation occurs as a result of the roof and floor cells extending filopodia as they interact with the ECM and the stretch cells, respectively (Dorman *et al.,* 2004).

DA tube formation is a process that requires precise communication and cooperation of different cell types at different stages of oogenesis (Boyle *et al.,* 2010; Zimmerman *et al.,* 2017; reviewed by Osterfield *et al*., 2017). The signals responsible for orchestrating the changes that make the dorsal appendages are not fully understood. We have begun to solve part of a pathway that drives dorsal appendage formation, a pathway in which the gene *bullwinkle (bwk)* participates (Rittenhouse and Berg, 1995). *bwk* encodes a transcription factor active in the nurse cells (Rittenhouse, 1996). Through unknown signals, *bwk* communicates with the stretch cells using Shark and Src42A tyrosine kinases (Tran and Berg, 2003). Loss-of-function mutations in *bwk* cause aberrant dorsal appendages that include incomplete tube closure and reduced anterior-directed migration (Dorman *et al.,* 2004), leading to moose antler-like DAs (Figure 1.2D).

Overexpression of the tyrosine kinases using a stretch-cell-specific *GAL4* and *UAS-Shark* or *UAS-Src42A* suppresses the *bwk* mutant phenotype (Tran and Berg, 2003). These findings led to a proteomic analysis discussed below that identified an interesting gene family, the *Imaginal disc growth factors* (*Idgfs*), as being up-regulated in the stretch cells of *bwk* mutant egg chambers (Zimmerman *et al.,* 2017).

**What are the *Idgfs?***

Previously, Sandra Zimmerman, a postdoctoral fellow in our lab, pondered about the DA defects resulting from the *bwk* germline mutation and the role of Shark and Src42A in this process. To explore this process, she carried out a proteomic analysis of stretch cells, purified from either *bwk* or wild-type egg chambers, aimed at identifying post-translational modifications or protein dysregulation in the *bwk* mutant. The stretch cells of *bwk* mutants had significantly higher levels of Idgfs compared to the stretch cells of wild-type egg chambers.

The fly genome has six annotated *Idgf* genes: *Idgf1, Idgf2, Idgf3, Idgf4, Idgf5,* and *Idgf6.* Sandra's general, discovery-based proteomic analysis identified *Idgf1, Idgf2, Idgf4*, and *Idgf6* as up regulated in *bwk* stretch cells, while a more specific, targeted proteomic analysis also revealed up regulation of *Idgf3* and *Idgf5*. Interestingly, overexpressing *Idgf1* or *Idgf3* (the only available over-expression constructs) resulted in a significant number of eggs displaying a DA phenotype that resembled *bwk* eggs. Additionally, lowering the expression of *Idgf4, Idgf5*, or *Idgf6* (the only RNAi constructs available on chromosome II – *bwk* is on III) ameliorated the *bwk/bwk* mutant phenotype. These results demonstrate that the Idgfs are part of the *bwk* pathway and that up-regulation of Idgf expression contributes significantly to the *bwk* phenotype. In support of this conclusion, Immunofluorescence and fluorescent *in situ* hybridization (IF/FISH) analysis

showed that all six *Idgfs* are expressed in the stretch cells of egg chambers, although the different cell types of the egg chamber presented different expression patterns of each of the *Idgfs*. All these lines of evidence suggest that the *Idgfs* play an important role in morphogenesis of the DAs, since they are part of the *bwk* signaling pathway that regulates dorsal appendage formation (Zimmerman *et al*., 2017).

One curious observation is that down-regulation of any one of the six *Idgfs* by RNA interference in the stretch cells also produces a *bwk* phenotype (Zimmerman *et al*., 2017). This result contrasts with the absence of DA phenotypes in true null mutants generated by CRISPR/Cas9 deletion of each gene (Sustar, Strand, Zimmerman, and Berg, *in preparation*). Loss of *Idgf6* alone does result in ~15% of eggs with thin DAs, and a strain bearing deletions of all six genes (sextuple knock out) does yield a high fraction of eggs with severe DA defects, but the phenotypes reveal a lack of tube formation, not the open, enlarged tubes produced by *bwk* mutants or by RNAi strains for individual *Idgf* genes. One hypothesis to explain these observations is that the genomic deletion of one member of the *Idgf* family, which is present throughout development in all tissues of the fly, allows the other members to accommodate their expression and compensate for the loss of function. In contrast, because RNAi acts as a temporal reduction of the gene, changes in expression of the other *Idgfs* to accommodate the sudden reduction of one *Idgf* gene's product might actually result in over-expression of their gene products, resulting in the gain-of-function phenotype similar to *bwk* mutants and *Idgf3* over expression.

From a broader context than the egg chamber perspective, there is additional evidence that the *Idgfs* might function in morphogenesis and immunity. *Idgf6* was the first *Idgf* to be identified, and it evoked a role in immunity (Kirkpatrick *et al*., 1995). *Idgf6* encodes a protein

highly secreted from *Drosophila* S2 cell lines, which are cultured cells isolated from fly embryos and thought to be derived from a macrophage lineage (Drosophila Genomics Resource Center, Indiana University). S2 cells engulf bacteria in a manner that resembles the endocytotic response phenotype of human macrophages (Rämet *et al*., 2002; reviewed by Ulvila *et al*., 2011). Idgf6 protein shares amino acid homology with the human glycoprotein HC gp-39 (Kirkpatrick *et al*. ,1995). Interestingly, HC gp-39 also known as or YKL-40, is abundant in human articular chondrocytes, which play a role in development, maintenance, and repair of the cartilage that covers the ends of the bones (Johansen *et al*., 1992; Fox *et al*., 2009). HC gp-39 is also abundant in synovial fibroblasts, which play a role in the innate immune system as local pathogen sensors and immune-system activators (Ospelt, 2017).

It was the identification of Idgf1, Idgf2, and Idgf3 from conditioned medium obtained from the imaginal wing disc cell lines that suggested a role of the Idfgs in having an effect on cellular morphology and thus suggesting their role during development (Kawamura *et al.,* 1999). Idgf1, Idgf2, and Idgf3 proteins were first identified and isolated from conditioned media of wing-disc cell lines. They were classified as growth factors because the Idgfs promote pseudopodia growth, cellular elongation, enhanced motility, and cell proliferation when added to wing-disc cells growing in unconditioned media *in vitro* (Kawamura, *et al.,* 1999). Using micro-sequencing of purified proteins, the authors designed PCR primers for use on genomic DNA to obtain probes to isolate cDNA from an imaginal disc cDNA library. Subsequent database searches looking for similar Idgf sequences identified Idgf4 (Kawamura *et al*., 1999). On the contrary, Idgf5 was identified for the first time as a member of the family through a computational search that aimed to identify the *Drosophila* chitinases-like proteins (Zhu *et al.,* 2004).

The *Idgf* expression patterns also support *Idgf* involvement in morphogenesis. Idgf6 protein and mRNA are present throughout the fly life cycle, but mRNA levels are higher at the beginning and end of embryogenesis than during mid embryogenesis relative to the internal control, actin-5C (Kirkpatrick *et al.,* 1995). During embryonic development, *Idgf1, Idgf2, Idgf3,* and *Idgf4* transcripts are expressed in cells adjacent to those involved in invagination events, such as the ventral furrow, cephalic furrow, and posterior midgut invagination. *Idgf1, Idgf2, Idgf3,* and *Idgf4* are also expressed in cells that experience migration, like the yolk cells at stage 11, which follow the germ band during retraction (Kawamura *et al.,* 1999).

Additionally, the Idgfs play an important role in immunity. Idgf6 protein accumulates in the extracellular spaces of the *Drosophila* hemolymph, and it is expressed in the fat body in third instar larvae and in the hemolymph tissue (Kirkpatrick *et al.,* 1995), which are the immune organs of flies (Krautz *et al*., 2014). C1.8 cell lines respond to Idgf2 treatment mainly by changing the transcription of genes involved in immunity and morphogenetic processes (Broz *et al*., 2017). Finally, *Idgf2* expression is induced by injury stress (Broz *et al.,* 2017), and, *Idgf3* loss-of-function mutants recover more slowly to injury and are more sensitive to nematode infections compared to wild type (Kucerova *et al.,* 2016). All these lines of evidence strongly indicate that the *Idgfs* facilitate changes in cell morphology, as well as development and immunity. Nevertheless, their specific role in these processes remains a mystery.

Amino acid sequence could also serve as a venue to elucidate the Idgfs biological role. The *Idgfs* share about 50% amino acid identity among each other (Kawamura *et al.,* 1999), a level of homology that could permit them to substitute roles during development if one or multiple family members are defective or missing. The Idgfs have a signal peptide domain, suggesting they are secreted molecules (Zhu *et al*., 2008); this feature is consistent with their

recovery from conditioned medium and larval hemolymph (Kawamura *et al.,* 1999; Kirkpatrick *et al.,* 1995). The Idgfs also share 15-25% amino acid similarity to chitinases (Kawamura *et al*., 1999). Chitinases are proteins responsible for breaking down a component of insect exoskeletons or fungal cell walls called chitin; chitinases are especially important for breaking down chitin during molting (Merzendorfer and Zimoch, 2003). The resolved crystal structure of Idgf2 shows structural and protein-folding similarities with Chitinases (Figure 1.5; Varela *et al.,* 2002). In the Idgfs, however, a non-catalytic residue takes the place of the catalytic residue responsible for break down of chitin in the Chitinase proteins. Additional amino acid substitutions in the Idgf2 sequence suggest changes of the protein properties, which further prevent hydrogen-bond mediated hydrolysis (Varela *et al.,* 2004). Thus Idgfs might be able to bind to chitin or similar polysaccharides, but Idgfs would not be able to break down chitin.

**Idgfs are related to human Chitinase-like proteins, which underlie human disease.**

As explained above, Idgfs share amino acid sequence and protein structure similarities with chitinases, which are proteins that bind to and hydrolyze polysaccharides like chitin. Because of amino acid substitutions, however, Idgfs lack the ability to break down chitin. In nature, there are more proteins that behave in a similar fashion, thus all of them are considered to be evolutionary conserved. All of these molecules are grouped into a larger family known as the Chitinase-like proteins (CLPs) (Funkhouser and Aroson Jr., 2006). Human CLPs include Chi3l1*,* Chi3l2, oviductin, and SI-CLP (Bussink *et al.,* 2007; Coffman 2008).

While, macrophages and other endothelial and immune cells normally express human CLPs, their up-regulation occurs in several immune-related diseases and infection, and in some cases, this up-regulation is used as biomarkers of disease (reviewed in Lee *et al.,* 2011). For

instance, *Chi3l1* codes for YKL-40 protein and is secreted by chondrocytes in explants or cultured cells; chondrocytes are cells that support the development, maintenance, remodeling, and repair of the cartilage matrix (Hakala *et al*., 1993). Chi3L1 is also secreted by synovial cells that make the synovial membrane, and by cells of immune character, such as macrophages and neutrophils (reviewed in Coffman 2008). Rheumatoid arthritis patients show elevated levels of Chi3L1 (Harvey *et al.,* 1998). Macrophages stimulated with cytokines express higher levels of Chi3L1 (Krause *et al*., 1996). Chi3L1 up-regulation is seen in some tumor tissues and in the serum of patients with a variety of cancers, in patients with osteoarthritis, in the chronic inflammatory rheumatic disease ankylosing spondylitis, in the liver of patients with alcoholic cirrhosis, patients with severe ulcerative colitis or active Chron's Disease (reviewed in Coffman 2008). Additionally, Chi3l1 is elevated in patients with pneumonia; here, Chi3l1 level is a predictor of mortality (Kronborg *et al.,* 2002). Similarly, Chi3l1 is elevated in the serum of patients with severe and fatal malaria, in which the level of the protein correlates with the severity of the disease (Erdman *et al.,* 2014).

In a similar way, *Chi3l2* expression is normally seen in chondrocytes and synoviocytes, while it is upregulated in microglia of Alzheimer's disease patients (Lee *et al.,* 2011). Chi3L2 is also upregulated in human brain sections of people infected with the Human Immunodeficiecy Virus (HIV) (Sanfilippo *et al*., 2017a) and in brain tissues of patients with neurodegenerative diseases like amyotrophic lateral sclerosis (LAS) (Sanfilippo *et al*., 2017b) and Alzehimer's disease (Sanfilippo *et al*., 2016). It is also known that up-regulation of Chi3L2 is negatively correlated with survival of LAS patients (Sanfilippo *et al.,* 2017b).

While there is less evidence that the other CLPs are associated with disease, SI-CLP is expressed in macrophages and up-regulated when macrophages are activated by different cytokines, suggesting their involvement in inflammation (Kzhyshkowska *et al.,* 2006).

Are the CLPs pathogenic or protective? Up regulation of the CLPs and their biomarker character suggest their active involvement with disease, but whether this increased expression causes tissue damage or helps prevent tissue damage is not clear. In some cases, CLPs appear to promote cancer growth and metastasis by up regulating the TGF-β signaling pathway (Qiu *et al.,* 2018), yet there is also evidence that they have the ability to protect against pathogenicity. For instance, Chi3l1 binds and activates the interleukin-13 receptor α2 (IL-13Rα2) and forms a multimeric complex with IL-13 (He *et al.,* 2013), a protective pathway that is normally activated upon pathogenic invasion (Junttila, 2018). Additionally, *Chi3l1/BRP-39* null mice show higher oxidant-induced injury and cell death, suggesting a conceivable beneficial role (He *et al*., 2013). Moreover, additional work is needed to understand if there is a causal relationship between the Chi3l1 ability to activate the TGF-β pathway and its role in disease (Qiu *et al*., 2018). Thus, the CLPs' actual role in diseases is still unclear. Characterizing how the Chitinase like proteins function at a cellular level could help us understand if they are pathogenic or protective, or if their pathogenicity results from an error during their protective role.

**Remaining questions about tube formation, *Idgfs,* and CLPs.**

Extensive experimental findings have helped us identify and partially characterize mechanisms of tube formation, especially related to the formation of the neural tube. In a similar way, different experimental models have helped us identify an underlying genetic basis for neural tube formation. Nevertheless, more work is needed to elucidate the specific role and

effect that these genes have during morphogenesis, especially their effects on cells that are coordinating movements within a larger tissue. In other words, what is the role that a specific genetic pathway plays on one cell of an epithelial sheet, and how does that effect influence the morphogenesis of the entire epithelium in order to form a biological tube?

Our knowledge of *Idgfs* is an example of this situation. *Idgfs* play a role in dorsal appendage tube formation. While their effect could be assessed by their function in other tissues, such as changing cell morphology or protecting against pathogenic infections, it is still unclear what their effect is at a cellular and molecular level. Specifically, it is unclear what pathways the *Idgfs* interact with and what their mechanism of action is to produce the effects mentioned above. Questions to be explored are, what genes are the *Idgfs* interacting with for tube formation, and how are these interactions affecting cells of an epithelium to drive tube formation?

Investigating the *Idgf* genetic pathway and mode of action, beyond helping us understand their nature, could give us insights into the nature of their human homologs. For instance, it is still unclear what the normal biological role of the CLPs is in nature. Understanding a cellular mechanism of action of the Idgfs could open a venue to investigate similar cellular mechanisms of actions of CLPs in human tissues.

**Dissertation overview**

In this dissertation, I present the work I have done to address the *Idgfs* mystery. Three and a half years ago, I embarked on a genomic expedition, searching for genes that interact with one of the *Idgfs, Idgf3,* with the aim of identifying novel genetic interactions in an unbiased manner. Based on what is known about the *Idgfs,* defining specific expectations was a difficult task. In fact, three tempting hypotheses on how the Idgfs act on the egg chamber (Figure 1.6;

Zimmerman *et al.,* 2017) point towards different gene prospects. Hypothesis 1 proposes that the *Idgfs* are secreted from the stretch cells and travel towards and interact with the DA making cells. This interaction could be the result of Idgfs interacting with either membrane receptors on the DA-making cells or with molecules inside the DA making cells. Upon the interaction, signaling cascades alter the genomic landscape of the DA making cells and ultimately lead to the formation of the dorsal appendage tubes. Hypothesis 2 predicts that the Idgfs modify the ECM physical properties by affecting expression of genes encoding ECM components (e.g. Collagen IV and Perlecan) and in this way affecting the stiffness of the ECM, which can affect tube growth. Hypothesis 3 proposes that the Idgfs act in an autocrine fashion, exerting an effect on the same stretch cells that secrete them, changing their physical properties and thereby affecting their interaction with the floor cells during tube elongation. Based on these hypotheses, I predicted to uncover genes like receptors, signaling pathway molecules, signal-transporting molecules, cytoskeleton-regulatory molecules, transcription factors, post-translational regulation factors, genes that encode ECM components, such as collagen and fibronectin, or enzymes that modify these structures by adding carbohydrates or producing other polysaccharides, and genes encoding vesicle components. Since my expectations were quite broad, I began my investigation using an unbiased modifier screen that would allow me to uncover genes expressed from all the follicular epithelium of the egg chamber.

In Chapter II, I explain how I exploited a gain-of-function allele to identify Idgf-interacting genes. Work in the lab has shown that the deletion of only one member of the Idgf family does not produce any DA defects, but instead, deletion of the six Idgfs is required to observe DA defects (unpublished). Because of these observations and the Idgfs' high amino acid homology, I believe that the members of the Idgf family might act redundantly in the cells. This

redundancy represents a challenge when intending to understand each of the Idgf's function using loss-of-function alleles. Therefore, as an indicator of genetic interactions, I used the incompletely penetrant phenotype of overexpressing *Idgf3* to scan for regions of the genome that could suppress or enhance the over-expression phenotype. In this way, I identified *combover (cmb),* a Rho-kinase substrate that plays a role in wing hair formation in *Drosophila.* Although *cmb* acts as a planar cell polarity effector during *Drosophila* wing hair development, in our system I found that *cmb* and *Idgf3* play a role in apical expansion during tube formation. Additionally, I was able to identify five regions that interact with *Idgf3,* and these regions uncovered 58 candidate genes.

In Chapter III, I go into more depth about one of those genes, *eIF3e,* which strongly enhanced the *Idgf3*-overexpression phenotype. The lack of genetic tools limited the investigation of this interesting interaction. Nonetheless, in this chapter I report different attempts to identify the relationship between *eIF3e* and *Idgf3* in dorsal appendage formation and how one of those attempts led me to identify the PlexA-Mical pathway as a hypothesized Idgf3-interacting pathway; this hypothesis will be worth pursuing in the future.

In Chapter IV, I present ideas on how to continue with these investigations in order to identify the *Idgf* pathway, which plays an important role in tube formation.

Chapter V contains the methods I used for all aspects of my project.

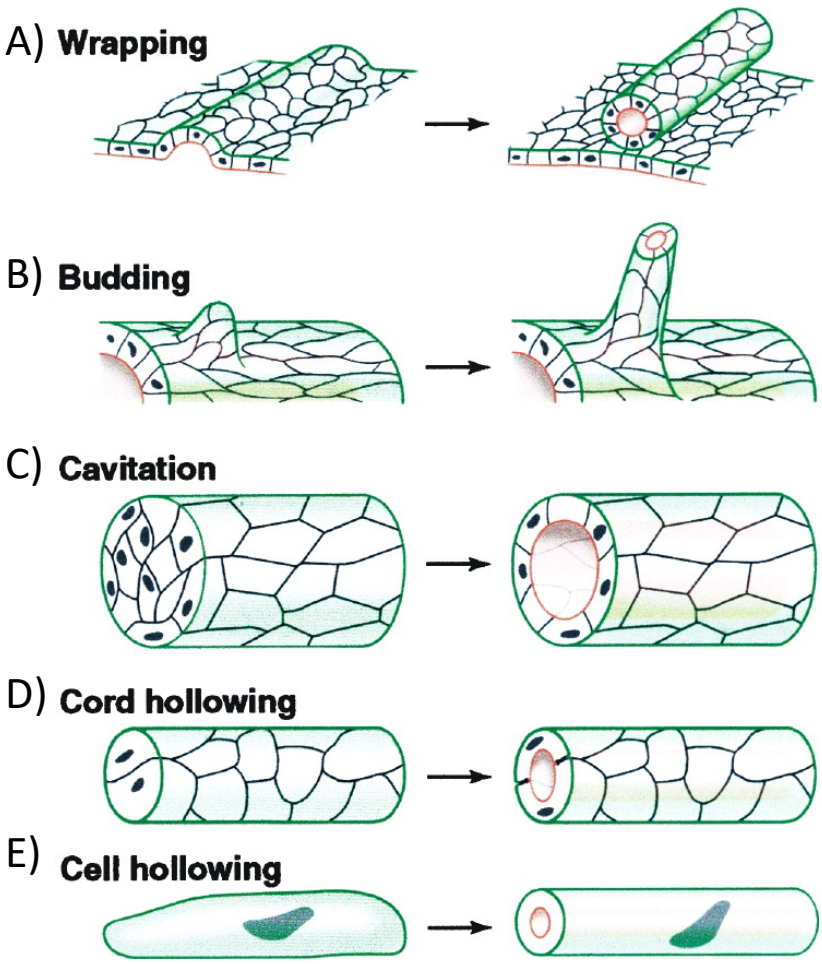


**Figure 1.1** Biological tubes form through different mechanisms of tube formation**.** (A) The **wrapping mechanism**, in which a flat sheet of epithelial cells bends, cells invaginate and the edges meet, sealing a tube that is parallel to the starting sheet. (B) The **budding mechanism,** in which cells from a flat epithelium bud and migrate out of the plane, creating a tube is is perpendicular to the starting sheet. (C) The **cavitation mechanism**, in which cells in the center of a cylindrical mass of cells are eliminated, creating the lumen of a tube. (D) The **cord hollowing mechanism** creates a de novo tube in between cells in a cylindrical cord. (E) The **cell hollowing mechanism** creates a tube lumen within the cytoplasm of a single cell. Image taken from Lubarsky and Krasnow, 2003.

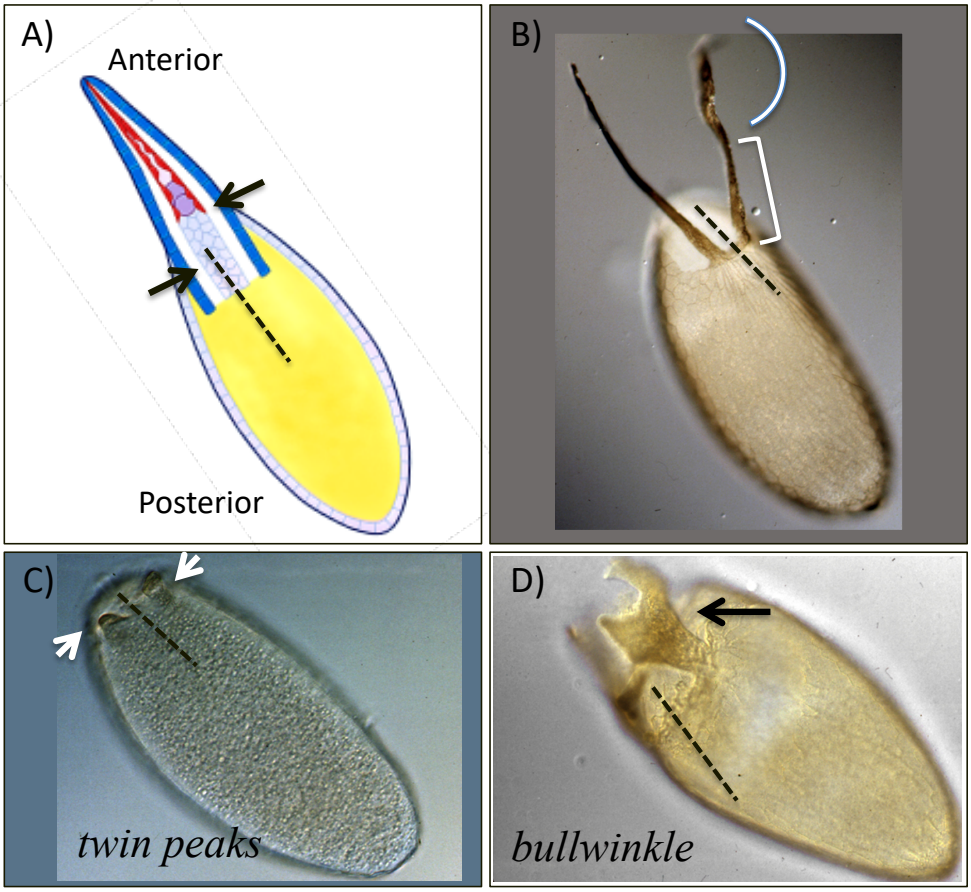


**Figure 1.2:** Dorsal appendage formation is a good model to study biological tube formation. (A) Schematic of a S14 egg chamber, arrows show the tube lumens (white). Different colors show the different cell types: nurse cells (solid purple), the oocyte (yellow) surrounded by body follicle cells, floor cells (red), roof cells (solid blue). Anterior is to the left upper corner and it applies for A-D. Dotted line shows the midline of the egg chamber and the eggs, and it applies for A-D. (B-D) Light-field micrographs laid eggs. Drawing obtained with permission from Dorman *et al*. 2004 (B) Egg laid by a wild type female, showing two normal dorsal appendages with a rounded stalk (square bracket) and a flat paddle (curved bracket). Picture obtained with permission from Berg, 2005. (C) Egg laid by a *TTK69* mutant female. White arrows show the two short dorsal appendages. (D) Egg laid by a *bwk* mutant female. Arrow shows one wide and short dorsal appendage. Credit for C and D to Celeste Berg.

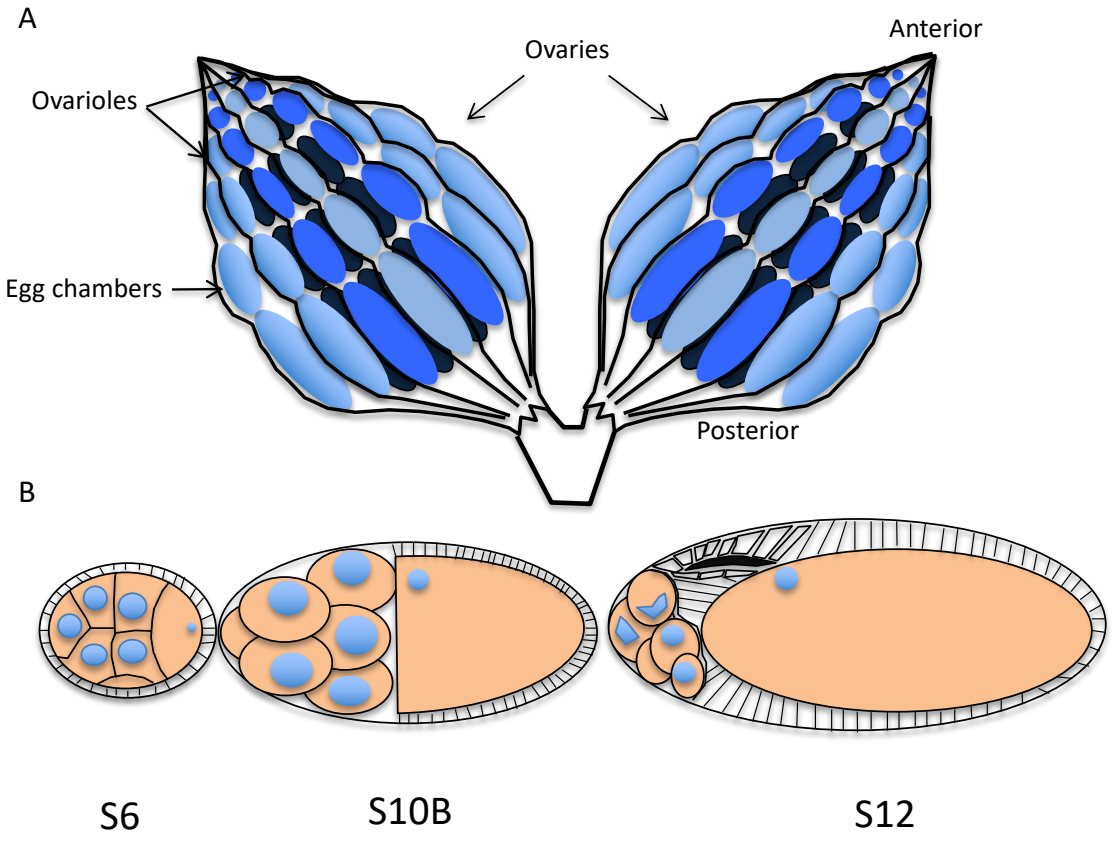


**Figure 1.3:** Egg chambers develop sequentially in the ovary. A) Schematic of *Drosophila* ovaries depicting egg chambers developing progressively in assembly lines called ovarioles. Each ovariole contains egg chambers organized sequentially with youngest at the anterior and most mature at the posterior. B) Schematic of three stages of egg chamber development shows somatic follicle cells in white and germline-derived nurse cells and oocyte in light orange. Nuclei are represented by blue circles. Dorsal appendage tube lumen is shown in black in S12.

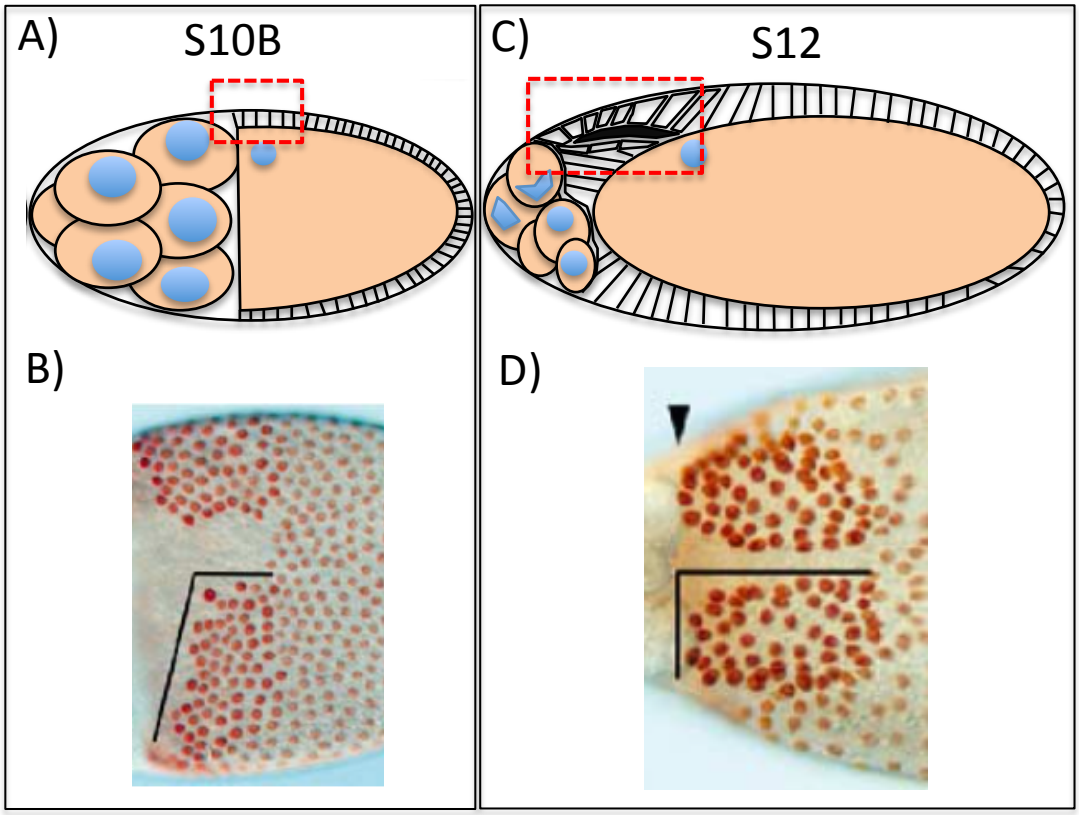


**Figure 1.4:** Dorsal appendage tube elongation is driven by rearrangement of roof cells. (A and C) Schematic of side views of an S10B egg chamber (A) and an S12 egg chamber (C). Germline nurse cells and oocyte are shown in light orange, nuclei are shown in blue, somatic follicle cells are shown in white and tube lumen is solid black. Red square shows the area that is zoomed in to show B and D. (B and D) Egg chambers stained with anti-Broad (red), a protein expressed in all body follicle cells before stage 10B. From stage 10B and forward, roof cells express *Broad* highly while the rest of the body follicle cells express lower to no expression of *Broad*. Brackets show roof cells rearranging from a patch with higher height than width to a patch with higher width than height. This type of rearrangement results from roof cell intercalating, a process also known as convergence extension. (B-D) adapted with permission from Ward and Berg. 2005.

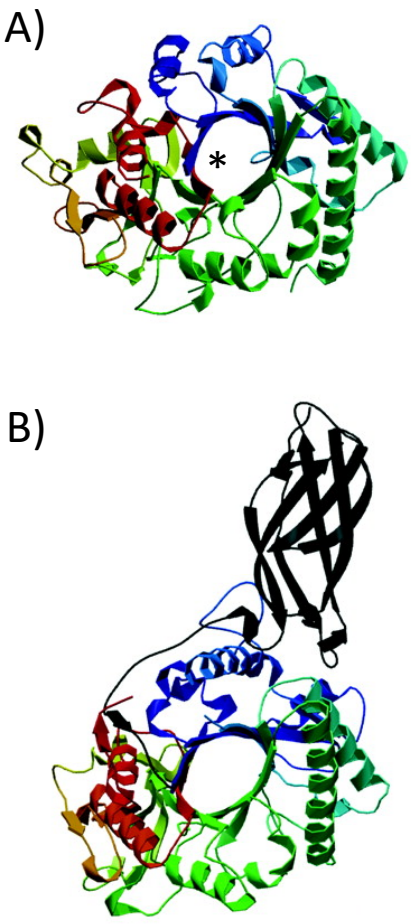


**Figure 1.5:** Idgf2 protein shares a similar folding organization to Chitinases. Idgf2 crystal structure (A), showing a classical $(\beta\alpha)_8$ barrel fold structure characteristic of chitinases (B). An amino acid sequence replacement in amino acid 132 of the Idgf2 sequence (by the *) abolishes catalytic activity in the Idgf2 protein. This figure was originally published in the Journal of Biological Chemistry. Varela, P., Llera, A. S., Mariuzza, R. A., and J. Tormo. Crystal Structure of Imaginal Disc Growth Factor-2 a member of a new family of growth-promoting glycoproteins from Drosophila melanogaster. J Biol Chem. 2002; 277: 13229-13236. © the American Society for Biochemistry and Molecular Biology.

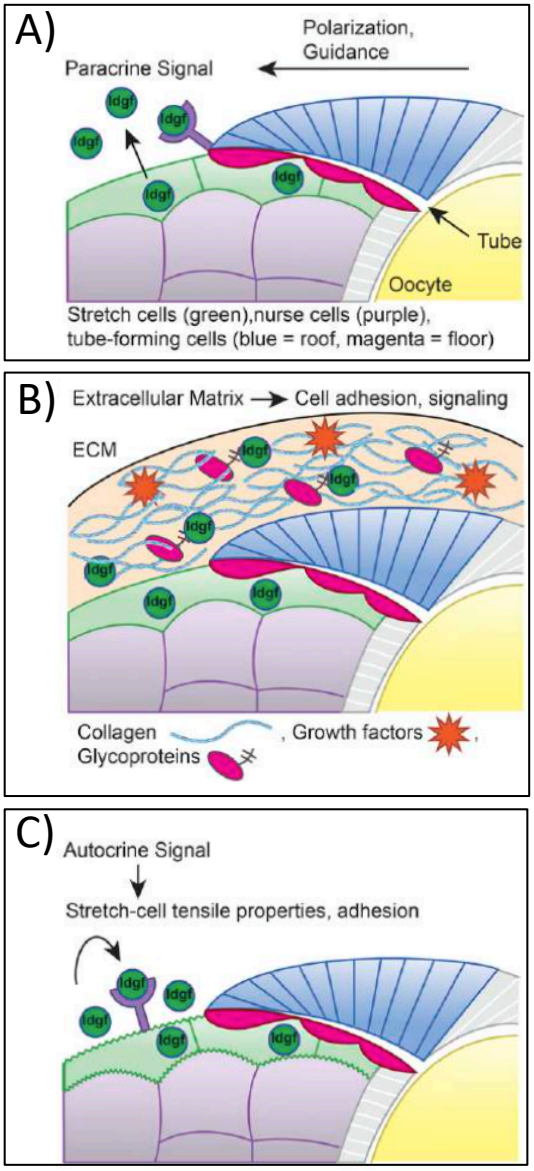


**Figure 1.6:** Three hypothesized mechanisms of action, explaining how the Imaginal Disc Growth Factors (Idgfs) could drive dorsal appendage formation. A) Idgfs (dark green) are secreted from the stretch cells (light green) and bind to receptors in the dorsal appendage making cells (blue), directing tube formation or anterior elongation. (B) Idgfs are secreted from the stretch cells, regulate or change proteins that make the extra cellular matrix (ECM), and change the physical properties of the ECM, affecting the interaction between the ECM and the DA-making-cells-interaction during DA tube elongation. (C) Idgfs act in an autcrine fashion. The Idgfs are secreted from the stretch cells and interact with receptors in the stretch cells, affecting how stretch cells and DA making cells interact during DA tube elongation. Image adapted with permission from Zimmerman *et al.* 2017

## CHAPTER II: Detecting new allies: Modifier screen identifies a genetic interaction between Imaginal disc growth factor 3 and combover, a Rho-kinase substrate, during dorsal appendage tube formation in Drosophila

The work presented in this chapter has recently been submitted and accepted for publication.

Biological tubes establish the primary design of all organs. For example, the spinal cord is made by the neural tube, which in many vertebrates begins to form by "wrapping" (Nievelstein *et al.,* 1993; Catala *et al.,* 1996). Wrapping is a mechanism of tube formation in which rows of cells within a sheet constrict their apices while adjacent outer rows of neighboring cells migrate towards each other, zipping together to form a tube that is parallel to the original plane (Lubarsky and Krasnow 2003). Tubes are clearly important both developmentally and physiologically, and yet the signals responsible for inducing epithelial cells to reorganize from a flat sheet into a complex tubular structure are still poorly understood [reviewed by Nikolopoulou *et al.,* 2017].

Understanding the genetic programs that drive wrapping is of great interest because their improper implementation gives rise to spinal cord defects such as *spina bifida* and *anacephaly*, which affect ~ 1 in 1000 births worldwide (Hogan and Kolodziej 2002; Copp *et al.,* 2015; Avagliano *et al.,* 2019) and represent a major health and economic problem in our society (Bamer *et al.,* 2010; Yi *et al.,* 2011). Although animal models and GWAS studies have helped identify genetic players that might be involved in tube formation during human development (Copp and De Greene 2010; Wang *et al.,* 2019), limited accessibility to the process impedes studies to understand how these genes influence morphogenesis. An important question that remains in the field is exactly how those, and other unknown genetic programs, drive tube

formation at a cellular level. Studies in the *Drosophila* system could help us overcome this challenge.

The *Drosophila* laid egg and the egg chamber that produces it serve as great models to study tube development (Berg 2005; Osterfield *et al.,* 2017). The laid egg has two eggshell structures, known as dorsal appendages (DAs), which facilitate gas exchange for the developing embryo by retaining pockets of air within the chorion (Hinton 1969). The dorsal appendages develop through the formation of two biological tubes that use the wrapping mechanism of tube formation (Dorman *et al.,* 2004) (Figure 1). Although the dorsal appendages are not tubes themselves, cellular tubes mold their physical form (Dorman *et al.,* 2004; Berg 2005). Therefore, by looking at the shape of the dorsal appendages on a laid egg, we can assess mistakes during the process of tube formation.

Dorsal appendage formation takes place before the egg is laid, while the egg chamber develops in the ovaries of the adult female (Figure 2.2A). The egg chamber consists of 16 germ-line cells (a single oocyte connected to 15 sibling nurse cells) surrounded by a mono-layered epithelium of somatic follicle cells (Figure 2.2B). Within the ovary, the egg chambers are organized in assembly lines, ranging from the youngest, stage-1 (S1) egg chambers, at the anterior, to mature, stage-14 (S14) egg chambers, at the posterior. This organization and the presence of multiple egg chambers within a single female allow us to simultaneously observe tube formation at different stages of development (King, 1970). By dissecting fly ovaries and fixing egg chambers, we can capture stationary processes of otherwise fast-moving events of morphogenesis (Hudson and Cooley 2014; Peters and Berg 2016A).

The morphological changes that form the dorsal appendage tubes begin at S10B of egg chamber development (Figure 2.1A and Figure 2.2B). At this stage, the nurse cells occupy the

anterior half of the egg chamber and the oocyte occupies the posterior half. The follicle cells that surround the nurse cells have become so thin and squamous they are called "stretch cells", while the follicle cells over the oocyte are columnar in shape. By S10B, among the columnar follicle cells, two patches of cells are differentially programmed to make the two tubes that mold the dorsal appendages (Figure 2.1A). Each patch is made of ~11 floor cells and ~52 roof cells (Dorman *et al.,* 2004), which will become the floor and the roof side of the DA tube, respectively (Figure 2.1A, arrows). From S10B to S14, these cells undergo cell-shape changes, cell intercalation, and cell migration in order to form two mature tubes (Dorman *et al*., 2004; Osterfield *et al.,* 2013). While the tubes are forming, the follicle cells release chorion protein into their lumen; these chorion proteins are later cross-linked to create an oar-shaped structure with a rounded stalk and a flat paddle (Fig 2.1A, B). Once this morphogenetic process is finished, the follicle cells undergo apoptosis and detach from the egg (Nezis *et al.,* 2002). Thus, the final shape of the dorsal appendages reflects the process of tube formation (Figure 2.1B).

We have used the dorsal-appendages model to identify and characterize genes involved in tube formation (Berg 2005). For example, we identified *bullwinkle (bwk)*, which when mutated results in wide and short dorsal appendages resembling moose antlers [hence the name] (Figure 2.1C; Rittenhouse and Berg 1995). In *bwk* egg chambers, the DA-forming tubes don't seal properly, and dorsal-appendage-making cells migrate more laterally than anteriorly (Dorman *et al.,* 2004). Interestingly, *bwk* acts outside the dorsal-appendage-making cells, in the nurse cells, by regulating expression of signals to the stretch cells (Rittenhouse and Berg 1995). The stretch cells act as mediators to then communicate with the dorsal-appendage-making cells, facilitating the proper formation and elongation of the DA tubes (Tran and Berg 2003). The signals involved in each of these processes are not completely understood.

To understand the molecular landscape of the stretch cells and how it drives dorsal appendage formation, we recently used proteomic analysis to assess stretch cells purified from wild-type and *bwk* egg chambers; we discovered that *bwk* mutants vastly over express a novel family of growth factors, the Imaginal disc growth factors (Idgfs). Lowering the expression of *Idgf4, Idgf5,* or *Idgf6* ameliorates the *bwk* mutant phenotype, suggesting they are part of the *bwk* signaling pathway that regulates dorsal appendage formation. Up-regulating only a single member of this family, e.g., *Idgf3*, is sufficient to produce a phenotype similar to the *bwk* mutant (Figure 2.1D) (Zimmerman *et al.,* 2017).

There is limited knowledge about the *Idgfs.* The first *Idgfs* were identified from conditioned medium and shown to act as growth factors, playing roles in cell-shape changes, cell proliferation, and cell migration in cell lines cultured *in vitro* (Kirkpatrick *et al.,* 1995; Kawamura *et al.,* 1999). Supporting the hypothesis that Idgfs might influence cell behaviors, transcripts from *Idgf1, Idgf2, Idgf3, Idgf4,* and *Idgf6* accumulate in sites of the embryo where major morphogenetic changes occur, such as the ventral furrow and midgut invaginations (Kawamura, *et al.,* 1999; Jambor *et al.,* 2015). The *Idgfs* encode proteins containing a signal-peptide domain (Zhu, *et al.,* 2008) and a mutation-bearing-chitinase catalytic domain (Varela, *et al.,* 2002), suggesting they are secreted molecules that evolved from chitanases but lack the ability to break down chitin. Their receptors and signaling pathway are not known.

In addition to helping us comprehend biological tube formation, elucidating the mechanism of action of the Idgfs could give insight into other human diseases since the human orthologues of the Idgfs, the Chitinase-Like Proteins (CLP's) (Zhu *et al.,* 2008), are up-regulated in immune diseases (reviewed in Ober and Chupp 2009), in numerous cancers (reviewed in Libreros *et al.,* 2013), and during infections (Erdman *et al.,* 2014). In spite of their well-known

association with these diseases, relatively little is known about their mechanism of action. Indeed, it is not clear whether the CLPs are pathogenic, protective, or both, depending on circumstances. Characterizing the cellular mechanisms of Idgfs in tube formation could facilitate studies of human CLPs by providing testable hypothesis on how Chitinase-like proteins could be acting in these contexts.

The main goal of this study was to increase our understanding of the *Idgfs* and their role in tube formation by identifying a genetic pathway that interacts with the *Idgfs* during dorsal appendage formation. We designed an unbiased screen to uncover genes that suppress or enhance the DA defects produced by over-expressing *Idgf3*. We identified large regions of chromosome 3L that, when removed by half, showed a possible genetic interaction with *Idgf3* for tube morphogenesis. Using the same approach with smaller, overlapping deletions, we narrowed down a subset of those possible interacting regions to a few candidate genes. Using RNAi lines and mutant alleles, we discovered a genetic interaction between *Idgf3* and *combover (cmb)*, a Rho-kinase substrate that physically interacts with a Planar Cell Polarity (PCP) pathway component. Through immunostaining, we go on to show how this interaction influences tube formation at a cellular level. In this way, we report the identification and first cellular characterization of an *Idgf*-interacting gene. Additionally, we identify other potential *Idgf3*-interacting candidates, some of which might also interact in the *cmb—Idgf3* pathway.

## RESULTS AND DISCUSSION

### Modifier-screen set up

Previous studies from our lab, using the *GAL4-UAS* system, demonstrated that overexpressing *Idgf3* in the stretch cells of the egg chamber causes dorsal appendage defects about 50% of the

time (Zimmerman *et al.,* 2017). We used this knowledge to identify possible genetic interactions with *Idgf3* by screening regions of the genome that, when reduced to a dosage half that of wild type, could suppress or enhance the frequency of dorsal appendage defects.

We chose chromosome 3L to scan for modifiers of the *Idgf3*-overexpression phenotype because we have limited knowledge of 3L genes that might be involved in dorsal appendage formation (Tran and Berg 2003; Berg 2005; Boyle *et al.,* 2010). We used the deficiency kit available at the Bloomington Stock Center (Cook *et al.,* 2010) and identified 72 lines that were the minimum number of stocks that uncover virtually all of 3L, a chromosome arm that comprises ~ one fifth of the genome (Table 1). All the lines have defined breakpoints and share the same genetic background (Parks *et al.,* 2004; Ryder *et al.,* 2007). Each deletion uncovers on average 58 genes, with a range of six to 159 genes.

We planned to use *UAS-RNAi* constructs to test individual genes within possible interacting regions, but since we did not know which cells of the egg chamber respond to the *Idgf3* signal, we needed a *GAL4* driver that would express in all follicle cells. We created a stock that uses *CY2-GAL4* (Queenan *et al.,* 1997) to drive expression of UAS-*Idgf3* in all follicle cells from stage 6 onward (Figure 2.2B). I considered *c415-GAL4* to not be an adequate driver for a the first round of the screen because it would have limited the expression of the RNAi lines to only the stretch cells later in the project.

We examined the dorsal appendage phenotype of this newly created stock. Flies that expressed *GAL4* alone produced eggs with DA defects 4% of the time, while flies that overexpressed *Idgf3* produced eggs with DA defects 29% of the time (Figure 2.3B). The reduced frequency of DA defects observed with overexpression of *Idgf3* using *CY2-GAL4* compared with *c415*, a stretch-cell-specific *GAL4* driver (50%, Zimmerman *et al.,* 2017), could

be due to spatial, temporal, or quantitative differences in *GAL4* expression (Figure 2.2C). For example, overexpression of *Idgf3* from the stretch cells could create a signal concentration gradient, while overexpressing *Idgf3* from all the follicle cells could create a uniform signal cloud, exposing the DA-making cells to different amounts of Idgf3. Alternatively, early overexpression of *Idgf3* using *CY2-GAL4* might cause the activation of pathways that counteract the effects of *Idgf3* overexpression, pathways that are ineffective if activated at S10. Although more investigation is needed to discover the mechanism that produces different frequencies of DA defects, the 29% frequency produced by *CY2-GAL4* allowed us to screen for modifiers of the *Idgf3*-overexpression phenotype. I considered to use the *c415-GAL4* driver in the modifier screen crosses or creating a stock that contain both drivers, but we chose to use the *CY2-GAL4* on its own instead because the *CY2-GAL4* driver on its own is already expressed in all the follicle cell types of the egg chamber (including the stretch cells) and its level of expression creates a threshold that allow us to look for and identify regions that can enhance or suppress the *Idgf3*-overexpression phenotype.

Subsequently, we observed that maintaining the *Idgf3*-overexpression stock at 25$^{o}$C caused a gradual decline in the frequency of defective DAs over time. Since the *CY2-GAL4* driver is moderately active at 25$^{o}$C (Queenan *et al.,* 1997), we hypothesized that this activity is enough to cause the accumulation of *Idgf3*-overexpression-suppressing mutations. To remedy this problem, we rebuilt the *CY2-GAL4 -> UAS-Idgf3* strain and maintained it at a lower temperature, 22$^{o}$C. This new strain (when shifted to 30$^{o}$C as described in the methods), continues to produce eggs with defective DA phenotypes at ~ 29% frequency.

**Screening for suppressors and enhancers**

We crossed females from the *Idgf3*-overexpression stock with males of each of the 72 deficiency lines or with males of a control stock, $w^{1118}$. By choosing non-Balancer flies, we obtained females that overexpressed *Idgf3* while also being heterozygous for a deficiency uncovering one part of chromosome 3L (Figure 5B); crosses to the control $w^{1118}$ males produced females that only overexpressed *Idgf3* (Figure 5A). We shifted the flies to 30°C to optimize Gal4 activity, then collected eggs and scored DA defects from each cross.

To determine whether each 3L deletion removed genes that interacted with *Idgf3*, we calculated the frequency of dorsal appendage defects on eggs laid by the *Idgf3*-overexpressing—deletion-heterozygous females and compared that value with the frequency of DA defects on eggs from females overexpressing *Idgf3* alone. We calculated *p*-values as an indicator of strength of interaction (Figure 2.3C) and drew a threshold of significance at $6.9 \times 10^{-4}$ after correcting for multiple testing (see methods). To our surprise, we found that 46% of the deficiencies significantly modified the *Idgf3*-overexpression phenotype: 38% of the deficiencies enhanced and 8% of the deficiencies suppressed (Table 1).

For this part of the screen, we did not test if each deficiency produced a dorsal appendage phenotype on its own because we wanted to quickly identify possible interacting deficiencies. Therefore, some deletions might have had a dorsal appendage phenotype independent of *Idgf3* overexpression. If so, we over-estimated the number of interacting deficiencies in this first stage of analysis.

We also noticed that our data are skewed towards enhancers. One possible factor contributing to this result is that the Idgfs are dosage sensitive for dorsal appendage formation: both down regulation and up regulation of each *Idgf* cause dorsal appendage defects

(Zimmerman *et al*., 2017). Therefore, genes that play a role in either type of regulation could perturb this balance and enhance the frequency of dorsal appendage defects. Also, since each deficiency reduces the copy number of many genes at one time, these large deletions could cause a cumulative effect if more than one cellular pathway is affected. Finally, the dorsal appendages are not critical structures of the fly; we therefore do not expect to find internal mechanisms that ensure proper DA development under such genetic alterations. Nonetheless, in this large screen, we identified several potential sites on chromosome 3L that genetically interact with *Idgf3*.

**Selecting regions to narrow down**

We used three criteria to pick deficiencies for further analyses. First, we wanted to identify both suppressors and enhancers of the *Idgf3* overexpression phenotype since these opposite phenotypes could reveal opposing inputs into how Idgfs are regulated or received. Second, we wanted to identify candidate genes that through their interaction with *Idgf3* would reveal critical processes for tube formation. In other words, removing only one copy of the gene while overexpressing *Idgf3* would disrupt tube formation drastically. Those candidate genes would be uncovered by the deficiencies with small *p*-values (Figure 2C, strong intensity). Alternatively, and our third criteria, we were interested in identifying important developmental pathways in which the *Idgfs* might play a role but that have back-up mechanisms to ensure robust function. In other words, removing one copy of a gene will produce only a mild effect on the *Idgf3*-overexpression phenotype because redundant genes or genes in parallel pathways could make up for the reduction of the gene product. Those genes would be uncovered by deficiencies with *p*-values near the threshold of significance (Figure 2.3C, weak intensity).

These three criteria led us to choose *Df(3L)ED4674*, *Df(3L)BSC289*, *Df(3L)BSC23*, *Df(3L)ED230* and *Df(3L)ED4502* for further study (Figure 2.3C, Table 2).

**Narrowing down the interacting regions**

We narrowed down the regions of interaction by using overlapping deficiencies. First, we took advantage of a tiling effect obtained from the original screen. 72% of the deficiencies from the primary screen partially overlapped with other deletions adjacent to their ends (Table 1, overlapping coordinates). Additionally, we obtained smaller, partially overlapping deficiencies from the Bloomington Stock Center, deficiencies that were produced using the same technologies as those used in the original modifier screen (See examples in Figure 2.4A and 2.3B).

Our strongest enhancer, *Df(3L)BSC4674*, overlapped with another deficiency from the original modifier screen, a deletion that suppressed the *Idgf3*-overexpression phenotype (Figure 2.4A). This result eliminated those genes in the proximal region of *Df(3L)BSC4674*. We tested six additional overlapping deficiencies in the region and found two that strongly enhanced the *Idgf3*-overexpression phenotype. Although these deletions increased the frequency of DA defects in the *Idgf3*-overexpression background, they did not result in a phenotype when *Idgf3* levels were normal (not shown), demonstrating that the defects depended on overexpressing *Idgf3*. By assessing the regions of overlap among these deletions, we ascertained the presence of an *Idgf3*-interacting gene among five candidate genes.

To narrow down the interacting regions uncovered by *Df(3L)BSC289*, *Df(3L)ED23*, and *Df(3L)ED230*, we used a similar approach and identified 5, 4, and 7 candidate genes, respectively (Table 2).

When investigating *Df(3L)ED4502*, we found one overlapping deficiency, *Df(3L)BSC614*, that enhanced the *Idgf3*-overexpression phenotype, confirming a genetic interaction with *Idgf3* and narrowing down the region to 51 candidate genes (Figure 3B). To refine the interaction further, we tested two additional deficiencies available in the region and found they did not enhance the *Idgf3*-overexpression phenotype. One of those deficiencies, *Df(3L)Exel6119*, resulted in a high number of dorsal appendage defects when *Idgf3* levels were normal, suggesting that a gene in that region plays a role in dorsal appendage formation but does not interact with the *Idgf3* pathway. Since this small deficiency is contained within the original deficiency *Df(3L)ED4502*, it explains why *Df(3L)ED4502* also results in dorsal appendage defects when *Idgf3* is at normal levels (Figure 2.5, lane 3). In contrast to *Df(3L)Exel6119*, however, *Df(3L)ED4502* interacted synergistically with *Idgf3*. We concluded that the genes uncovered by *Df(3L)BSC614,* but that fall outside *Df(3L)Exel6119*, were responsible for the enhancing effect seen with the large deficiency *Df(3L)ED4502* in an *Idgf3* overexpression background (Figure 2.5, lane 4). In total, our mapping suggested 37 candidate genes.

**Identifying interacting genes**

To identify the actual gene responsible for the interaction with *Idgf3*, we used *UAS-RNAi* constructs generously provided by the Bloomington or Vienna Stock Centers. Using the same DA assay, we tested those alleles for interaction with *Idgf3.* When evaluating the *UAS-RNAi* lines, we kept in mind that the amount of reduction of the gene product would likely differ from the original screen, in part because knockdown depends on the amount of Gal4p protein, which also drives expression of *Idgf3*. Since we were reducing transcripts only in the follicle cells, and the germ line produces a large amount of RNA to be loaded maternally into the embryo, we

could not assess the level of transcript reduction easily. Furthermore, protein products could perdure even if transcripts were completely degraded. We therefore interpreted a lack of phenotype from RNAi knockdown with caution, and we used null alleles when available, as nulls more closely mimic the conditions of the original deletion screen.

We narrowed down the region uncovered by *Df(3L)ED4674*, our strongest enhancer, to five candidate genes (Figure 2.4A, Table 2). RNAi alleles against four candidates, *CG9705*, *CG9706*, *CG9674*, and *nudC*, did not modify the *Idgf3*-overexpression phenotype. When we attempted to knock down expression of the fifth gene, *eIF3e,* by crossing a *UAS-RNAi* construct to either the *Idgf3*-overexpression stock or *CY2-GAL4* alone, pupae did not hatch and we were unable to obtain adult females to test their eggs for dorsal appendage defects. We also failed to obtain adults when using a temperature-sensitive *gal80* with *CY2-GAL4.* Unfortunately, no mutant alleles exist. Our observations suggest that *eIF3e*, which encodes a translation initiation factor, is an important developmental gene in *Drosophila*. Consistent with this hypothesis, the mammalian *eIF3e* is essential for mouse embryonic development (Sadato *et al*., 2018). As more null alleles become available, we will be able to test *eIF3e*, and other individual genes, for interaction with *Idgf3* with more confidence.

### ***Idgf3*** **genetically interacts with** ***combover***

After refining the interacting region for *Df(3L)ED4502*, one of our modest enhancers, 37 genes remained to be tested (Figure 3B, Table 2). We used a candidate gene approach and tested alleles of three genes whose function is relevant for development (Table 2). We identified a mild genetic interaction with a *combover* (*cmb)* RNAi line, which enhanced the *Idgf3*-overexpression phenotype. We tested a loss-of-function mutant and an overexpression line for this gene (Fagan

*et al*., 2014) and found complementary effects: *+/cmb*$^{KO}$ enhanced the *Idgf3*-overexpression phenotype, and the overexpression of *cmb-RB* suppressed the *Idgf3*-overexpression phenotype in three separate replicas (Figure 2.5).

We then asked: how are *Idgf3* and *cmb* interacting at the cellular level to impact the shape of the DA tubes? We tested two hypotheses: 1) they modify the narrowing and lengthening of the tube by regulating cell intercalation; and 2) they control the surface area of the tube lumen.

### *Idgf3* and *cmb* do not affect cell intercalation during dorsal appendage formation

The gene *cmb* was first identified as a substrate of Rho kinase, *in vitro* (Fagan *et al.,* 2014). This report suggested that *cmb* might play a role in the Planar Cell Polarity pathway (PCP) since the overexpression of *cmb* in the *Drosophila* wing causes the growth of multiple wing hairs, a phenotype that is characteristic of mutations in other PCP components. Moreover, Cmb physically interacts with one component of the PCP pathway (Multiple wing hairs) in both a yeast two-hybrid system and by immuno-precipitation (Fagan *et al.,* 2014).

PCP genes set up planar directionality of the epithelium, defining the orientation of static tissues such as those that produce mammalian hairs, bird feathers, and fish scales (reviewed by Butler and Wallingford 2017). The PCP pathway also coordinates the behavior of cells in morphogenetic tissues, directing movements that drive cell intercalation during a variety of developmental processes (Keller *et al*., 2000; Wallingford and Harland 2001; Park and Moon 2001; Darken *et al.,* 2002).

In our system, cell intercalation facilitates tube formation (wrapping) at stage 11, and it helps narrow and lengthen the tubes during S12 – S13 (Dorman *et al*., 2004; Osterfield *et al*., 2013; Ward and Berg 2005). When the DA patches are defined at S10B, they are longer along

the Dorso-Ventral (DV) axis compared to the Anterior-Posterior (AP) axis (Figure 2.6A, I). During S11, the floor cells zip up the tube underneath the roof cells, and the roof cells contract their apices. At the same time, more lateral cells move toward the dorsal midline, exchanging neighbors and altering the shape of the DA patch (Dorman *et al*., 2004; Osterfield *et al*., 2013; Ward and Berg 2005). During S12, as the roof cells release apical tension in a biased fashion (Peters and Berg 2016B), cell intercalation continues, producing a patch that is now longer along the AP axis than the DV axis (Figure 2.6E, J; Dorman *et al*., 2004; Ward and Berg 2005).

To test if the *Idgf3-cmb* interaction was affecting cell intercalation during DA formation, we quantified this transition by measuring the aspect ratio of S10B and S12 DA patches. We compared egg chambers produced by *CY2-GAL4* (control) females with those produced by *+/cmb*$^{KO}$ females, *Idgf3*-overexpressing females, and *cmb*$^{KO}$ */Idgf3*-overexpressing females. If *Idgf3* and *cmb* affected cell intercalation, we expected to see similar aspect ratios among genotypes at S10B, but significant differences between control and experimental groups at S12. To mark the exact boundary of the dorsal appendage patches, we used an antibody against Broad (Br), a transcription factor required to specify DA-forming cells (Tzolovsky *et al*., 1999): high levels of Broad ("High Br") define the DA patches, while moderate or low Broad ("low Br") marks lateral and posterior main-body follicle cells (Dorman *et al.,* 2004). To avoid introducing any bias, we conducted the image acquisition and quantification blind to the genotypes we were analyzing (see methods).

High-Br staining revealed the basal location of the nuclei in the dorsal-appendage-making cells (Figure 2.6A-H). As expected, at S10B, the shapes of the patches were similar for all genotypes (Figure 2.6A-D), except for a small but significant difference between the *Idgf3*-overexpression group and the control. Since the means of the aspect ratios of all the genotypes

were tightly clustered (0.66+/-0.04; Figure 5I), however, this small difference ($p = 0.03$) might simply have resulted from slight timing differences in S10B stage. That is, some eggs from the *Idgf3*-overexpression genotype might be at the end of S10B, transitioning to S11, when the patch nuclei condense slightly as roof cells begin to constrict their apices.

When looking at S12 egg chambers, we were surprised that the DA patches from both control and experimental egg chambers had elongated and narrowed to a comparable degree (Figure 2.6E-H), with aspect ratios that again exhibited similar means (1.71+/-0.06; Figure 5J). Moreover, the slight differences among genotypes at each stage were not significant ($P > 0.05$), and the small difference seen in the *Idgf3*-overexpression group at S10B was not present at S12. Based on these results, we concluded that the *Idgf3-cmb* interaction was not directly affecting cell intercalation in our system. This result was consistent with studies in the *Drosophila* testis demonstrating a non-PCP role for *cmb* in sperm individualization (Steinhauer *et al*., 2019).

### *Idgf3* and *cmb* affect apical area of dorsal appendage tubes

To examine the effect of the *Idgf3-cmb* interaction on tube lumen morphology, we stained egg chambers with an antibody against E-Cadherin (E-Cad) to reveal cell shapes (Figure 2.7A-D). E-Cad localizes on the apico-lateral sides of cells and is an important component of cell junctions, controlling cellular adhesion (Ratheesh *et al.,* 2012).

We quantified the area of the apical side of the dorsal appendage tubes at stage S12 (Figure 2.7). We used nurse-cell morphology at S12, which was unaffected by Idgf3 over expression, to stage egg chambers. Importantly, we had to account for the migration of the dorsal appendage tubes because tube migration, with its accompanying cell rearrangements and apical surface expansion, is an ongoing process during stage S12 (Peters and Berg 2016B).

Slight differences in the distance migrated during this stage of DA development could affect apical area (Figure 2.7E). To account for this problem, we normalized the area of the apical side of the dorsal appendage tubes by the length of the tubes (see methods).

We found that the apical area of the dorsal appendage tube, when controlled by the distance migrated at S12, averaged 16.50+/-1.5 μm in eggs laid by control flies (Figure 2.7A, 2.6F). The normalized apical area was similar in eggs laid by +/$cmb^{KO}$ mutants (18.04+/-1.2 μm; Figure 6B, 6F). In contrast, eggs laid by the *Idg3*-overexpression females had significantly higher values (20.045 +/- 1.4 μm; Figure 6C, 6F) than the controls, and knocking out one copy of *cmb* in the *Idgf3*-overexpression background significantly enhanced the *Idgf3*-overexpression effect (24.20 +/- 1.7 μm). Since $cmb^{KO}$/+ did not produce a phenotype on its own, this change in apical area was dependent on the overexpression of *Idgf3*, similar to what we found in the genetic analysis of laid eggs.

**Role of *Idgf3* and *cmb* during dorsal appendage formation**

To explain how *cmb* and *Idgf3* might interact together to regulate the apical area of cells during DA tube elongation, we propose two mechanisms. Both mechanisms rely on the fact that *cmb* is a substrate for Rho kinase (Rok) and that Rok directly affects actomyosin network tension (Munjal *et al.,* 2015; Riento and Ridley 2003). Changes in actomyosin network tension likely control the behavior of DA-making cells during tubulogenesis.

During wrapping, in the first steps of tube formation, roof cells constrict their apices and floor cells elongate to seal the tubes. These cell behaviors require high apical network tension (Osterfield *et. al* 2013). Following this step, tubes begin to elongate. Transcription factors that modulate expression of actin-regulatory genes control this transition, and changes in tension then

allow biased apical expansion and anterior crawling (French *et al*., 2003; Boyle *et al.,* 2010; Peters *et al.*, 2013). Since *cmb* is a Rok substrate, it is possible that *cmb* might be involved in regulating tension in dorsal-appendage-making cells during this transition. Experimental work measuring the actomyosin network tension in a *cmb* mutant could help test this hypothesis.

Under this hypothesis, how can *Idgf3* interact with *cmb* to regulate dorsal-appendage-tube elongation? One idea is that *Idgf3* acts upstream of the *Rok-cmb* pathway. That is, *Idgf3* could interact with an unidentified receptor in the dorsal-appendage-making cells, activating Rok and thus inhibiting *cmb* and reducing actin polymerization, as seen in wing hair formation (Fagan *et al.,* 2014).

To explain our experimental observations, removing only one copy of *cmb* might not be enough to cause changes in actin polymerization on its own, but overexpressing *Idgf3* might be enough to push the system over a threshold. In this way, the combination of *Idgf3*-overexpression and the removal of one copy of *cmb* might enhance the effect of *Idgf3*-overexpression alone. Analyzing the amounts and distribution of actin in the dorsal-appendage-making cells of *Idgf3*-overexpression and $cmb^{KO/+}$/*Idgf3*-overexpression mutants could provide evidence to support or reject this hypothesis.

There is another mechanism that can explain our observations. While *cmb* regulates apical tension of the dorsal appendage tube, *Idgf3* could be acting in a parallel pathway to *cmb*. This alternative mechanism recognizes that apical expansion is normally coordinated with anterior crawling (Boyle and Berg 2009), which involves roof cells physically interacting with the extracellular matrix (ECM) (Dorman *et al*., 2004). We propose that *Idgf3* influences this interaction by modulating the stiffness of the ECM (Zimmerman *et al*., 2017), possibly by activating enzymes that degrade the ECM around the elongating dorsal appendage tubes. Since

the leading cells contact the ECM along their basal surfaces, lowering the stiffness of the ECM could lower the resistance the leading cells encounter and alter integrin-mediated intracellular actin dynamics. These changes would then trigger the coordinated expansion of apical surfaces regulated by *cmb*. A similar change in ECM stiffness is critical for the cell-shape changes that drive *Drosophila* wing elongation (Diaz-de-la-Loza *et al.,* 2018).

In our experimental observations, removing one copy of *cmb* might not be sufficient to expand apical area because the ECM exerts a force containing the elongating tubes. Overexpressing *Idgf3,* which leads to an abnormal decrease of the ECM stiffness around the tubes, could lower the ECM force that counteracts the expansion of the tubes. Under these circumstances, removing one copy of *cmb* enhances cell expansion, resulting in the phenotype seen in the $cmb^{KO/+}$*; Idgf3* mutants. Experiments in which we artificially manipulate the stiffness of the ECM could help us understand if the ECM does play a role in dorsal appendage formation. In addition, quantifying the width of the ECM in *Idgf3* and *cmb* mutants would provide evidence to support or reject our hypothesis.

Although more work is needed to fully understand the *cmb*-*Idgf3* interaction, we have successfully identified one biological effect on tube shape when the expression of these genes is altered. It would be interesting to explore if human CLPs affect apical cell area of an epithelium or if the human orthologue of *combover*, *PCM1*, contributes to actin dynamics in metastatic cancer when the CLPs are up regulated (Libreros *et al*., 2013).

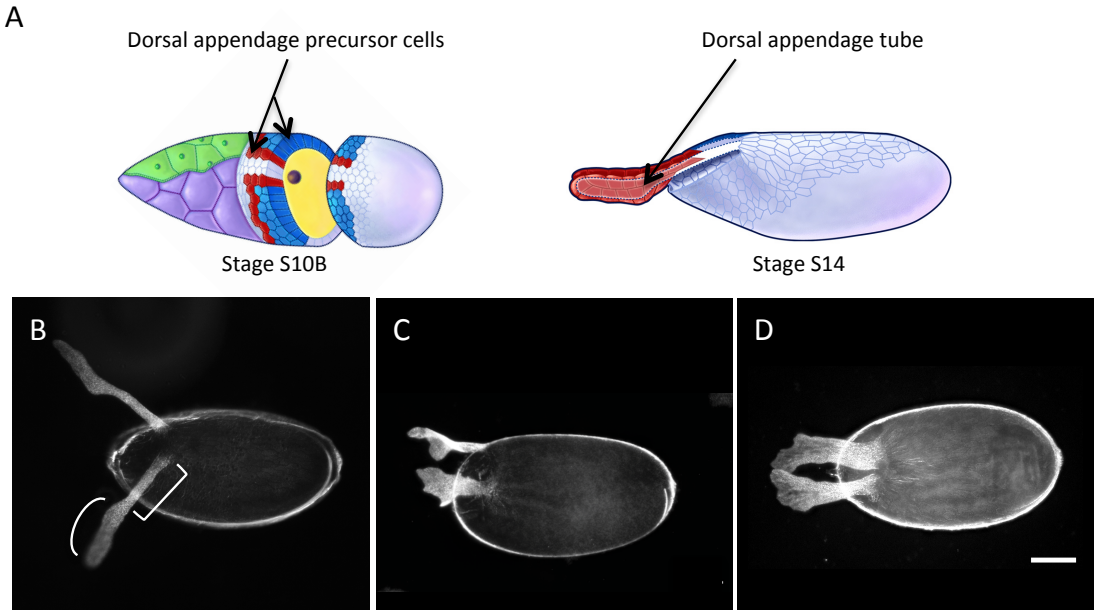


**Figure 2.1** Dorsal appendage formation is a good model to study biological tube formation. (A) Schematic drawings of two later stages of oogenesis, S10B and S14, depicting the cells that make the egg chamber. On the left, arrows indicate the cells programmed to build the dorsal appendages in red (floor cells) and blue (roof cells). On the right, an arrow points to the tube lumen, defined by a dotted line. Drawings obtained with permission from Dorman *et al*. 2004. (B-D) Dark-field micrographs of laid eggs. Anterior is to the left, dorsal is up in B and C, facing out of the page in D. (B) Egg from a wild-type female shows the rounded stalk (square bracket) and flat paddle [curved bracket] of normal dorsal appendages. (C) An egg laid by a *bullwinkle* (*bwk*) loss-of-function mutant exhibits short, wide, dorsal appendages with flat stalks and wavy paddles. (D) An egg laid by an *Idgf3*-overexpression mutant has short, wide, dorsal appendages similar to *bwk*. Pictures in C and D were obtained with permission from Zimmerman *et al.* 2017. The scale bar in D = 100 microns and applies to B, C, and D.

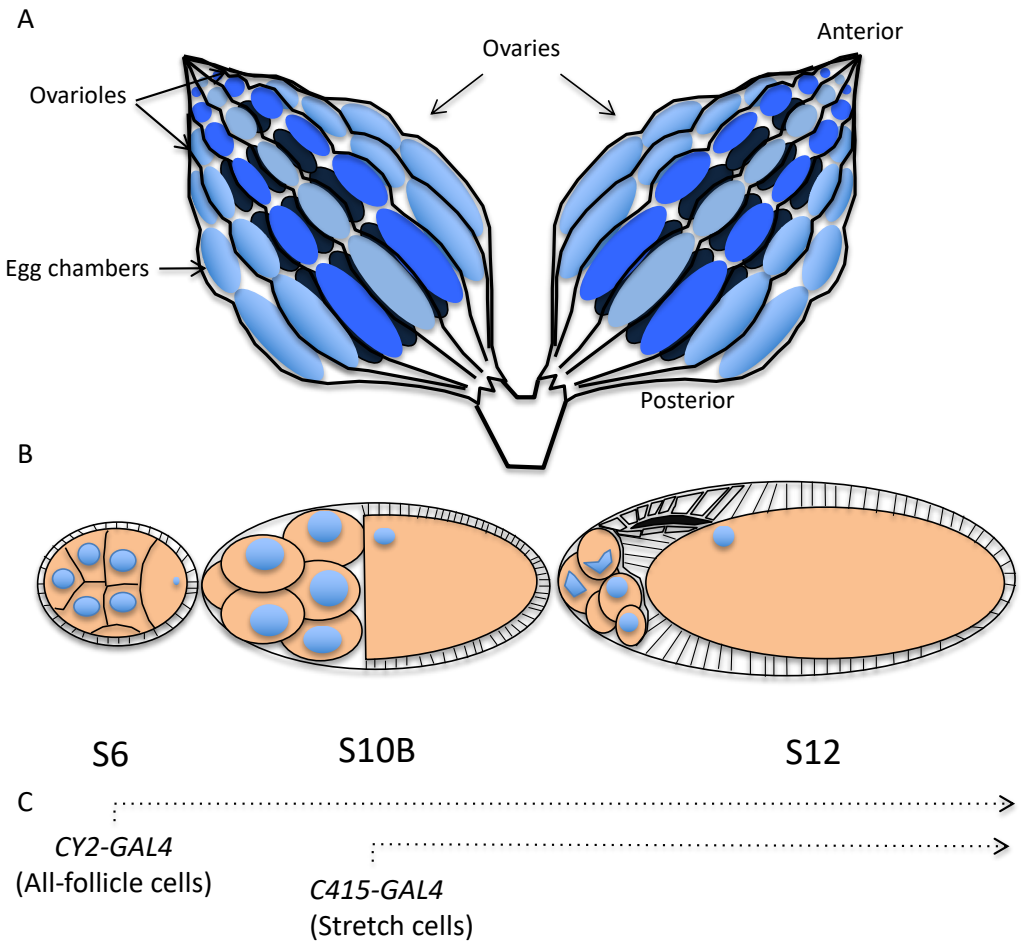


**Figure 2.2:** Egg chambers develop sequentially in the ovary. A) Schematic of *Drosophila* ovaries depicting egg chambers developing progressively in assembly lines called ovarioles. Each ovariole contains egg chambers organized sequentially with youngest at the anterior and most mature at the posterior. B) Schematic of three stages of egg chamber development shows somatic follicle cells in white and germline-derived nurse cells and oocyte in light orange. Nuclei are represented by blue circles. Dorsal appendage tube lumen is shown in black in S12. C) Timing of *GAL4* expression. *CY2-GAL4* is expressed at stage S6 in all follicle cells, while *C415-GAL4* is expressed at stage S10B only in the stretch cells; in both cases the expression continues to the end of oogenesis.

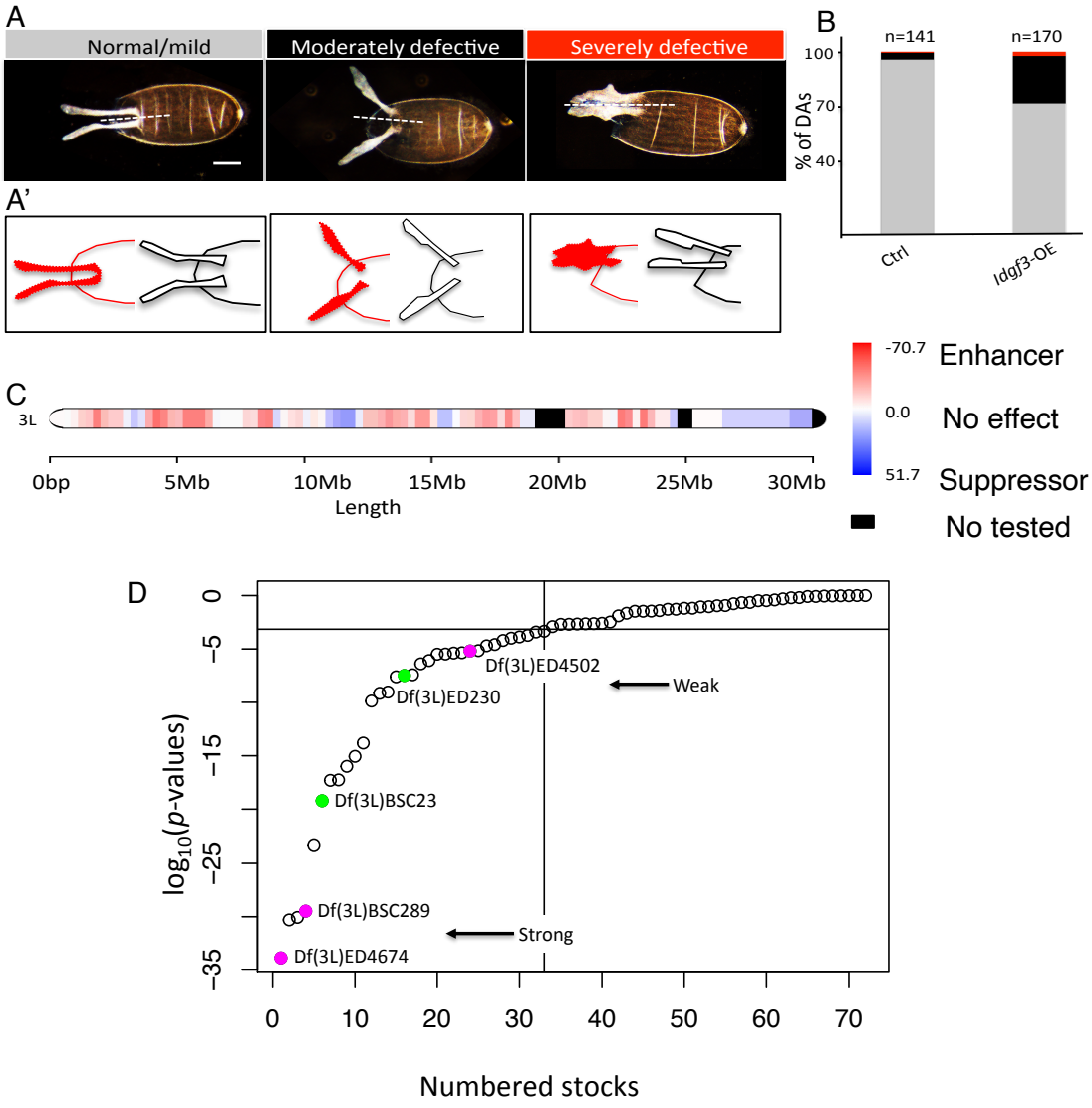
A
Normal/mild
Moderately defective
Severely defective
A'
B
n=141
n=170
100
70
40
% of DAs
Ctrl
Idgf3-OE
C
3L
0bp
5Mb
10Mb
15Mb
20Mb
25Mb
30Mb
Length
-70.7
Enhancer
0.0
No effect
51.7
Suppressor
No tested
D
0
−5
−15
−25
−35
log10(p-values)
Df(3L)ED4502
Df(3L)ED230
Df(3L)BSC23
Df(3L)BSC289
Df(3L)ED4674
Weak
Strong
0
10
20
30
40
50
60
70
Numbered stocks

**Figure 2.3** Modifier screen identifies regions on chromosome 3L that enhance or suppress the dorsal-appendage defects due to overexpressing *Idgf3*. (A) Representative images of dorsal appendage phenotypes observed in modifier screen, grouped and color coded into normal/mild (gray), moderately defective (black), or severely defective (red). Images are oriented with anterior facing left and dorsal facing out of the page. Dotted line shows the midline of the egg chamber. Scale bar is 100 microns and applies to all the pictures. The egg shown on the normal/mild category is slightly ventralized, which we considered to be mild. (A') Schematic outlining the DAs from their corresponding panels above (red) to contrast with the expected a normal DA shape (black), which is the rounded stalk and flat paddle. (B) Graph: proportions of eggs with normal/mild, moderately defective, and severely defective dorsal appendages produced by females of genotypes: $w^{1118}$*; CY2-GAL4/+; +/+ (*right) and $w^{1118}$*; CY2-GAL4/+; UAS-Idgf3/+* (left). (C) Chromosome 3L, mapping the modifier screen results and following the color code on the right side. (D) $\log_{10}$ of Chi-squared *p*-values calculated from comparing the dorsal appendage phenotypes between the $w^{1118}$*; CY2-GAL4/+;UAS-Idgf3/+* (control) and *CY2-GAL4/+;UAS-Idgf3/Df(3L*) (tested). Significance threshold is y= -3.1, which corresponds to the $\log_{10}$ of the Bonferroni correction of 0.05. Filled circles indicate the deletion lines that we chose for further analysis, in magenta (enhancers) and in green (suppressors). Arrows indicate strong and weak interactions.

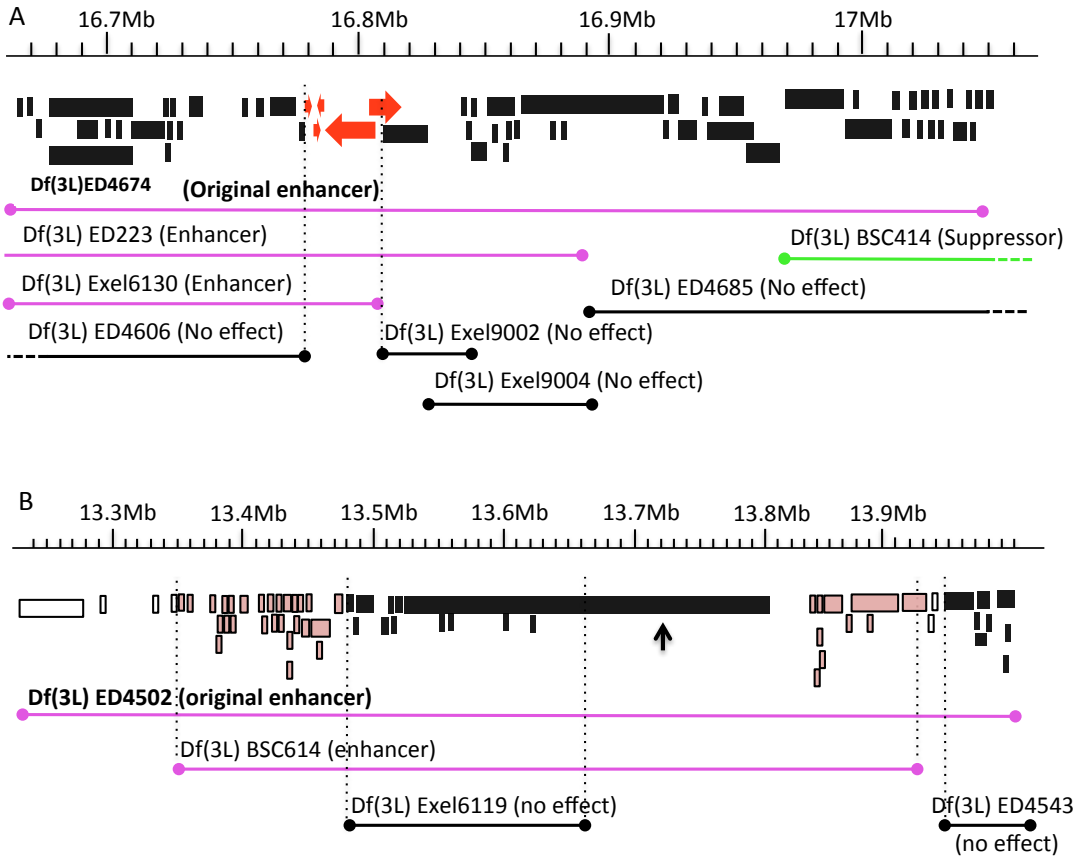
A
16.7Mb
16.8Mb
16.9Mb
17Mb
Df(3L)ED4674
(Original enhancer)
Df(3L) ED223 (Enhancer)
Df(3L) BSC414 (Suppressor)
Df(3L) Exel6130 (Enhancer)
Df(3L) ED4685 (No effect)
Df(3L) ED4606 (No effect)
Df(3L) Exel9002 (No effect)
Df(3L) Exel9004 (No effect)
B
13.3Mb
13.4Mb
13.5Mb
13.6Mb
13.7Mb
13.8Mb
13.9Mb
Df(3L) ED4502 (original enhancer)
Df(3L) BSC614 (enhancer)
Df(3L) Exel6119 (no effect)
Df(3L) ED4543
(no effect)

**Figure 2.4:** Overlapping deficiencies across chromosome 3L were used to narrow down the regions that interact with the *Idgf3* gene. (A, B) Genome browser maps showing two examples of interacting regions and the deletions we used to refine the list of potential interacting genes. Each block indicates the coding and non-coding regions of a gene. Unfilled blocks are genes whose interaction was neither confirmed nor discarded; black blocks are genes that failed to interact with *Idgf3*; red or pink blocks indicate potential candidate genes. Magenta lines show the span of the deficiencies that enhanced the *Idgf3*-overexpression phenotype. A green line shows the span of a deficiency that suppressed the *Idgf3*-overexpression phenotype. Black lines show the span of the deficiencies that did not change the percentage of defects observed by overexpressing *Idgf3*. Dotted regions indicate deletions that extend distally or proximally from the region shown here. (A) Example of a simple narrowing-down process. *Df(3L)BSC4674* strongly enhanced *Idgf3* overexpression. *Df(3L)ED223* and *Df(3L)Exel6130* confirmed and narrowed down the region of enhancement; these deletions did not produce a phenotype on their own. All the other deficiencies tested in the region did not have any effect on the *Idgf3*-overexpression phenotype, narrowing down the region to five candidate genes, shown in red. (B) Example of a complex narrowing-down process. *Df(3L)ED4502* identified an enhancer region, which was confirmed and narrowed down with *Df(3L)BSC614*. Two other deficiencies uncovered portions of the region; neither produced any effect on the *Idgf3*-overexpression phenotype. These results left 37 candidate genes remaining to be tested. The small arrow points to a gene that was discarded as a candidate gene because the coding regions for all its transcripts lay within the non-interacting deficiency. Ruler above each browser map shows the span of DNA in Megabases (Mb).

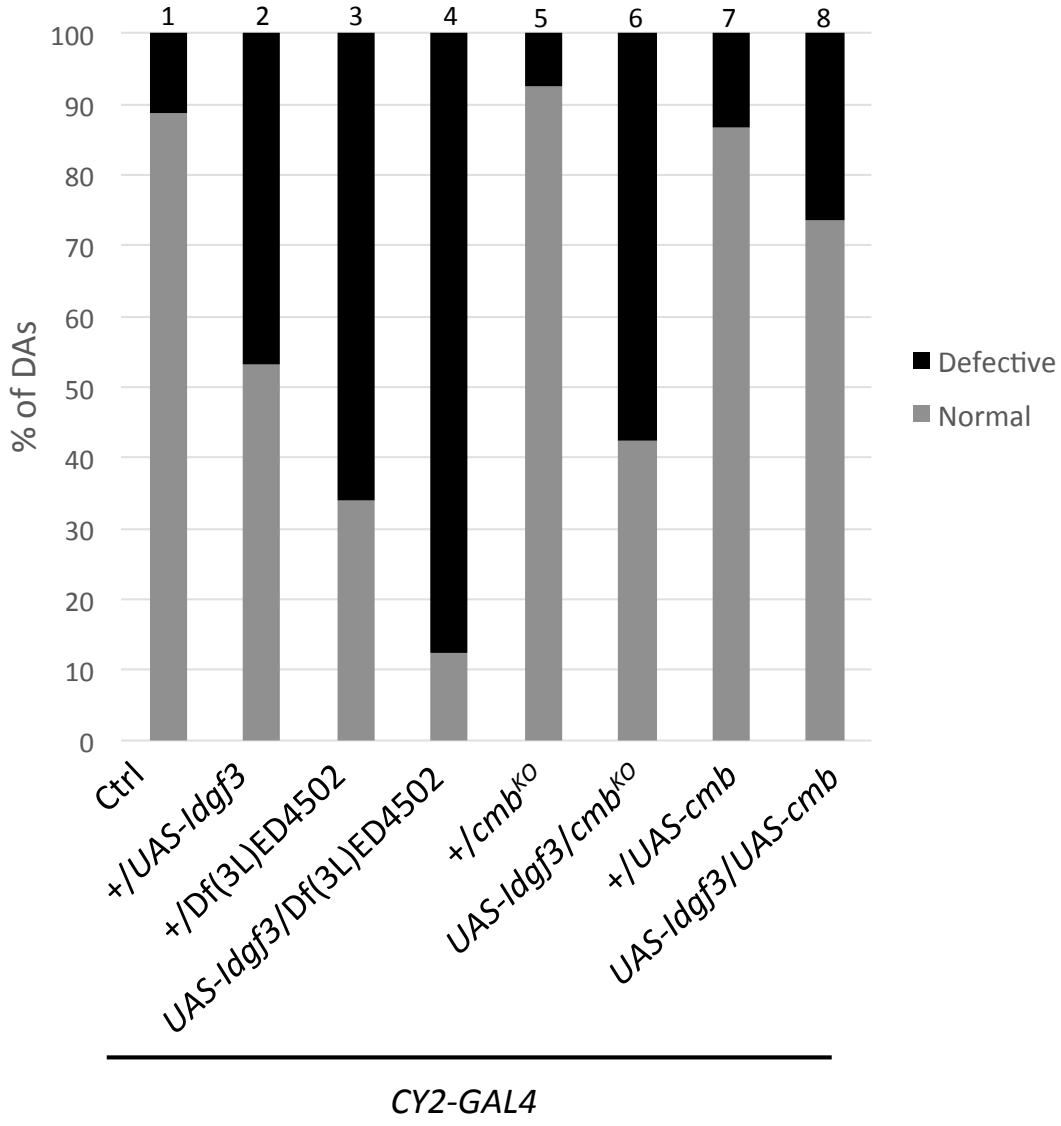
1
2
3
4
5
6
7
8
100
90
80
70
60
50
40
30
20
10
0
% of DAs
Defective
Normal
Ctrl
+/UAS-Idgf3
+/Df(3L)ED4502
UAS-Idgf3/Df(3L)ED4502
+/cmbKO
UAS-Idgf3/cmbKO
+/UAS-cmb
UAS-Idgf3/UAS-cmb
CY2-GAL4

**Figure 2.5**: *cmb* genetically interacts with *Idgf3.* Dorsal appendage phenotypes were quantified as normal (gray) or defective (black). Control female *($w^{1118}$; CY2-GAL4/+)* produced approximately 11% eggs with defective dorsal appendages (lane 1). The *Idgf3*-overexpression females (*$w^{1118}$; CY2-GAL4/+;UAS-Idgf3/+)* produced approximately 46% of eggs with defective dorsal appendages (lane 2). *Df(3L)ED4502* uncovered the *cmb* gene and produced a phenotype that was enhanced by the overexpression of *Idgf3* (lane 3 and lane 4). Removing one copy of *cmb* resulted in a small number of defective dorsal appendages (lane 5), similar to the *CY2-GAL4* control (lane 1). Removing one copy of *cmb* in an *Idgf3*-overexpression background (lane 6) enhanced the *Idgf3*-overexpression phenotype (lane 2). Overexpressing *cmb* resulted in a small number of defective dorsal appendages (late 7). Overexpressing *cmb* simultaneously with *Idgf3* (lane 8) suppressed the *Idgf3*-overexpression phenotype.

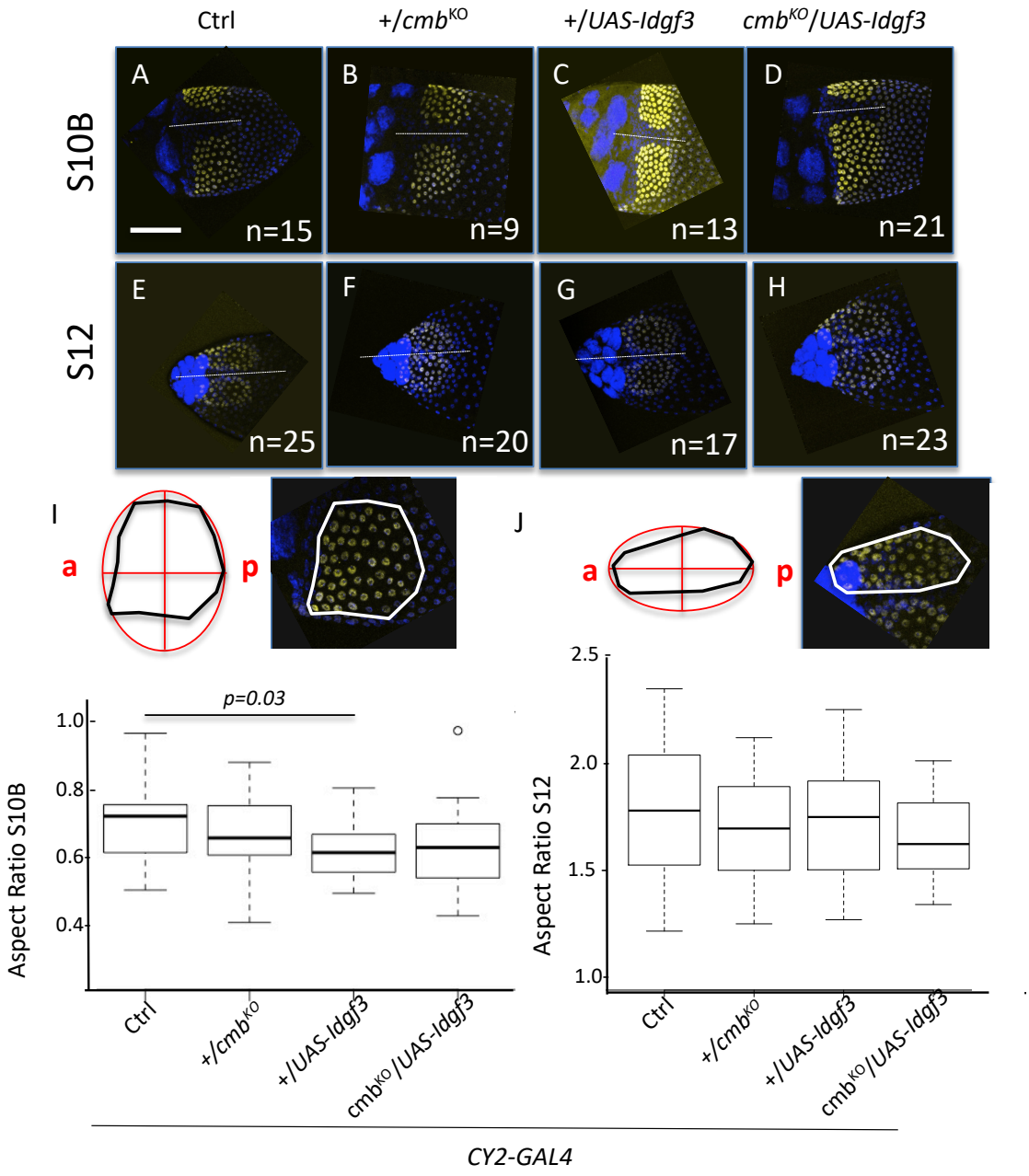
Ctrl
+/cmb^KO
+/UAS-Idgf3
cmb^KO/UAS-Idgf3
S10B
S12
A
B
C
D
E
F
G
H
n=15
n=9
n=13
n=21
n=25
n=20
n=17
n=23
I
J
a
p
a
p
p=0.03
Aspect Ratio S10B
Aspect Ratio S12
1.0
0.8
0.6
0.4
2.5
2.0
1.5
1.0
Ctrl
+/cmb^KO
+/UAS-Idgf3
cmb^KO/UAS-Idgf3
CY2-GAL4

**Figure 2.6:** *Idgf3-cmb* genetic interaction does not affect cell intercalation during dorsal appendage tube formation. (A-H) Representative examples of central dorsal views of S10B egg chambers (A-D), and anterior dorsal views of S12 egg chambers (E-H). Images represent eggs from three different experimental replicas, in which the intensity of background might vary, but the focus is on the shape of the DA patch. Scale bar is 100 microns and applies to all pictures. (A and E) $w^{1118}$*; +/CY2-GAL4*. (B and F) $w^{1118}$*; +/CY2-GAL4; +/cmb*$^{KO}$. (C and G) $w^{1118}$*; +/CY2-GAL4;+/UAS-Idgf3*. (D and H) $w^{1118}$*; +/CY2-GAL4; UAS-Idgf3/cmb*$^{KO}$. Each image is a projection of confocal slices (average ~38) showing the dorsal appendage patches stained for Broad protein (roof cell nuclei, yellow), and DAPI (DNA, blue). The number of egg chambers scored per genotype is indicated on each panel. Dotted lines show the midlines of each egg chamber. (I, J) Quantification of the aspect ratio of each dorsal appendage patch. Schematics on each panel show the outline area of each dorsal appendage patch, enlarged to the right, that was considered for aspect-ratio calculation using FIJI (See methods). "a" indicates anterior, "p" indicates posterior. Box plots show the mean, quartile, and range of aspect ratios measured for each genotype.

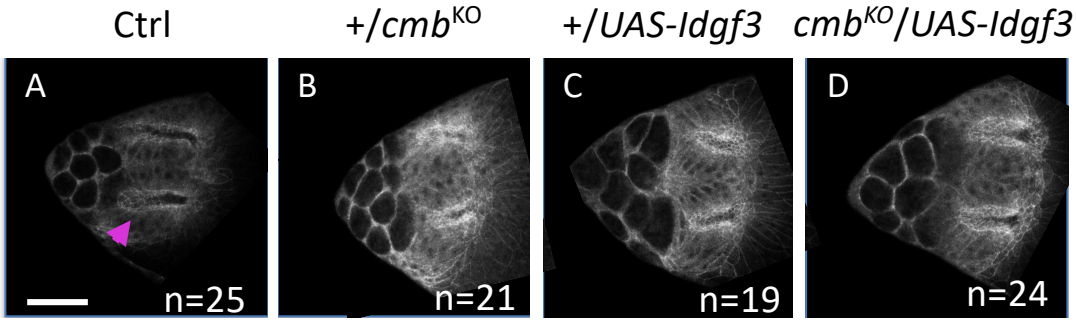
Ctrl
+/cmb^KO
+/UAS-Idgf3
cmb^KO/UAS-Idgf3
A
B
C
D
n=25
n=21
n=19
n=24

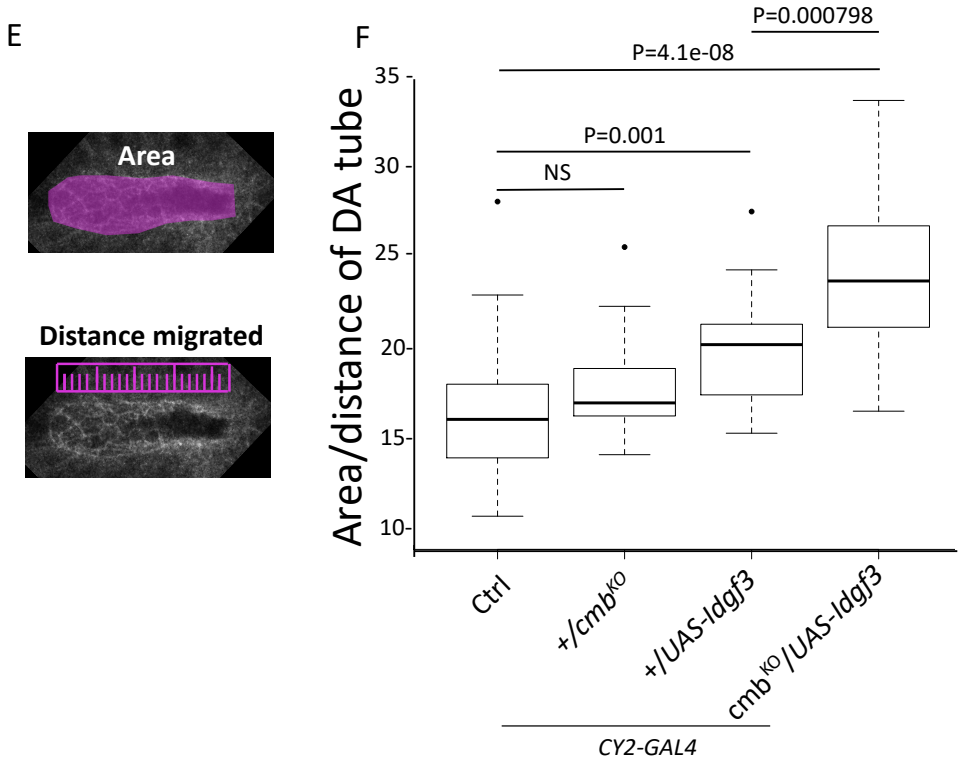
E
Area
Distance migrated
F
P=0.000798
P=4.1e-08
P=0.001
NS
Area/distance of DA tube
35
30
25
20
15
10
Ctrl
+/cmb^KO
+/UAS-Idgf3
cmb^KO/UAS-Idgf3
CY2-GAL4

**Figure 2.7**: *Idgf3-cmb* genetic interaction affects apical area of the dorsal appendage tubes. (A-D) Representative examples of anterior dorsal views of S12 egg chambers stained for E-Cadherin protein. Scale bar is 50 microns and applies to all pictures. (A) $w^{1118}$*; +/CY2-GAL4.* (B) ) $w^{1118}$*; +/CY2-GAL4; +/*$cmb^{KO}$. (C ) $w^{1118}$*; +/CY2-GAL4; +/UAS-Idgf3*. (D) $w^{1118}$*; +/CY2-GAL4; UAS-Idgf3/*$cmb^{KO}$. Images are a single, 0.5-micron slice taken at the most apical region of the cells that make the dorsal appendage tube. The number of egg chambers scored for each genotype is indicated on each panel. Magenta arrow on A points to the DA tube expanded as example in E. (E) A schematic drawing showing two factors that affect apical tube measurements: apical area of tube-making cells (magenta space). The temporal progression of dorsal appendage tube elongation (magenta ruler). F) Quantification of the area of the tube normalized by tube elongation (See methods). Box plots show the mean, quartile, and range of aspect ratio/distance migrated measured for each genotype. Since apical area increases as the tube cells move forward, we normalized the apical area by the distance migrated

## Chapter III: Does Idgf3 interact with the eukaryotic translation initiation factor 3 subunit e (eIF3e) and the Mical pathway during Drosophila dorsal appendage formation?

In this chapter I report my efforts to pursue a promising result, a potential interaction between *eIF3e* and *Idgf3*, that originated from the large modifier screen. As I continued unraveling information, however, I faced limitations on genetic tools that complicated the completion of the project. Building the needed tools, e.g., a null allele of *eIF3e*, would have required months of effort without a guarantee of a positive result. Nonetheless, my studies revealed intriguing discoveries that are worth following up with in the future.

### Modifier screen identifies a region that strongly interacts with Idgf3.

Using deficiency lines that uncover genes located on the 3L chromosome, I identified regions that enhanced or suppressed the *Idgf3*-overexpression phenotype. From these lines, *Df(3L)ED4674* strongly enhanced the *Idgf3*-overexpression phenotype (*p*-value = 1.36e-34) (Figure 3.1). 64 genes are located within this region, and when removed by half in an *Idgf3*-overexpression background, 45.2% of the eggs showed severely defective phenotypes. Most of these eggs were significantly smaller in size than the WT eggs and had chorion material of irregular shape on the dorsal side of the egg; although clearly different from the main-body eggshell, this material did not resemble dorsal appendages (Figure 3.1A). In this same line, 52.5% of eggs had moderately defective dorsal appendages and showed variable defects. These defects ranged from the absence of paddles to uneven edges. Finally, only 2.3% of eggs had a WT phenotype. On the other hand, when *Idgf3* was at normal levels, the removal of the *Df(3L)ED4674* region had a mild effect on dorsal appendage formation (Figure 3.1B), indicating that the severe defects seen in the modifier screen are coming strictly from an interaction with

*Idgf3.* These results revealed the presence of a gene that has a crucial impact on dorsal appendage formation, an impact that is dependent on the *Idgf3* pathway.

**Tiling deficiencies narrowed down the strongest enhancer to one candidate gene, *eIF3e.***

Testing partially overlapping deficiencies allowed me to identify smaller regions that enhanced or suppressed the *Idgf3*-overexpression phenotype. If the results were congruent with the results using the large deficiency, the smaller overlapping deficiencies allowed me to narrow down the interactions into smaller windows. For example, *Df(3L)ED4606* and *Df(3L)BSC414,* which I used in the original modifier screen, narrowed down the boundaries of the strongest enhancer *Df(3L)ED4674* (Figure 3.1C). I identified five additional overlapping deficiencies that uncovered the region (Figure 3.1C), from which *Df(3L)ED223* and *Df(3L)Exel6130* strongly enhanced the *Idgf3*-overexpression phenotype (Table 3). The fact that two different overlapping deficiencies showed a strong enhancing effect supported the hypothesis that an interesting *Idgf3*-interacting gene is present within the overlapped region. In this way, I narrowed down the interaction to *CG9705, CG9706, eIF3e, CG9674,* and *nudC,* as candidate genes.

Using available RNAi lines under the control of either *CY2-GAL4*, which is expressed in all follicle cells from S6 onward, or the stretch-cell specific *c415-GAL4* driver, I discarded *CG9705, CG9706, CG9674,* and *nudC* as possible *Idgf3*-interacting genes (Table 3). In some cases, multiple RNAi lines were available, and all showed congruent results. These results narrowed down the interaction to *eIF3e.* Because the deficiencies uncovering this gene showed remarkably small *p*-values and RNAi lines for the other genes in the region did not reveal any interaction, this screen pinpointed *eIF3e* as an attractive *Idgf3*-interacting gene candidate.

**Efforts towards verifying a genetic interaction between *eIF3e* and *Idgf3* lead to additional routes to elucidate a possible interaction.**

The *eIF3e* gene encodes one of ten subunits of the eIF3 protein complex that aids mRNA binding to the 40S ribosomal subunit (Asano *et al*., 1997). As such, it is an essential gene; indeed, *P*-element alleles are recessive lethal (Spradling *et al*., 1999). Unfortunately, using an RNAi line and the *CY2-GAL4* driver, I found that the reduction of *eIF3e* transcript, with and without *Idgf3* overexpression in the background, was lethal. That is, I was unable to obtain adult flies, as the pupae did not eclose, suggesting that *CY2-GAL4* is expressed in pupae and that *eIF3e* plays a role in pupal development; this effect is independent of *Idgf3* overexpression.

To overcome the challenge of not being able to obtain the females of the desired genotype, I created a temperature-sensitive strain that could allow me to lower the expression of *eIF3e* after pupal development. I recombined a *gal80[ts]* construct onto the same chromosome where the *UAS-Idgf3* construct is located (Figure 3.2A). At 18ºC, the Gal80 protein is functional and inhibits Gal4p, stopping the exogenous expression of *Idgf3* and *eIF3e*-RNAi, since their expression relies on the *CY2-GAL4* driver. In this way, I was able to obtain females that overexpressed *Idgf3* while down-regulating *eIF3e,* but unfortunately, none of these females laid eggs at 30ºC.

Since *CY2-GAL4* produces reduced effects at 25ºC compared to 30ºC (Queenan *et al*., 1997), I exploited this lowered activity to test if the *eIF3e-RNAi* line, with and without *Idgf3,* laid any eggs at 25ºC. At first glance it appears as if the down-regulation of *eIF3e* did not change the *Idgf3*-overexpression phenotype at 25ºC (Figure 2B). However, the *Idgf3*-overexpression control in this experiment showed a troublesome number of defects. Since the Gal4 driver is less active at 25ºC than at 30ºC, I was expecting to see a less severe phenotype than what I observed when incubating the *Idgf3*-overexpression flies at 30ºC. Surprisingly, this

experiment showed a higher fraction of DA defects compared to when females were incubated at 30°C, and the DA defects were similar to the ones seen when flies are incubated at 30°C. The results from the *Idgf3*-overexpression control might suggest that a fly of the wrong genotype was erroneously incubated with females of the right genotype. Since it was not possible for me to discern if this mix-up had occurred, from these results I could not conclude whether or not *Idgf3* interacted with *eIF3e*. Because this experiment requires raising the flies at 18°C in order to obtain new females of the right genotype, I chose not to redo the crosses and test whether these results were meaningful. Instead, I focused my efforts on *combover*, as described in chapter II. Simultaneously, I was investigating one other *eIF3e* allele for interaction with *Idgf3,* as well as other *eIF3e*-pathway genes on the assumption that *eIF3e* was the interacting gene responsible for enhancing the *Idgf3* overexpression phenotype. I discuss these results below and in the next section.

The eIF3e protein is highly conserved, in mammals, *Drosophila* and other species (Marchetti *et al*., 1995). In fact, *Drosophila* and mammalian eIF3e protein sequences are 71% similar, and most of this conservation occurs between residues 207 and 395 (Miyazaki *et al.,* 1999). The mammalian *eIF3e* gene was first identified and characterized as one of the integration sites for the mouse mammary tumor virus (MMTV). Thus, *eIF3e* is also known as *Int6*. The integration of this virus results in a truncated form of *eIF3e* that has oncogenic properties (Marchetti *et al*., 1995).

Although transposon insertion alleles had been described for *eIF3e*, at the time, the only other available allele for *eIF3e* (besides the RNAi constructs I had already tested) was a *UAS* construct containing a fragment of *eIF3e* that was tagged with GFP at the C-terminus (Richardson, 2015). This fragment expresses the first 138 out of 435 amino acids of eIF3e, and

the truncation resembles the mutation that, in mammals, is linked to breast cancer (Marchetti *et al*., 1995). Both second chromosomes of this *eIF3e*-overexpression line had dominant markers. Thus, it required several crosses to obtain flies that would overexpress both *Idgf3* and *eIF3e* while having wild-type second chromosomes.

First, I tested the effects of overexpressing *Idgf3* and the *eIF3e* fragment with either marker on the second chromosome. I found that in the Kr[If-1]/+ background, *eIF3e*-fragment overexpression suppressed the *Idgf3*-overexpression phenotype. On the contrary, in the *CyO*/+ background, *eIF3e*-fragment overexpression enhanced the *Idgf3*-overexpression phenotype, and this enhancement effect was less severe than when *eIF3*e was removed using the deficiency that uncovers it (Figure 3.2C). Thus, I was unable to draw any conclusions based on these incongruent results.

Following, I crossed the original strain containing the *eIF3e* fragment to a strain that lacked second chromosome markers to obtain females in the F2 generation that had wild type second-chromosomes. I crossed the F2-generation females to either the *Idgf3*-overexpression stock, or a stock that only contained the *CY2-GAL4* driver as a control for dorsal appendage phenotype at normal levels of *Idgf3*. I found that when *Idgf3* is at normal levels, 9.2% and 8% of eggs laid by female flies that originated from either the CyO or the Kr[If-1] marked second-chromosome, respectively, had defective dorsal appendages. On the other hand, when *Idgf3* is overexpressed in the background, females that originated from the *CyO* marked chromosome laid 15.6% of eggs with defective DAs and females that originated from the Kr[If-1] marked chromosome laid 29.23% of eggs with defective DAs. What these results mean statistically is that only females that originated from the Kr[If-1] marked chromosome showed an enhancing genetic interaction with the *Idgf3* (Figure 3.2D). These were interesting results because when the

marked chromosomes were present, females containing the Kr[If-1] marked-chromosome suppressed and females containing the *CyO* marked chromosome enhanced the *Idgf3* overexpression phenotype (Figure 3.2C). These results suggest that the marked-chromosomes were responsible for the observed interactions in the previous crosses, and that each third chromosome bearing the *eIF3e* construct contain mutations that might be affecting the *Idgf3* pathway.

My plan to follow through cleaning up the background of the strains using back crossings on the strains lacking the second-chromosome markers fell through when the COVID-19 pandemic forced a shutdown of the lab. For this reason, I also was not able to test the effect of reducing *eIF3e* only in the stretch cells of an *Idgf3* overexpression background, using the *c415-GAL4* driver, which might not have the same lethal effects as using the *CY2-GAL4* driver. As the lab resumes activities, cleaning up the background of the *eIF3e* truncated allele, in addition to testing *eIF3e* RNAi with the *c415-GAL4* driver, are experiments that should be given priority in order to test that *eIF3e* is indeed the gene responsible for the enhancing effect produced by the large deficiency at high levels of *Idgf3*.

Finally, ideally, a null allele of the *eIF3e* would have recapitulated the dosage sensitivity effect that the deficiency that uncovered *eIF3e* showed, without eliminating all the other flanking genes uncovered by such deficiency, thus confirming a genetic interaction between *eIF3e* and *Idgf3*.

Because an *eIF3e* null allele is not available and because I was intrigued by the strong enhancement effect identified with the deficiency *Df(3L)ED4674,* which uncovers *eIF3e*, I explored one other gene that interacts with *eIF3e.* My goal was to identify genes that are known to interact with *eIF3e* and test them as possible *Idgf3*-interacting genes.

***eIF3e* regulates *Mical* translation for dendrite pruning.**

eIF3e protein is best known for its role in translational regulation of mRNAs. It takes part as a subunit of the preinitiation complex (PIC) that includes the 40S ribosomal subunit. Specifically, eIF3e binds to the cap region of the mRNA to facilitate PIC scanning of the 5' untranslated region to identify the initiation codon (Marygold *et al*., 2017). Recently, Rode and colleagues found that for dendrite pruning of sensory neurons of class c4 da, the translation of Mical mRNA is dependent on eIF3e as well eIF3c subunits (Rode *et al*., 2018). Once translated, Mical binds the cytoplasmic region of Plexin A. When the Plexin A are bound by their ligands, the Semaphorins, they activate Mical's redox-dependent actin disassembly, driving dendrite pruning (Hung *et al.,* 2010). These observations motivated me to see if *Idgf3* interacted with *Mical* for dorsal appendage formation. Because I was working on validating the interaction between *Idgf3* and *eIF3e,* as described above, in parallel to testing if other genes that interact with *eIF3e* also interact with *Idgf3,* and I was waiting for those results to test other *eIF3* components, I did not test if the *eIF3c* subunit interacts with *Idgf3;* this subunit was the only additional subunit of the eIF3 complex tested and found to interact with *Mical* during neuronal pruning (Rode *et al.,* 2010). Testing if the *eIF3c* subunit interacts with *Idgf3* will serve as additional evidence that Idgf3 activity is influenced by the eIF3 complex and its role in translation, rather than a specific interaction between *Idgf3* and *eIF3e.*

***Mical* constructs combined with the *Idgf3*-overexpression mutant reveal intriguing dorsal-appendage phenotypes**

*Mical* spans a 41-kb region of chromosome 3R and consists of ~25 exons that produce at least 14 RNA isoforms and five protein isoforms (FlyBase). Mical interacts with PlexA at the

Mical C terminus, by a heptad-repeat coiled-coil structure. *Mical* also contains a calponin homology domain, which binds to actin filaments, and a flavoprotein monooxygenase-conserved domain with hydroxylase enzymatic activity that hydrolyses actin (Figure 3.3A). These domains are required in neurons for dendrite pruning (Terman *et al.,* 2002; Hung *et al.,* 2010).

At the time I was looking specifically for null alleles or a deletion specific to *Mical*, but there was none available. While I could have ordered deletions that uncovered *Mical* from the deficiency kit, I first tested overexpression alleles that were generously donated by professor Sebastian Rumpf and that were under the control of the *UAS* system (Rode *et al*., 2018; Hung *et al*., 2010). These strains included two lines containing the full length of Mical transcript, one tagged with GFP and another one without GFP (Hung *et al*., 2010); one line containing only the 5'UTR of Mical tagged with GFP (Rode *et al*., 2018); one line containing the entire protein tagged with GFP but deleting the REDOX domain (Hung *et al*., 2010); one line containing the entire protein tagged with GFP but deleting the Calponin Homolgy (CH) domain (Hung *et al*., 2010); and one line containing the entire protein (not tagged with GFP) but deleting the Coiled-coil (C) domain (Hung *et al*., 2010) (Figure 3.3B).

When scoring dorsal appendage phenotypes, using the same scoring system as for the original modifier screen, I found that overexpressing full-length *Mical* strongly enhanced the fraction of defects seen in the *Idgf3* overexpression phenotype (Figure 3C). Importantly, these defects appeared to be of opposite phenotypes. That is, while *Idgf3* overexpression leads to wide appendages, overexpressing full-length *Mical* leads to DAs that are thin, and the DA bases have chorion material accumulated at the end of each DA (Figure 3.3D yellow arrows). However, the same genotype produced a few eggs with wide dorsal appendages (Figure 3.3D). While it would be interesting to quantify the number of eggs with wide vs. thin defective appendages, for now,

since the thin DA defects are specific to overexpressing these *Mical* constructs, I considered that this effect could be a suppression of the *Idgf3*-overexpression phenotype (Table 4). Nonetheless, I need to test what phenotypes this constructs produce on their own to be able to draw any conclusions.

Interestingly, when investigating how the expression of Mical-deletion constructs affected DA formation, I found that constructs lacking the C domain (the Plexin-binding domain) slightly suppressed the *Idgf3*-overexpression phenotype ($p$=0.01). One caveat though is that I was unable to collect more than 59 eggs, which is too low of an n to be able to draw a conclusion with confidence (Figure 3.3C). Similarly, I was not able to collect at least 100 eggs from females expressing the 5'UTR-GFP construct or the construct lacking the REDOX domain. Both of these constructs slightly enhanced the *Idgf3*-overexpression phenotype. Although intriguing, more work is needed to increase the n of these categories in order to draw any conclusions.

Amazingly, expressing a construct that lacked the Calponin Homology domain, which binds actin, enhanced the fraction of eggs with DA defects associated with *Idgf3* overexpression (Figure 3.3C). However, it would also be interesting to quantify the range of thin and wide dorsal appendage defects to understand if it is the same range as for when overexpressing full-length *Mical* construct.

Based on only these results I cannot draw any conclusions confidently regarding the structure/function analysis. However, the appearance of thin appendages is specific for the overexpression of the *Mical* constructs; the *Idgf3* overexpression completely lacks this type of phenotype. Therefore, I hypothesize that *Mical* could be suppressing the *Idgf3*-overexpression phenotype, but I need to quantify the different phenotypes to draw that conclusion confidently.

Also, I need to test if the expression of these constructs produces a dorsal appendage phenotype when Idgf3 is present at normal levels. I suspect that if expressing these constructs of *Mical* is suppressing the *Idgf3*-overexpression effect, I suspect to see higher levels of skinny dorsal appendages as a phenotype of the constructs on their own, which are reduced in number at higher levels of *Idgf3*.

Since these results did not allow me to verify an interaction between *Idgf3* and the *eIF3e-Mical* pathway, I sought to find evidence through analyzing *Mical* translation.

**Does eIF3e regulate translation of Mical during dorsal appendage formation?**

*eIF3e* codes for a translation factor that is required for Mical translation during neuronal dendrite pruning (Rode *et al*., 2018). Based on this knowledge, I wanted to see if *eIF3e* also regulated the translation of *Mical* during the formation of dorsal appendages. I took advantage of the construct containing the 5'UTR of Mical linked to the coding region for GFP. My goal was to measure if the amount of translation of this transcript changed under different levels of Idgf3. Since loss of *eIF3e* enhances the *Idgf3*-overexpression phenotype, I predict that *Idgf3* negatively regulates *eIF3e*. Thus, if eIF3e does regulate the translation of *Mical* during dorsal appendage formation, overexpressing *Idgf3* should result in lower levels of the GFP in the *Idgf3*-overexpression background compared to the amount of GFP I would see with normal levels of *Idgf3* (Figure 3.4A).

Using confocal microscopy, I attempted to measure the GFP signal in S10B and S11 egg chambers that carry the 5'UTR of *Mical* driving GFP, either at normal levels of *Idgf3* or higher levels of *Idgf3*. Unfortunately, I found that the distribution of GFP was uneven throughout the follicle cell layer, making quantification difficult (Figure 3.4B).

Finally, since *Mical* interacts with *Plexin A*, I tested whether an interaction could occur between *Idgf3* and *Plexin A*.

**_PlexA_ plays a role in dorsal appendage formation and enhances the _Idgf3_-overexpression phenotype.**

PlexA, but not PlexB, is able to physically bind to Mical in a yeast two hybrid system (Terman *et al.,* 2002). Similarly, *PlexA* activates Mical for actin break down and dendrite pruning (Terman *et al.,* 2002). Since I was interested in testing if the *eIF3e-Mical* pathway interacts with *Idgf3,* I used this information to find additional evidence to support or reject my hypothesis that *Idgf3* interacts with this pathway.

Using the same dorsal appendage assay, I tested if *PlexA* RNAi constructs genetically interacted with *Idgf3*. Although there is no evidence that *PlexB* interacts with *Mical, PlexA* and *PlexB* share similar characteristics. PlexA and PlexB both have an effect on cytoskeletal reorganization and bind to ligands known as semaphorins. However, the semaphorins that bind to *PlexB* are of a different class (class 2) than semaphorins that bind to PlexA (class 1), and they sometimes have opposing roles (Wingberg *et al*., 1998; Ayoob *et al*., 2006; Neufeld *et al*., 2011). Because, of these complexities, I was also curious to test PlexB for *Idgf3* interaction.

I found that *PlexA* was down-regulated in an *Idgf3* overexpression background, ~91% of eggs had defective phenotypes (Figure 3.5B). The defective dorsal appendages were wider and shorter than the WT dorsal appendages (Figure 3.5C). When *PlexA* was down-regulated under normal levels of *Idgf3,* ~77% of eggs showed a defective phenotype. These results suggest a role of *PlexA* in dorsal appendage formation that might be independent from *Idgf3* overexpression. However, there is a significant enhancement in the presence of high levels of *Idgf3* ($p=8.929e^{-5}$),

suggesting a genetic interaction between *Idgf3* and *PlexA*. It would be important to test *PlexA* null heterozygotes to see if that background produced a stronger enhancing effect on the *Idgf3*-overexpression phenotype.

On the other hand, I found that down-regulation of *PlexB* had a mild suppressing effect on the *Idgf3*-overexpression phenotype ($p=0.02$) (Figure 3.5A). Since there is no evidence that PlexB interacts with Mical, I did not test the effect that down regulating *PlexB* on its own has on dorsal appendage formation, because I focused on the strong *PlexA* phenotype. However, since PlexB does show a slight modifier effect, it will also be important to test the effects of reducing *PlexB* on its own either by using RNAi against *PlexB* or using a null heterozygous *PlexB* allele under normal levels of *Idgf3*. Such an experiment will help test the possibility that *Idgf3* overexpression is suppressing a DA phenotype caused by reducing PlexB on its own. Nevertheless, these experiments show evidence that PlexA might be playing a role in DA formation and that lowering *PlexA* transcript through RNAi enhances the *Idgf3* overexpression phenotype. Importantly, since I only tested one RNAi line to lower the expression of *PlexA*, I need to verify these results by testing additional RNAi lines, or a deficiency that uncovers *PlexA,* to make sure that the DA defects observed in these experiments are not originating from the side of insertion of the construct but the reduction of *PlexA*.

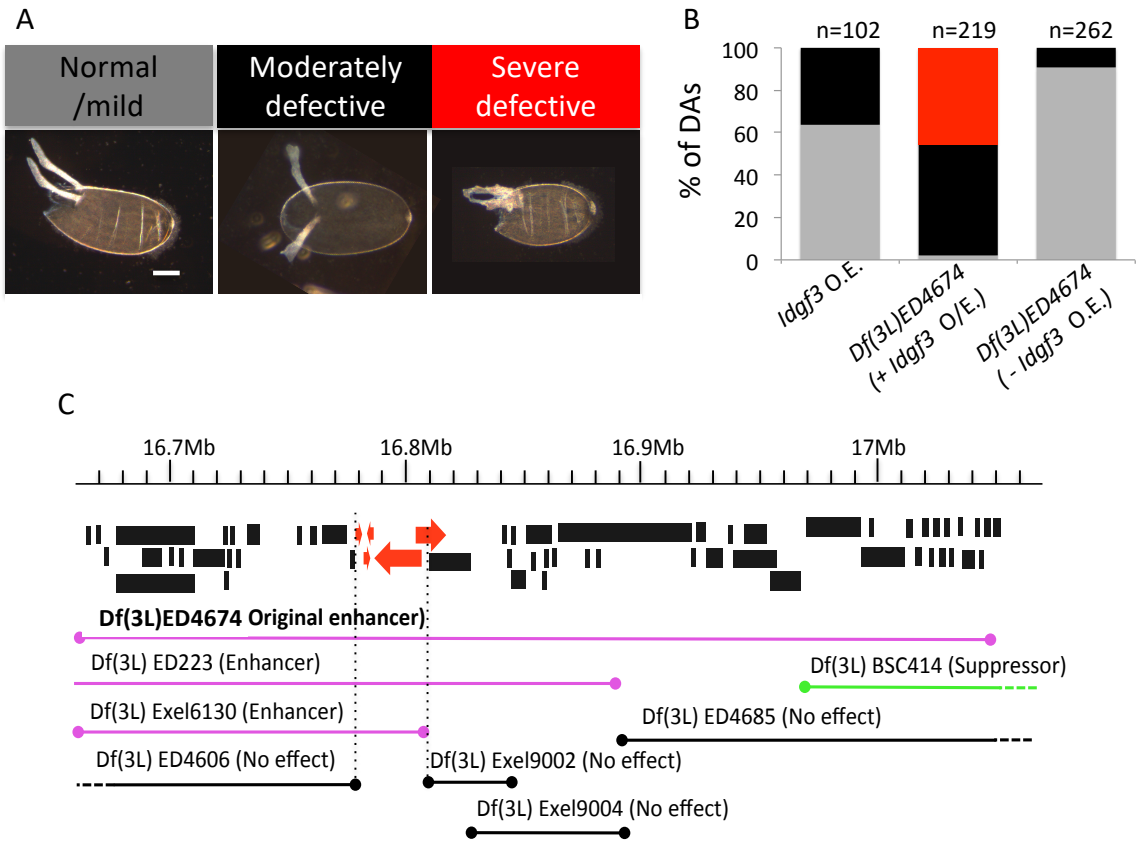
A
Normal /mild
Moderately defective
Severe defective
B
n=102
n=219
n=262
% of DAs
100
80
60
40
20
0
Idgf3 O.E.
Df(3L)ED4674 (+ Idgf3 O/E.)
Df(3L)ED4674 ( - Idgf3 O.E.)
C
16.7Mb
16.8Mb
16.9Mb
17Mb
Df(3L)ED4674 Original enhancer)
Df(3L) ED223 (Enhancer)
Df(3L) BSC414 (Suppressor)
Df(3L) Exel6130 (Enhancer)
Df(3L) ED4685 (No effect)
Df(3L) ED4606 (No effect)
Df(3L) Exel9002 (No effect)
Df(3L) Exel9004 (No effect)

**Figure 3.1**: Quantification of dorsal appendage phenotypes identifies region of chromosome 3L that strongly interacts with *Idgf3.* (A) Representative dorsal appendage phenotypes that were seen when overexpressing *Idgf3* and when combined with the deficiency *Df(3L) ED4674,* grouped and color coded into normal/mild (gray), moderately defective (black) or severely defective (red). Images are oriented with anterior facing left and dorsal facing out of the page (moderate) or facing slightly up (normal and severe). Scale bar is 100 microns and applies to all pictures. (B) Graph: proportion of eggs with normal/mild, moderately defective, and severely defective dorsal appendages produced by females of genotypes $w^{1118}$*; CY2-GAL4/+ ; UAS-Idgf3/+ (*left) or $w^{1118}$ *; CY2-GAL4/+ ; UAS-Idgf3/Df(3L)ED4674* (center) or $w^{1118}$ *; CY2-GAL4/+ ; +/Df(3L)ED4674* (right). The number of eggs quantified per genotype is shown over each box plot. (C) Schematic of the genome browser map showing overlapping deficiencies used to narrowed down the interaction between *Df(3L)ED4674* and *Idgf3* overexpression. Each block indicates the coding and non-coding regions of a gene. Black blocks are genes that failed to interact with *Idgf3*; red or pink blocks indicate potential candidate genes. Magenta lines show the span of the deficiencies that enhanced the *Idgf3*-overexpression phenotype. A green line shows the span of a deficiency that suppressed the *Idgf3*-overexpression phenotype. Black lines show the span of the deficiencies that did not change the percentage of defects observed by overexpressing *Idgf3*. Dotted regions indicate deletions that extend distally or proximally from the region shown here.

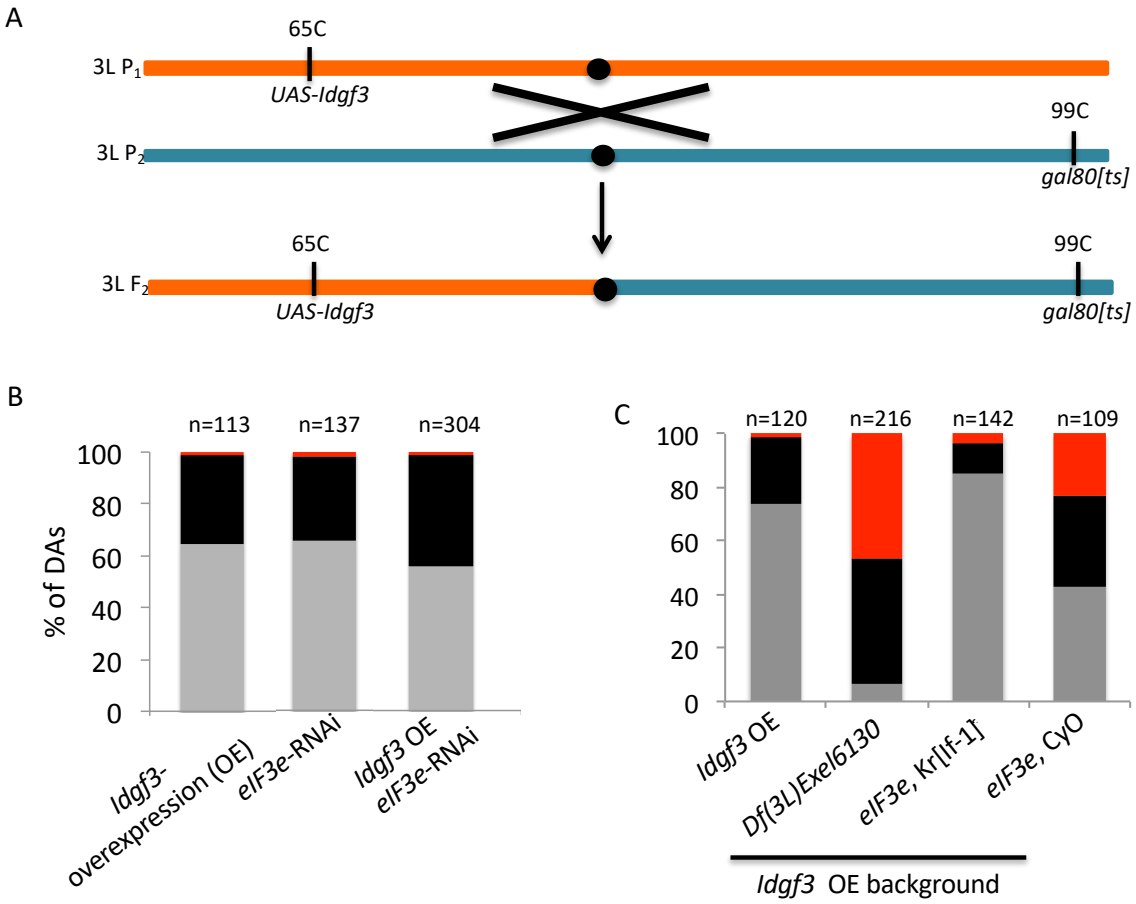
A
65C
3L P1
UAS-Idgf3
99C
3L P2
gal80[ts]
65C
99C
3L F2
UAS-Idgf3
gal80[ts]
B
n=113
n=137
n=304
% of DAs
100
80
60
40
20
0
Idgf3-overexpression (OE)
eIF3e-RNAi
Idgf3 OE eIF3e-RNAi
C
n=120
n=216
n=142
n=109
Idgf3 OE
Df(3L)Exel6130
eIF3e, Kr[If-1]
eIF3e, CyO
Idgf3 OE background

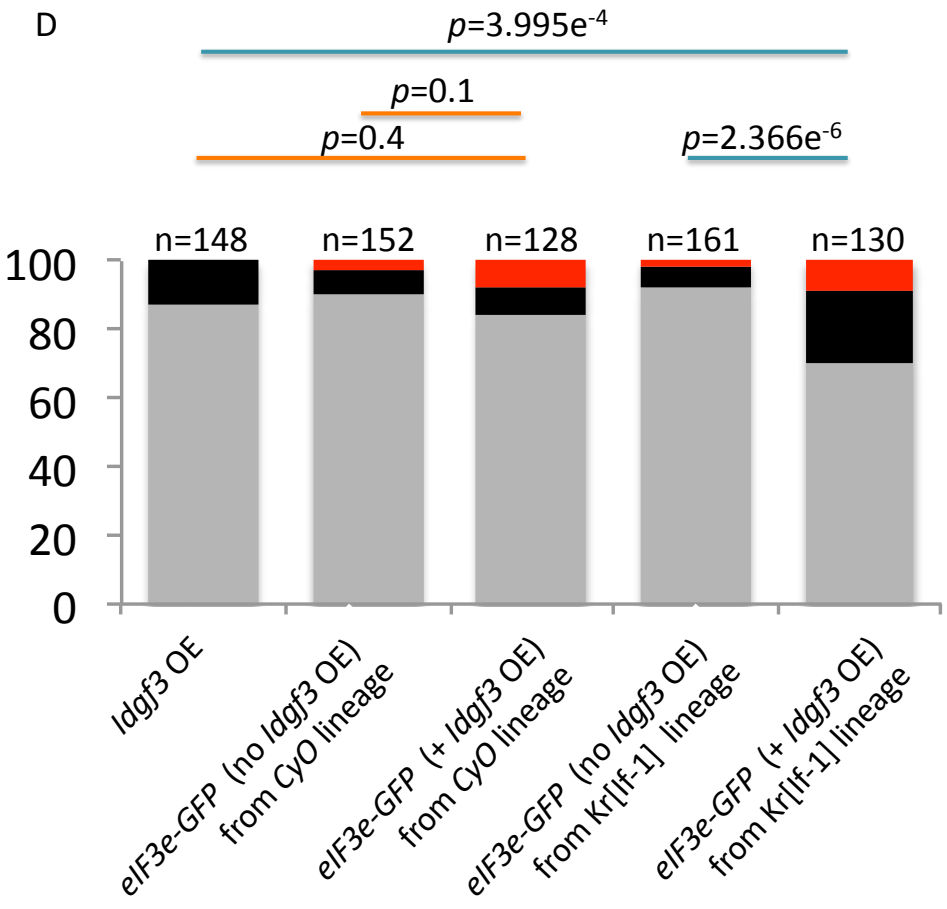
D
p=3.995e-4
p=0.1
p=0.4
p=2.366e-6
n=148
n=152
n=128
n=161
n=130
100
80
60
40
20
0
Idgf3 OE
eIF3e-GFP (no Idgf3 OE) from CyO lineage
eIF3e-GFP (+ Idgf3 OE) from CyO lineage
eIF3e-GFP (no Idgf3 OE) from Kr[If-1] lineage
eIF3e-GFP (+ Idgf3 OE) from Kr[If-1] lineage

**Figure 3.2:** Testing interaction between *Idgf3* and *eIF3e.* (A) Generation of a strain that could overexpress *Idgf3* under the control of a temperature-sensitive *gal80[ts]* allowed testing of an *eIF3e*-RNAi allele. Schematic of the genomic map showing the location of the *UAS-Idgf3* construct (at 65C cytogenetic map units) of one of the parental strains (orange) and of the *gal80[ts]* construct (at 99C cytogenetic map units) of the other parental strain (blue-green). The resultant recombined chromosome in the F2 generation (bottom) was verified by PCR of both constructs (B) Graph: proportion of eggs with normal/mild, moderately defective, and severely defective dorsal appendages produced by females of genotypes: $w^{1118}$ *; CY2-GAL4/+ ; UAS-Idgf3,gal80[ts]/+* (left) or $w^{1118}$ *; CY2-GAL4/+;-gal80[ts]/UAS-eIF3e-RNAi* (middle), $w^{1118}$ *; CY2-GAL4/+ ; gal80[ts]/UAS-eIF3e-RNAi* (right). The last two strains used the temperature-sensitive strain *GAL4/gal80* to down-regulate *eIF3e* in adult ovaries, in either normal or high levels of Idgf3, while Idgf3 overexpression alone (left) served as a control. (C) Graph: proportion of eggs with normal/mild, moderately defective, and severely defective dorsal appendages produced by females of genotypes: $w^{1118}$ *; CY2-GAL4/+ ; UAS-Idgf3/+* (left) *or* $w^{1118}$ *; CY2-GAL4/+; UAS-Idgf3/Df(3L)Exel6130* (second to the left), or *w[*]; Kr[If-1]/+; P{w+mC]=UAS-eIF3e.Frag.GFP}31/UAS-Idgf3* (second to the right), or *w[*]; +/CyO; P{w+mC]=UAS-eIF3e.Frag.GFP}31/UAS-Idgf3* (right). (D) Graph: proportion of eggs with normal/mild, moderately defective, and severely defective dorsal appendages produced by females of genotypes: $w^{1118}$ *; CY2-GAL4/+ ; UAS-Idgf3/+* (left) or *w[*]; +/+; P{w+mC]=UAS-eIF3e.Frag.GFP}31/+* from the *CyO* lineage (second to the left) or *w[*]; +/+; P{w+mC]=UAS-eIF3e.Frag.GFP}31/UAS-Idgf3* from the *CyO* lineage (third to the left) or *w[*]; +/+; P{w+mC]=UAS-eIF3e.Frag.GFP}31/+* from the *Kr[If-1]* lineage (second to the right), or *w[*]; +/+; P{w+mC]=UAS-eIF3e.Frag.GFP}31/UAS-Idgf3* from the *Kr[If-1]* lineage (right). The number of eggs quantified on each genotype is showed over each graph for B, C and D.

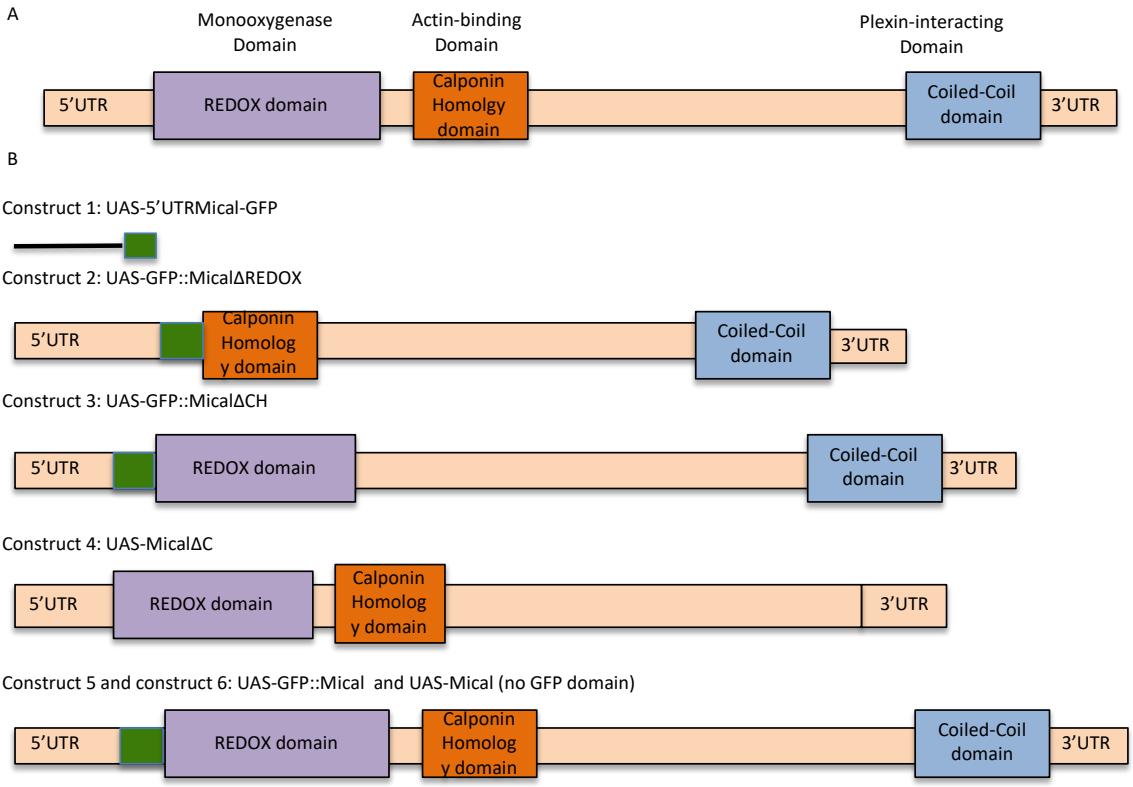
A
Monooxygenase Domain
Actin-binding Domain
Plexin-interacting Domain
5'UTR
REDOX domain
Calponin Homolgy domain
Coiled-Coil domain
3'UTR
B
Construct 1: UAS-5'UTRMical-GFP
Construct 2: UAS-GFP::MicalΔREDOX
5'UTR
Calponin Homolog y domain
Coiled-Coil domain
3'UTR
Construct 3: UAS-GFP::MicalΔCH
5'UTR
REDOX domain
Coiled-Coil domain
3'UTR
Construct 4: UAS-MicalΔC
5'UTR
REDOX domain
Calponin Homolog y domain
3'UTR
Construct 5 and construct 6: UAS-GFP::Mical and UAS-Mical (no GFP domain)
5'UTR
REDOX domain
Calponin Homolog y domain
Coiled-Coil domain
3'UTR

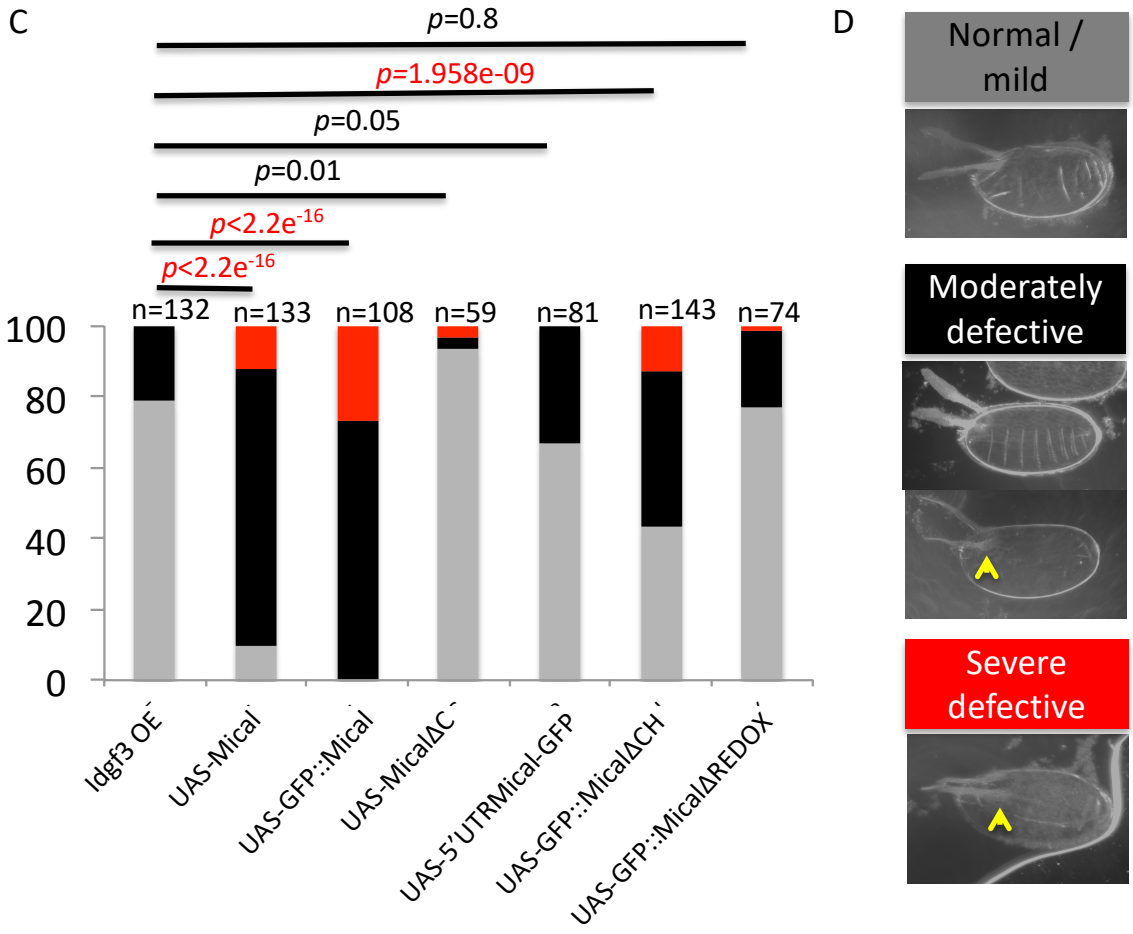
C
p=0.8
p=1.958e-09
p=0.05
p=0.01
p<2.2e-16
p<2.2e-16
n=132
n=133
n=108
n=59
n=81
n=143
n=74
100
80
60
40
20
0
Idgf3 OE
UAS-Mical
UAS-GFP::Mical
UAS-MicalΔC
UAS-5'UTRMical-GFP
UAS-GFP::MicalΔCH
UAS-GFP::MicalΔREDOX
D
Normal / mild
Moderately defective
Severe defective

**Figure 3.3:** *Mical* overexpression constructs expressing different sections of the short *Mical* isoform (*Mical-RA)* were tested for *Idgf3* interaction. (A) Schematic map of three different domains encoded by *Mical*. The listed domains are color-coded and include, a monooxygenase domain (purple), an actin-binding domain (orange), and a Plexin interacting domain (light blue). These domains play a role in breaking down F-actin, which occurs when Mical is activated by PlexA. (B) Schematic of the *Mical* constructs generously donated by Sebastian Rumpf, who created the *UAS-5'UTRMical-GFP;* all the other constructs were created by Hung, *et al.* 2010 and Terman, *et al.* 2002. (C) Four out of the six constructs are tagged with Green fluorescent protein (GFP), which is shown by a green box at the end of each construct. All these constructs were built using a pUASt vector. (C) Fraction of dorsal appendage phenotypes of eggs laid by females expressing each indicated construct while *Idgf3* was overexpressed in the background. Their corresponding n and *p* values are shown above each boxplot. Significant *p* values are color coded in red. (D) Dorsal appendage phenotypes grouped into Normal (gray), Moderately defective (black) and Severely defective (red). Moderate and Severe groups contained phenotypes ranging from wide dorsal appendages to skinny dorsal appendages. Yellow arrows point out a feature unique to the expression of the *Mical* constructs in an *Idgf3* overexpression background: the base of the dorsal appendages appear to have extra chorion material.

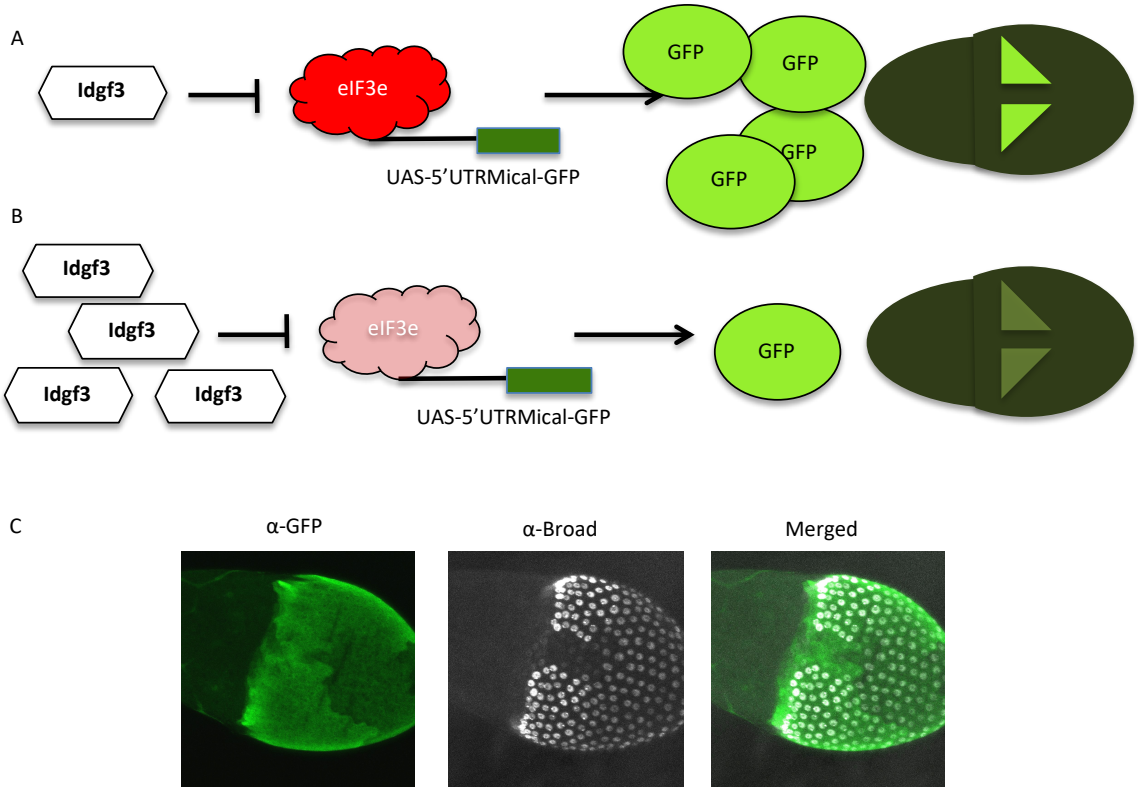
A
Idgf3
eIF3e
UAS-5'UTRMical-GFP
GFP
GFP
GFP
GFP
B
Idgf3
Idgf3
Idgf3
Idgf3
eIF3e
UAS-5'UTRMical-GFP
GFP
C
α-GFP
α-Broad
Merged

**Figure 3.4:** 5'*UTRMical-GFP* construct could allow us to test the hypothesis that Idgf3 inhibits eIF3e function. Based on the modifier screen result that the deficiency that uncovers *eIF3e* enhances the *Idgf3* overexpression phenotype, we hypothesize that *Idgf3* inhibits *eIF3e.* Since eIF3e is required for Mical translation in other contexts, we sought to use the 5'UTRMical-GFP construct to test the hypothesis. (A) At normal levels of *Idgf3,* we should be able to detect a basal amount of GFP signal. (B) Under this hypothesis, overexpressing *Idgf3* should lower the amount of GFP signal. (C) We found an unexpectedly variable distribution of GFP in the columnar follicle cells that did not allow us to measure GFP in the DA patches.

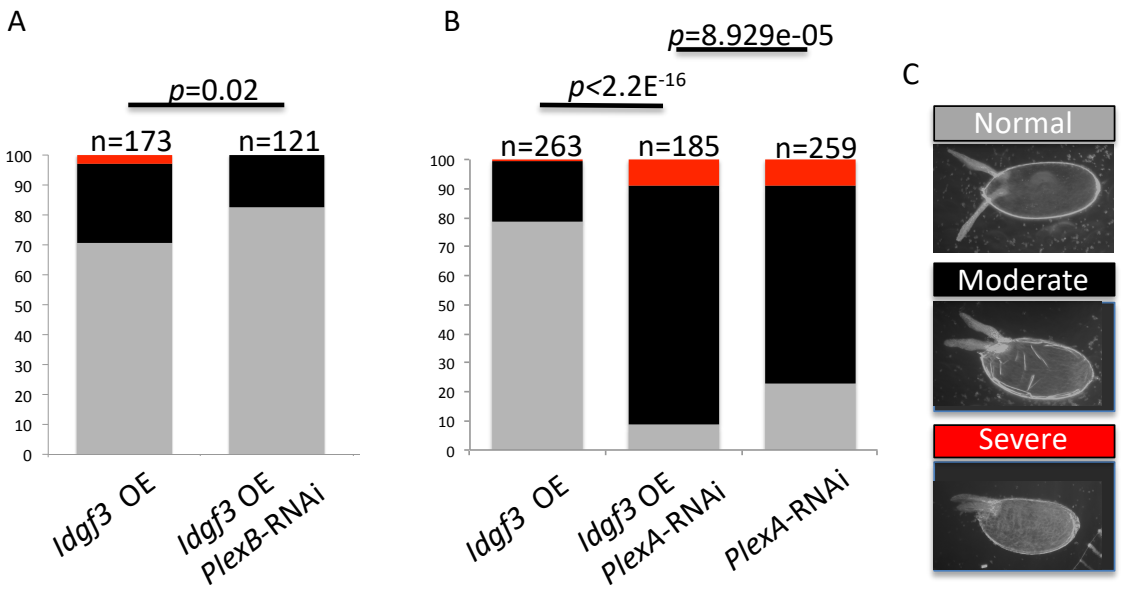
A
p=0.02
n=173
n=121
100
90
80
70
60
50
40
30
20
10
0
Idgf3 OE
Idgf3 OE PlexB-RNAi
B
p=8.929e-05
p<2.2E-16
n=263
n=185
n=259
Idgf3 OE
Idgf3 OE PlexA-RNAi
PlexA-RNAi
C
Normal
Moderate
Severe

**Figure 3.5:** *Plexins* genetically interact with *Idgf3.* (A) Quantification of dorsal appendage phenotypes of the *Idgf3*-overexpression control: $w^{1118}$ *; CY2-GAL4/+ ; UAS-Idgf3/+* and the *PlexB*-RNAi in an *Idgf3*-overexpression background: $w^{1118}$ *; CY2-GAL4/P{PlexB-RNAi} ; UAS-Idgf3/+.* (B) Quantification of dorsal appendage phenotypes of the *Idgf3*-overexpression control: $w^{1118}$ *; CY2-GAL4/+ ; UAS-Idgf3/+,* a *PlexA-RNAi* line in an *Idgf3* overexpression background: $w^{1118}$ *; CY2-GAL4/P{PlexA-RNAi} ; UAS-Idgf3/+* and a *PlexA-RNAi* line in normal levels of *Idgf3:* $w^{1118}$ *; CY2-GAL4/P{PlexA-RNAi} ; +/+.* The number of eggs collected per genotype was >100 for A and B. (C) Dorsal appendage phenotypes were categorized into Normal (gray), Moderately defective (black) and Severely defective (red).

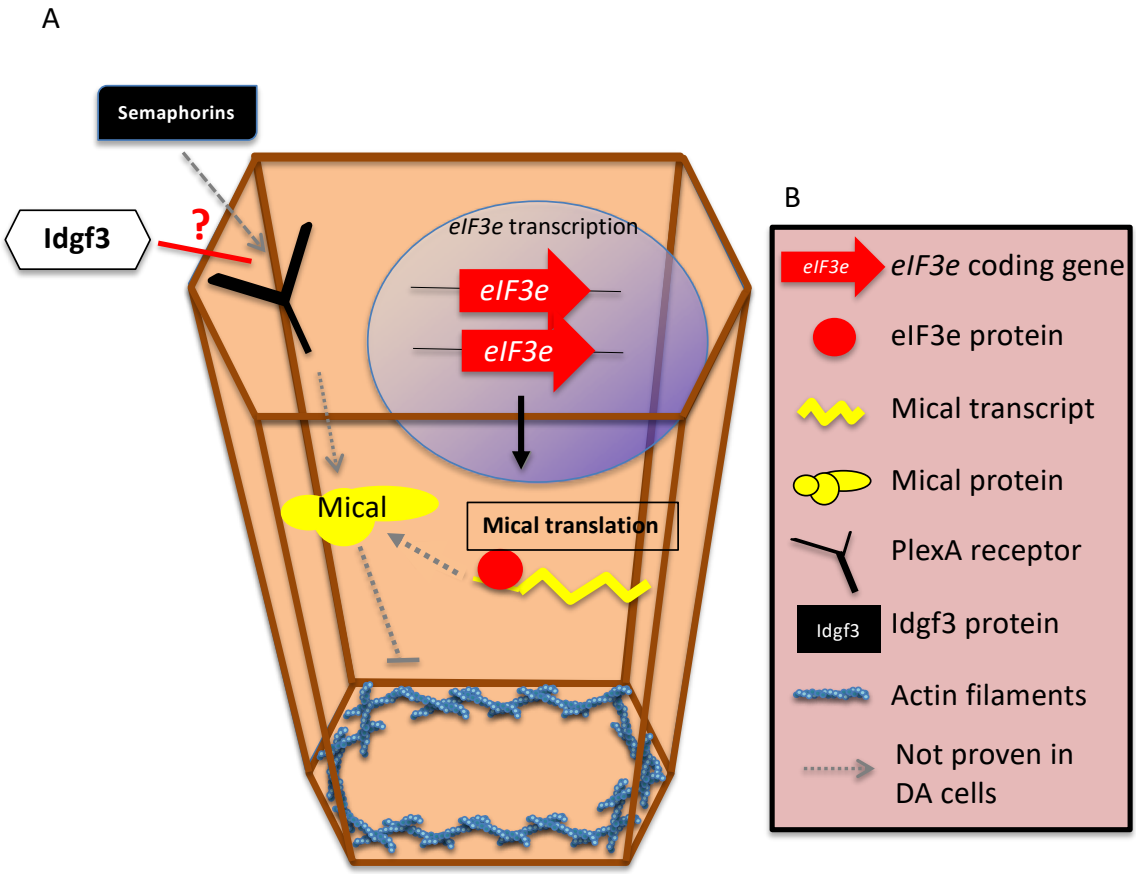
A
Semaphorins
Idgf3
?
eIF3e transcription
eIF3e
eIF3e
Mical
Mical translation
B
eIF3e
eIF3e coding gene
eIF3e protein
Mical transcript
Mical protein
PlexA receptor
Idgf3
Idgf3 protein
Actin filaments
Not proven in DA cells

**Figure 3.6:** A highly speculative model hypothesizing that Idgf3 competes with Semaphorins to interact with and inactivate the PlexA receptor in DA cells. (A) Schematic of the model in which Idgf3 and semaphorins could bind to PlexA. Under this hypothesis, semaphorins and Idgf3 are balanced and can bind to PlexA, either activating Mical (semaphorins), which leads to the break down of actin filaments, or inactivating Mical (Idgf3), which leads to the conservation of actin filaments. This dynamic interaction among molecules allows the regulation of cell-shape changes. The overexpression of *Idgf3* or the loss of specific *Mical* domains will affect the balance of this signaling pathway and result in defective dorsal appendages. (B) Code for schematic in A. Dotted gray lines are highly speculative interactions that have been shown in other cell types but have not been proven in DA cells.

## Chapter IV: Additional implications and future directions

Before this work, our most recent breakthrough was the identification of a novel *Drosophila* gene family, the *Imaginal disc growth factors (Idgfs),* and of their role in dorsal appendage formation. This discovery was exciting to us because the *Idgfs* and their broader gene family, the Chitinase-like proteins (CLPs), are associated with disease, infection, development, and cell growth (cell proliferation and cell size) (Broz, *et al.,* 2017; Kawamura, *et al*., 1999; Coffman 2008). Our finding was also intriguing because the *Idgfs*, although biologically important, are not linked to any genetic pathway; their mechanism of action was unclear.

Since we previously found the Idgfs to be up-regulated in a *bwk* background, and their increased expression affected the formation of the dorsal appendages, I sought to use the dorsal-appendage model to identify and characterize the *Idgfs'* genetic pathway. In this dissertation, I presented my efforts and achievements towards addressing those goals, by exploiting a gain-of-function *Idgf3* allele, which led me to identify and characterize one *Idgf3* genetic partner. Future experiments expanding on these findings can eventually lead us to elucidate the pathway in which the *Idgfs'* participate in for dorsal appendage formation.

### Modifier screen identifies *Idgf3*-interacting gene candidates but is limited by dosage sensitivity and efficacy of constructs.

In the second chapter, I described how I began this project by using a discovery-based modifier screen approach, using a gain-of-function allele of one of the *Idgfs, Idgf3*. Current work in the lab carried out by Anne Sustar and Liesl Strand has found that *Idgfs* might act redundantly during DA formation; knocking out each member of the *Idgfs* family does not produce obvious DA defects, but knocking out all six *Idgfs* reveals strong loss-of-function

phenotype, with the exception of *Idgf6* which causes higher DA defects than knocking out each of the other *Idgf* but less defects than deleting all six of the *Idgfs* (Unpublished). Therefore, my first approach allowed me to identify *Idgf3*-interacting genes in an unbiased fashion, while overcoming the possible redundancy among the *Idgf* family members. Additionally, I used this approach because there had not been any characterized *Idgf*-interacting genes.

Briefly, I scanned chromosome 3L, in part because it was one of the least-explored chromosome arms in the context of genes involved in dorsal appendage formation. As an indicator of a genetic interaction, I searched for regions that, when removed by half, could suppress or enhance the defects seen when *Idgf3* is overexpressed. This approach pinpointed several deficiencies that modified the *Idgf3*-overexpression phenotype significantly. I successfully narrowed down five of those deficiencies into a few candidate genes by using smaller tiling or overlapping deficiencies. Using null and RNAi alleles, I identified *cmb* as an *Idgf3*-interacting gene.

The original modifier screen approach limited me, however, to only identifying gene candidates that biologically act in a dosage dependent manner. That is, removing one of the two copies of a gene was enough to modify the *Idgf3*-overexpression phenotype. Genes that interact with *Idgf3,* but for which one gene copy is sufficient to maintain normal biological processes, might be present along the tested regions but were not uncovered in my screen.

One way to overcome this dosage sensitivity limitation is by using homozygous deficiencies. Unfortunately, the deficiencies, which delete a large number of genes per region, have a high-risk of deleting genes that are homozygous lethal. Thus, the modifier screen approach will only be possible to do in such scenario if overexpressing *Idgf3* suppresses the lethality of the homozygous deletion. Such results, while informative, will not reveal genes that

are not dosage sensitive and enhance the *Idgf3* overexpression phenotype. Analyzing differences of transcriptome profiles at high or normal levels of *Idgf3* could identify some of the *Idgf3*-overexpression enhancers that are not dosage sensitive, only if *Idgf3* levels affect the expression of those genes.

Another limitation of the modifier screen was the use of RNAi lines when null alleles were not available. Ideally, the use of null alleles would have been a more direct comparison to the original modifier screen in terms of dosage sensitivity; the null alleles and the deficiency lines were missing one copy of a gene (or multiple genes in the case of the deficiency) in all the cells of the egg chamber at all stages throughout development. Using RNAi alleles limited me to, first, not having control over how much gene product I eliminated, which could have been more or less than the amount of gene product from the deficiency, depending on the quality of the RNAi construct. Likewise, I did not have control over how fast I silenced the expression of a targeted gene. Although I used a GAL4 driver that is active from S6 and on, more than half the gene product could have still been present at stages that are critical for and affect dorsal appendage formation, depending on how long the proteins perdures in the system.

On the other hand, using RNAi has benefits. One benefit is the availability of RNAi lines for almost all the genes of the *Drosophila* genome, which made it possible for me to test almost all the genes I was interested in. A second benefit of the RNAi lines used in this screen is that they are dependent on the Gal4p activity, which expression is cell specific. Therefore, by using different GAL4 drivers that are specific for different cells of the egg chamber one could reveal a spatial map of the interaction between the *Idgf3* and an uncovered gene. This type of spatial information was not tested as part of my project, but it is vital information to determine since we still do not know what cells (if any) act as substrate for the Idgfs.

**Modifier screen identified *eIF3e* as an interesting *Idgf3*-interacting gene candidate and directed attention towards the *Mical* pathway.**

Chapter III details my efforts on trying to test the interaction between *Idgf3* and *eIF3e.* *eIF3e* was uncovered by the strongest enhancing deficiency and was the only gene candidate I was not able to eliminate using RNAi alleles because of lethality. Also, there are no available *eIF3e* null alleles. Because the deficiency that uncovered *eIF3e* results in high number of eggs with severely defective DAs, and this effect is seen when *Idgf3* is overexpressed and not at normal *Idgf3* levels, it is of high priority to verify that *eIF3e* interacts with *Idgf3*. This experiment will be possible if null mutant *eIF3e* alleles become available in the fly community, or using CRISPR/Cas9, one can create an *eIF3e* mutant allele. An eIF3e null allele is preferred over an RNAi line because it will replicate the effects of the deficiency that uncovered it without eliminating the genes that flank *eIF3e.*

In the future, several experiments are critical to do in order to confirm the interaction between *eIF3e* and *Idgf3* and in order to move forward with characterizing a possible *Idgf3* pathway that is linked to *eIF3e.* Besides testing the newly created *eIF3e* null allele as a modifier of the *Idgf3*-overexpression phenotype, one could seek to rescue the DA defects by additionally introducing a *UAS-eIF3e* construct into the $eIF3e^{KO}$/+, *Idgf3*overexpression line. This experiment would allow us to distinguish between *eIF3e* being the gene responsible for modifying the DA defects of the *Idgf3* overexpression line, or a sequence along the same region acting as an enhancer of the gene that interacts with *Idgf3* but is located in another region. Moreover, investigating if overexpression of *eIF3e* suppresses the *Idgf3*-overexpression phenotype would also help supporting the hypothesis that *eIF3e* and *Idgf3* genetically interact. However, depending on the gene's nature, an interaction could exist without necessarily show

such a trend. For instance, if *eIF3e* exact levels are important for normal dorsal appendage formation, overexpressing *eIF3e* could also show an enhancement of the DA defects.

If these tests provide evidence for a genetic interaction, one could move forward into characterizing the interaction at a cellular level, similarly to what was done with *cmb* (described in chapter II). One aspect that is expected to be different with this *eIF3e-Idgf3* interaction is the cellular process under investigation, as the DA defects seen when combining *Idgf3* overexpression and the deficiency that uncovers *eIF3e* are extremely different from the defects seen when combining $cmb^{KO/+}$ and *Idgf3*-overexpression. As described in the following paragraphs, *eIF3-Idgf3* interaction could be regulating actin (as it is hypothesized for the effect of *cmb-Idgf3* interaction). However, the *eIF3e-Idgf3* interaction leads to a high percentage of small egg chambers with chorion material that does not resemble DA in place of the DAs. Looking at what is known about *eIF3e* could help us identify the process that might lead to such phenotypes.

In chapter III, I described how I sought in the literature for information that allowed me to decide if *eIF3e* was an interesting *Idgf3* candidate to pursue and to identify alternative ways to test this interaction. To summarize what was presented in chapter III, *eIF3e* is a translation elongation factor, part of a the eIF3 complex, and one the eIF3 complex roles is to regulate translation of *Mical* transcript in c4 da neurons in *Drosophila* (Rode *et al*., 2018). Mical protein interacts with Plexin A to break down actin during dendrite pruning (Terman *et al.,* 2002). This information made me wonder if the *Idgfs* were part of the PlexA-Mical signaling pathway. Because my overall goal was to identify the pathway in which *Idgf3* play a role, I sought to pursue the question, do Mical or Plexins genetically interact with *Idgf3*? In chapter III I presented my work testing *UAS-Mical* constructs. Because new DA phenotypes surfaced when

crossing these available Mical constructs with *Idgf3*-overexpression mutants, I was not able to confidently conclude that *Mical* and *Idgf3* are genetically interacting. Below I propose different ideas to pursue the question further.

It would be interesting to test how removing one copy of *Mical* in the *Idgf3*-overexpression background affects dorsal appendage formation. Until null alleles of *Mical* become available, one could test several deficiencies that uncover *Mical* for interaction with *Idgf3*. Using available overlapping deficiencies, one could narrow down the region of interaction to uncover nearly only Mical (Figure 4.1). Assuming that the strong enhancing effect seen with one of the deficiencies I did test comes from removing one copy of *eIF3e,* and since eIF3e positively regulates the translation of *Mical,* one would expect to find that removing one copy of *Mical* enhances the *Idgf3*-overexpression phenotype. However, just as with the *Idgfs,* it could be that the right levels of *Mical* are necessary for the pathway to function, leading to an enhancing effect.

I presented additional work in chapter III that would be helpful to repeat and finish that can serve as additional evidence to understand if there is an interaction between *Idgf3* and *Mical.* I tested if *Idgf3* has an effect on *Mical* translation (through eIF3e), by using the strain that expresses a GFP-tagged construct of the 5'UTR of *Mical* under *UAS* control (Figure 3.3B). Briefly, I tried to measure levels of GFP in the presence of normal or high levels of *Idgf3.* Unfortunately, I found a random distribution of GFP-positive cells among all the main-body follicle cells of S10B egg chambers. Before repeating this work, it would be interesting to investigate if that patterning effect is S10B specific, or if the patterning stays through egg chamber development. Alternatively, those observations could be an artifact that needs to be addressed during the staining procedure. If we could overcome this challenge and measure the

amounts of GFP levels, we could understand if *Idgf3* overexpression indeed affects *Mical* translation, which can serve as strong evidence that *Idgf3* is interacting in this pathway.

Additional evidence for *Idgf3* interacting with the *Mical-PlexA* pathway could come by answering the question, do Idgfs interact with the PlexA receptor? In chapter III I presented results that show a genetic interaction between *PlexA* and *Idgf3.* My results first show that PlexA does play an important role in dorsal appendage formation because lowering its expression in the follicle cells from S6 onward results in a high frequency of eggs with DA defects that resemble the *bwk* phenotype. Fascinatingly, overexpressing *Idgf3* in the background of reduced PlexA enhances the frequency of DA defects.

In the next few paragraphs, I propose three different hypothesized ways that could explain these results, and I include experiments to test those hypotheses.

One hypothesis that can explain how the down-regulation of PlexA enhances the *Idgf3*-overexpression phenotype is if Idgf3 acts as a ligand for PlexA and competes with semaphorins, well known PlexA ligands (Wingberg *et al.,* 1998). In such a scenario, Idgf3 must be negatively regulating PlexA and deactivating its downstream effects (Figure 3.6).

One way to test this hypothesis is by using a GFP reconstitution approach. This method consists of splitting GFP and inserting the two complementary fragments into two genes of interest so that the fragments will be fused separately with the proteins of interest. If the two proteins of interest come into contact with each other, GFP protein reconstitutes and green fluorescent is detectable in the tissue (Feinberg *et al.,* 2008). With this method in mind, I can create mutant flies that have the *Idgf3*-overexpression construct fused with one fragment of GFP, while fusing the second GFP fragment to the endogenous *PlexA* in the extracellular region near

the ligand-binding domain. If Idgf3 binds to PlexA for dorsal appendage formation, I will be able to visualize the green fluorescent marker on the egg chambers.

While GFP reconstitution experiments sound alluring for positive results, negative results will be difficult to understand. Specifically, it will be difficult to discern if a negative result (which is no GFP signal) is the outcome of Idgf3 and PlexA not interacting with each other, or a malfunction of the protocol. Therefore, an alternative direction to test if Idgf3 inactivates PlexA is by carrying out competition experiments between semaphorins and Idgf3. For example, by overexpressing semaphorins at the same time as *Idgf3*, I would expect a suppression of the *Idgf3*-overexpression phenotype. As controls, I would assay DA phenotypes resulting from overexpression of each gene on its own. One important consideration in such experiment is that the location of the semaphorins and the *Idgf3* in the genome must be the same to control for the amount of expression of both genes because given that PlexA plays a role in DA formation, overexpressing semaphorins will probably have an effect on DA formation. Nevertheless, these experiments could reveal genetic competition between a known PlexA ligand and a proposed PlexA ligand.

To test a direct physical interaction, I can design a coaffinity purification assay combined with tandem mass spectrometry (coAP-MS) by tagging either the *Idgf3* or *PlexA* of *Drosophila* cultured cells. The aim using this assay is to pull down the tagged protein and identify proteins from the collected material using mass spectrometry. This experiment will assess if the other untagged protein can be identified. This type of assay has been successfully used to create protein-protein interaction maps previously (Guruharsha *et al*., 2011), with the only caveat that the interaction is taken out of a biological context. Therefore, if a specific cell function is needed for the two proteins to interact, the interaction will not be revealed using this method.

Hypothesis two explains that Idgf3 could negatively regulate semaphorins at the transcriptional or translational level. If this hypothesis is true, Idgf3 can inactivate the PlexA-Mical-actin pathway by downregulating semaphorin expression (Figure 4.2A). One could test this hypothesis by isolating follicle cells from wild-type or Idgf3-overexpression egg chambers and use quantitative Polymerase Chain Reaction (qPCR) to compare the amount of semaphorin transcript in the different egg chambers. The results can be validated using FISH analysis on egg chambers of both genotypes and intent to quantify or, if quantification is not possible, find evidence of semaphorins down regulation by comparing the levels of semaphorins in both samples. Additionally, I can use antibody staining against semaphorins on egg chambers of the two different genotypes and, using confocal microscopy, measure and compare the amount of the protein in the egg chambers.

Finally a third hypothesis that can explain the interaction of Idgf3 and PlexA is that Idgf3 acts in a parallel pathway regulating *eIF3e* expression or translation or activity, and that the PlexA-Idgf3 interaction identified through the DA model is reflecting the eIF3e role in regulating Mical translation (Figure 4.2B). One way to test this third hypothesis would be by inserting the green fluorescent protein downstream of the *eIF3e* transcript, so when *eIF3e* is transcribed, the product is tagged with GFP at the C terminus. We can then measure the amount of GFP at normal or high levels of Idgf3. To test if Idgf3 is affecting eIF3e function, I could use this same GFP-tagged eIF3e construct (full length construct) and an antibody against Mical (there is a polyclonal antibody reported in FlyBase or alternatively, there are antibodies against the human Mical that I can test in preliminary experiments to see if they cross react with the *Drosophila* Mical) and quantify and analyze if the levels of Mical are correlated with levels of eIF3e.

**Additional investigation of the modifier screen could increase our understanding of the *Idgfs.***

Additionally, one could move forward using the results from this modifier screen is to use a reverse screen approach to identify more *Idgf3*-interacting genes. One could make use of the findings that *cmb-Idgf3* interaction affect the apical side of the DA cells and select candidate genes from throughout the genome whose function is associated with defining or regulating apical area, such as polarity proteins such as Bazooka (Par3), cytoskeletal proteins or cytoskeleton-regulating proteins, or genes that interact with the *Rho-kinase* pathway.

In principle, this same reverse approach could be used to evaluate the remaining candidates from my original screen. Unfortunately, it will be difficult to predict which of the 58 candidate genes that were uncovered in the modifier screen could interact in the pathway, for many of these genes' functions have not been characterized under any circumstance. Therefore, one way to identify new *Idgf3*-interacting genes is by narrowing down additional deficiencies that significantly enhanced or suppressed the *Idgf3*-overexpression phenotype. After narrowing them down to a few candidate genes, one can test if the newly identified candidate genes interact with *Idgf3*.

A third way to proceed with the results of the modifier screen is by investigating if any of the 58 candidate genes uncovered in the modifier screen has an effect on dorsal appendage formation independently of *Idgf3*-overexpression. By looking at the dorsal appendages of eggs that have low expression of each of the 58 candidate genes using RNAi lines, one could pursue this question and identify genes involved in DA morphogenesis in a short period of time. The advantage of this approach is that the results will identify genes that play a role in DA formation

in just one generation, in the F1 generation. Additionally, since most of the 58 candidate genes have not been characterized previously, DA formation can be their first annotated feature. The drawback of this approach is that genes that interact with *Idgf3* for dorsal appendage, but that depend on *Idgf3*-overexpression to show a DA phenotype, e.g. *cmb,* would not be identified in this screen.

A fourth way to proceed with the modifier screen results is by scanning the other chromosome arms using a strategy similar to what I did with the 3L chromosome. Such a genome-wide approach will identify a large number of *Idgf3*-interacting gene candidates and get us closer to elucidate the pathway as near to completion as this approach can achieve.

Finally, testing the other *Idgfs,* in a similar fashion as how I tested *Idgf3* could provide crucial information that will support or reject the idea that *Idgfs* act redundantly (See Chapter I, page 13).

**How are *cmb-Idgf3* affecting the apical area of the dorsal-appendage-making cells? - Proposed experiments.**

Chapter II goes further into detailing how I validated the genetic interaction between *Idgf3* and the candidate gene *cmb,* a Rho-kinase substrate involved in *Drosophila* wing-hair formation. Successfully, I characterized this interaction as playing a role in defining the apical area of the cells that make the dorsal appendages during the phase of tube elongation (S12). I ended the chapter by hypothesizing two different mechanisms of action and proposing future work that could allow us to identify the actual role of both *Idgf3* and *cmb* during this phase. Both hypotheses assume *Rho*-kinase is also involved in the *Idgf3-cmb* pathway.

Hypothesis one proposes that the *Idgf3-cmb* interaction affects the actomyosin tension network of the apical side of the DA-making cells. I would test this hypothesis by quantifying the levels of actin present in the DA-making cells during tube formation using rhodamine-phalloidin staining against actin or an antibody against an actin reporter (Kiehart *et al.,* 2000). For this approach, I would compare wild type, *Idgf3-overexpression*, and $cmb^{+/KO}$/*Idgf3-overexpression* egg chambers and use antibody staining against Broad to identify the DA-making cells. Confocal images of S10B, S11, and S12 egg chambers of each genotype will capture the levels of actin present in the DA making cells during DA morphogenesis. One important aspect to consider is that S12 egg chambers must be imaged right after the transition of S11 to S12, before the DAs had elongated over the stretch cells; the ring canals of the nurse cells express elevated levels of actin (Warn *et al.,* 1985), which in late S12 could obscure actin signal from the overlaying DAs and make it difficult to quantify actual levels of actin of the DA-making cells.

If *Idgf3-cmb* interaction affected the actomyosin network, one would expect to see similar levels of actin among egg chambers at stage S10B, but significantly different levels of actin as DA-tube morphogenesis progresses. The major differences among genotypes should be seen at the beginning of S12, when DA cells arrest apical constriction and begin to expand. If no differences in actin levels are seen at the beginning of S12, it could mean that *Idgf3-cmb* interaction does not affect actin-myosin network. Alternatively, a negative result could suggest that *Idgf3* and *cmb* affect actin-myosin later in S12.

The second hypothesis suggests that *Idgf3* has an effect on the stiffness of the ECM that surrounds the elongating DAs, exerting pressure on the tissue and thus affecting tube growth. To test this hypothesis one could manipulate the stiffness of the ECM by using *CY2-GAL4* to drive expression of RNAi lines for genes that encode ECM components, like laminin (Gutzeit, 1991),

and quantify DA defects. By using a combination of RNAi lines with *Idgf3* overexpression and *cmb* mutant alleles, we could identify an association between EMC stiffness and the *Idgf3-cmb* pathway.

To find additional evidence for the two hypotheses, one could characterize the protein localization pattern of Idgf3 and of Cmb in the different cell types of the egg chamber. These experiments can be achieved by developing GFP-tagged *Idgf3* and *cmb* alleles to be imaged using confocal microscopy on fixed tissues or by live imaging. This experiment could tell us if Idgf3 accumulates in the ECM while Cmb is localized and acting in the dorsal-appendage-making cells.

**What is the earliest stage of egg chamber development that is affected by the *cmb-Idgf3* interaction?**

While I demonstrated that the *cmb-Idgf3* interaction produces visible effects on S12 egg chambers, I cannot discard the possibility that this interaction could have effects on previous stages, especially because the apical area of the roof cells is a dynamic rather than a static feature throughout oogenesis. In fact, during S11, roof cells constrict their apices, changing the cells from columnar to wedge shaped (Dorman *et al.*, 2004). During the S11-to-S12 transition, the apical side of cells changes in an orderly fashion - the most anterior roof cells release constriction before the posterior roof cells (Peters and Berg, 2016B); note that roof cell apical expansion helps elongate the tube anteriorly.

Since the *cmb-Idgf3* interaction affects apical cell area, is it possible that *cmb-Idgf3* affect apical constriction in S11? Although I assessed the progression of cell shapes from S10B to S12, and I specifically focused on the shapes of the patches that make the DAs and quantified their

aspect ratios looking for differences among mutants, I did so by dissecting ovaries and handpicking individual S10B and S12 egg chambers before applying antibodies. While I did not notice any obvious differences among genotypes at S10B, it is possible that changes did occur as early as S11.

It would be interesting to analyze differences of apical constriction among the wild type, *Idgf3*-overexpression, and $cmb^{+/KO}$ – *Idgf3 overexpression* genotypes. One way to analyze these differences is by using an actin reporter and confocal life imaging. One could live image the process of apical constriction and quantify the smallest apical area reached by the constricting cells when moving from S10B to S12. This experiment would be difficult to do in fixed tissue, for it is not possible to guarantee capturing the exact S11 stages in all the egg chambers.

**Additional tested deficiencies**

In the course of this work, I tested additional genes, but more work is needed to draw any conclusions. Some of those tested alleles included the *lkb1* and *pten* genes, which were identified as *eIF3e*-interacting genes in a genome-wide proteomics screen that aimed to resolve the insulin pathway (Vinayagam *et al.,* 2016). I tested these genes because when *Idgfs* were first discovered, it appeared that their cellular function was part of the insulin pathway (Kawamura *et al.,* 1999). I found that an RNAi line and a loss-of-function allele of *pten* did not modify the *Idgf3*-overexpression phenotype. On the other hand, two out of three alleles of *lkb1* enhanced the *Idgf3*-overexpression phenotype (Table 4). This discordant result might be due to the levels of *lkb1* and the nature of the strain; the two loss-of-function alleles, which I obtained from different sources, enhanced the *Idgf3*-overexpression phenotype, but the RNAi allele did not have any effect. These data are the results of only one replicate, and I did not test if the alleles

had a phenotype when *Idgf3* is at normal levels. In the future, validating a possible *lkb1-Idgf3* interaction could inform us if *Idgf3* affects the pathway related to Lkb1, a serine/threonine kinase (Hemminiki *et al.,* 1998).

Additionally, I tested *mxt,* a novel gene that can bind to other components of the eIF3 complex (Hernandez, 2013), in order to see if the *eIF3e-Idgf3* interaction acted through this pathway. I found that lowering the expression of *mxt* using an RNAi allele mildly enhanced the *Idgf3*-overexpression phenotype. However, testing if the strain had a dorsal appendage phenotype at normal levels of *Idgf3* is important to investigate before drawing any conclusions. Additionally, this result needs to be validated in triplicates.

After validation experiments and after making sure the *mxt* phenotype enhances the *Idgf3*-overexpression phenotype, one could ask if *mxt* is also part of the *cmb-Idgf3* pathway; *mxt* might be part of a complex (maybe with *eIF3e)* that facilitates the translation of *cmb* or *cmb* interacting genes. The simplest approach would be to test for a genetic interaction between *cmb* and *mxt.* This experiment, however, would only be possible to do if lowering the expression of *mxt* shows a dorsal appendage phenotype that could allow the identification of modifiers.

Finally, based on experimental lab data, we had a list of genes that we knew played a role in dorsal appendage formation (Table 4), and I was curious to see if they interacted with *Idgf3*. These genes included Tramtrack69, for which I tested a null allele and a partial-loss-of-function allele that only disrupts late oogenesis, and both block aspects of DA tube formation (French *et al.*, 2003; Peters *et al.,* 2013); Gβ13F and Gγ, which are required in a specific group of DA cells for tube remodeling (Boyle *et al*., 2010); and the non-receptor tyrosine kinase Btk29A, which plays an essential role in actin cytoskeletal organization during dorsal closure and salivary invagination in fly embryos (Chandrasekaran and Beckendorf, 2005) and interacts with Src42A

(Tateno *et al.,* 2000), which we found regulates DA formation downstream of the *bwk* signal (Tran and Berg, 2003). We also wanted to test members of other signaling pathways, such as *Rac1* and *Rac2*, as well as *unpaire*d *1*, *unpaired 2*, and *unpaired 3*, which are *Drosophila* cytokines that activate the JAK-STAT pathway involved in tissue repair, similar to the CLPs (Wright *et al.,* 2011; Low *et al.,* 2015). Additionally, from a large mutant screen that aimed to identify genes involved in dorsal appendage formation, I was interested in testing alleles of *fs(3)02534*, *l(2)01326a l(2)01326b*, and *l(3)AtPα* for *Idgf3* interaction.

From all these alleles (Table 4), I was surprised that *Btk29A* only mildly enhanced the *Idgf3*-overexpression phenotype. I was hoping to see a strong interaction between *Btk29A* and *Idgf3,* since as described above, *Btk29A* is characterized by playing a role in tissue invagination during *Drosophila* embryonic development, and tissue invagination is led by apical constriction of the cells making the tube, like the apical constriction that drives the roof cells to make DA tubes in the egg chamber model (Dorman *et al*., 2004). In contrast, I found that the null allele of *Tramtrack69* and the *fs(3)02534* allele strongly enhanced the *Idgf3*-overexpression phenotype. We do not have much biological information about *fs(3)02534*, so a deeper investigation to characterize this gene's function during dorsal appendage formation could be a direction of a whole new and interesting project. On the other hand, it was fascinating to find a strong interaction between the null allele of *Tramtrack69* because of its function during DA tube morphogenesis. Moreover, it was exciting to find that *Gγ* suppressed the *Idgf3*-overexpression phenotype because this allele is capable of suppressing the *Tramtrack69* phenotype, serving as extra evidence that *Tramtrack69* and *Idgf3* could be acting together to play a role in DA formation. The partial-loss-of-function allele of *Tramtrack69* showed no interaction with *Idgf3,* which could suggest that enough of the Tramtrack69 protein is available in this mutant to not

cause any further defects than the ones seeing when *Idgf3* is overexpressed. Alternatively, because the null allele of *Tramtrack69* affects patterning in early stages and it is the allele that is showing an interaction with *Idgf3,* it could suggest that *Idgf3* is having an affecting DA formation from early on in the process through an interaction with TTK69.

Finally, G proteins activate the Rho-kinase signaling for wound repair in flies (Verboon and Parkurst, 2015), suggesting these genes might also play a role in the here-reported *cmb-Idgf3* pathway. Nonetheless, these crosses need to be validated by doing at least three replicas and measuring the DA phenotypes that each allele has under normal levels of *Idgf3*.

**Final remarks**

This dissertation describes three years of work that led me to identify and characterize *cmb* as a gene that interacts with *Idgf3* to regulate dorsal appendage formation. This work also proposes new venues of research by identifying 58 candidate genes that could be investigated further to assess their role in dorsal appendage formation and to assess their interaction with the *Idgf3* pathway. Additionally, through this project, I hypothesized two pathways that might interact with *Idgf3*'s in dorsal-appendage formation. One pathway surfaced by identifying *cmb,* a Rho-kinase substrate, and verifying and characterizing the cellular effects of *cmb-Idgf3* interaction. The other pathway is the *PlexA-Mical* pathway, which surfaced by identifying *eIF3e* as a possible *Idgf3* interacting gene. However, this interaction remains to be verified. If this interaction is real, in the future, these two hypotheses would be fascinating to explore.

The results of this project also allowed me to propose additional experiments in flies to expand our understanding of *Idgfs* and work towards identifying its pathway in dorsal appendage formation. Exploring whether the genes uncovered in this screen also interact with the other

*Idgfs* would be of great interest but beyond the scope of all the experiments and proposed experiments presented in this dissertation. One experiment that can briefly allow us to see if what is truth for *Idgf3* could also apply for the other *Idgfs,* is an experiment using the only additional *Idgf* overexpression allele, which is *Idgf1,* and testing if it also interacts with *cmb, eIF3e, Mical,* and *PlexA*. Congruent results between *Idgf1*- and *Idgf3*-overepxression allele could serve as additional evidence that the members of this family are acting in a redundant manner. If the results between the two *Idgf* overexpression constructs are incongruent, it could point to possible gene or pathway specificity. Identifying some kind of specificity among the members of this family could facilitate research into characterizing the normal function of the Idgfs at a cellular level during dorsal appendage formation. Such function is difficult to assess by only using the gain of function allele of one member.

Finally, my studies lay the foundation for experiments on the human homologs, the CLPs, to test if they also affect cell shape changes in normal and diseased tissue.

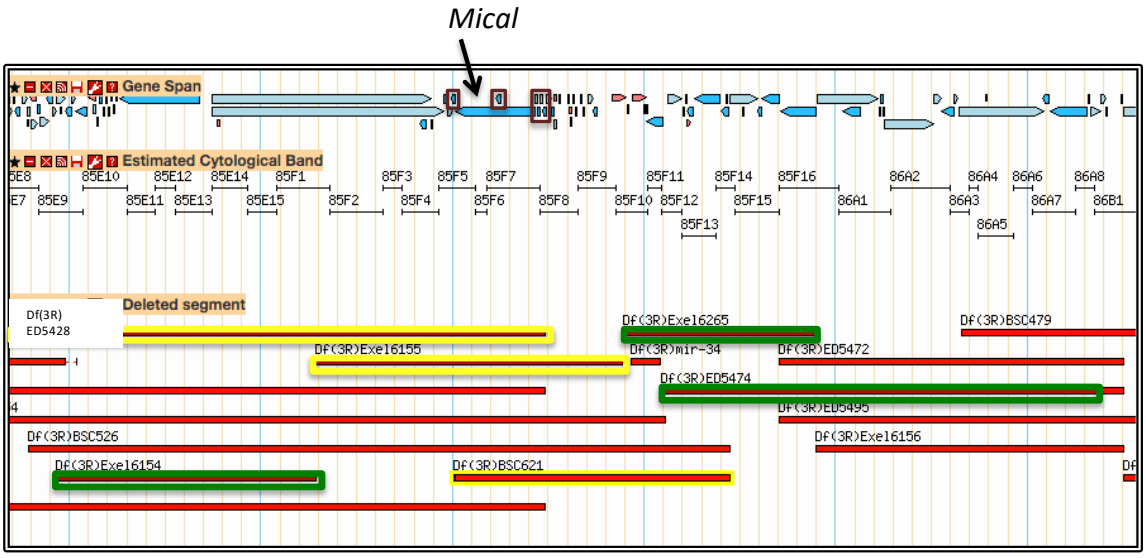
Mical
Gene Span
Estimated Cytological Band
Deleted segment
Df(3R)
ED5428
Df(3R)Exel6265
Df(3R)BSC479
Df(3R)Exel6155
Df(3R)mir-34
Df(3R)ED5472
Df(3R)ED5474
Df(3R)ED5495
Df(3R)BSC526
Df(3R)Exel6156
Df(3R)Exel6154
Df(3R)BSC621

**Figure 4.1** Deficiency lines that uncover *Mical* can be used to assess the effects of *Mical* heterozygous deletion on the *Idgf3* overexpression phenotype. Screen shot of the FlyBase genome browser showing the deficiencies that uncover the genes that flank *Mical.* The schematic shows the genes (blue, light blue and pink boxes), cytological band coordinates and the deleted regions (red rectangles), which are highlighted to indicate expected interaction (yellow) or not interaction (green) if *Mical* interacts with *Idgf3.* Genes inside the dark red boxes will have to be tested by RNAi to discard their role in the the interaction with *Idgf3.*

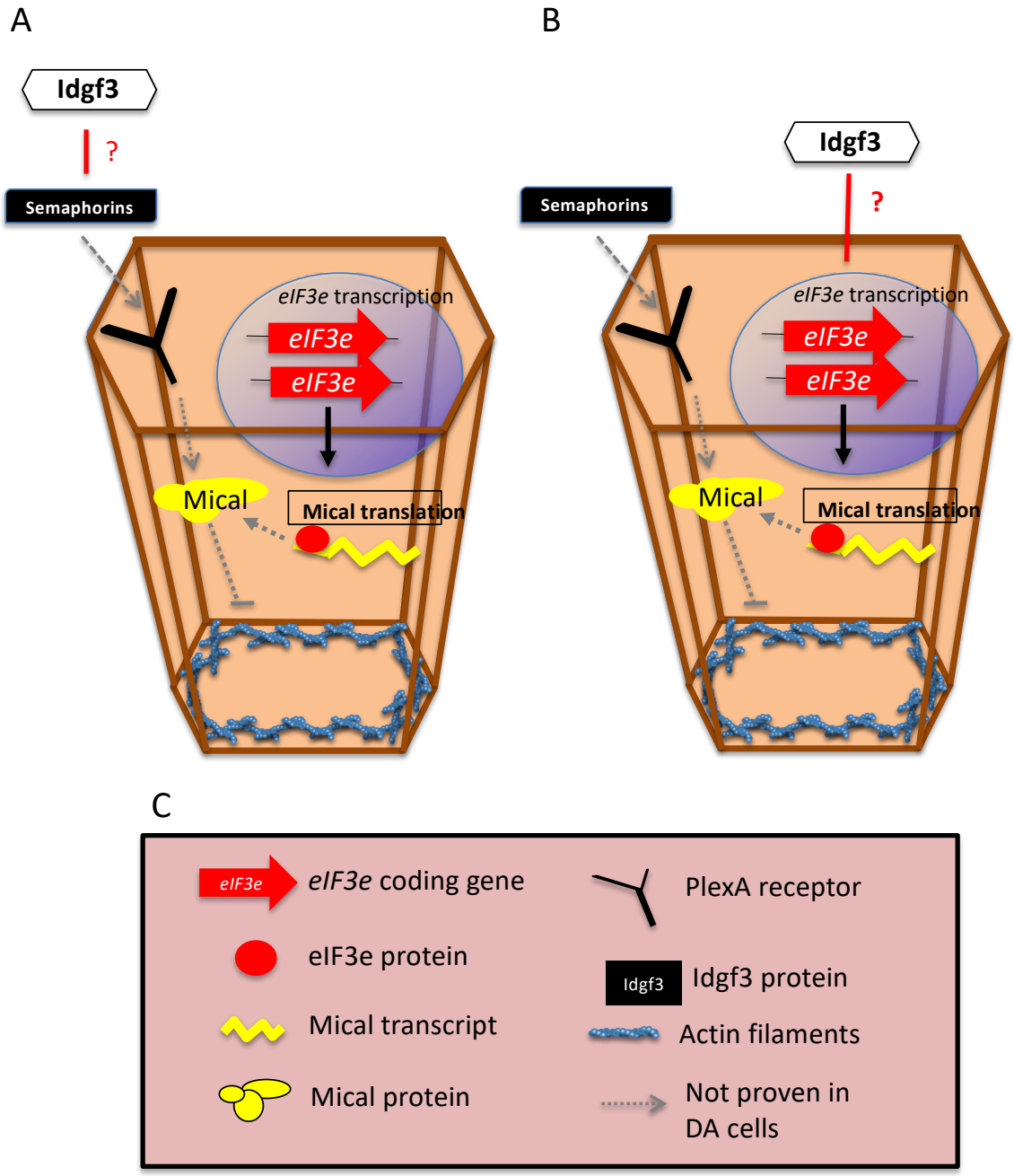
A
Idgf3
?
Semaphorins
eIF3e transcription
eIF3e
eIF3e
Mical
Mical translation
B
Idgf3
?
Semaphorins
eIF3e transcription
eIF3e
eIF3e
Mical
Mical translation
C
eIF3e
eIF3e coding gene
eIF3e protein
Mical transcript
Mical protein
PlexA receptor
Idgf3
Idgf3 protein
Actin filaments
Not proven in DA cells

**Figure 4.2** Two additional hypothesized mechanisms by which *Idgf3* might interact with *Mical* (Highly speculative in DA cells). (A) Direct interaction: Idgf3 inhibits transcription or translation of semaphorins, thus inactivating PlexA and Mical's function. (B) Parallel pathway: Idgf3 regulates *eIF3e* transcription or translation. In this way, because eIF3e regulates *Mical* translation, Idgf3 could be acting upstream this pathway regulating levels of Mical in the cell. Gray arrows show interactions that have been proven in other cell types but have not been proved in DA cells and also applies for A. (C) Code for the schematics.

## Chapter V: MATERIALS AND METHODS

### Fly Stocks used

$w^{1118}$ and the other stocks used in this work are available upon request. $w^{1118}$; *CY2-GAL* (Queenan *et al.,* 1997) was provided by Trudi Schüpbach and was used in lieu of a wild type strain. $w^{1118}$*; UAS-Idgf3/TM3,Sb* was obtained from the Bloomington Stock Center (BL# 52658). Using these strains we created the stock $w^{1118}$*; CY2-GAL4; UAS-Idgf3/TM3, Sb*. All deficiency lines were provided by the Bloomington Stock Center (Table 1). *UAS-RNAi* lines were obtained from the Bloomington or Vienna Stock Centers (Table 2, Ni *et al.,* 2011; Dietzl *et al.,* 2007). The *combover* loss-of-function (LOF) strain, $w^{1118}$*; +/+ ;* $cmb^{KO}$*/TM6B, Hu*, and an overexpression allele $w^{1118}$ *P{UAS-cmb-RB}* (Table 2) were generously donated by Andreas Jenny's laboratory (Fagan *et al.,* 2014). The $cmb^{KO}$ LOF allele is null for both of the Cmb protein isoforms due to the deletion of an ~ 1 kb fragment early in the coding region and its replacement with a $white^{+}$ marker. The overexpression allele used in this paper produces only the smaller of the two Cmb isoforms, Cmb-PB.

### Modifier-screen crosses

Six-to-ten virgin females from the *Idgf3*-overexpression stock were crossed to four males of each stock from the deficiency kit, or to males from overlapping deletion lines, or to RNAi or mutant-allele strains. For the modifier screen, crosses were done at 25 ºC, while for narrowing down regions, crosses were performed at 22 ºC. From each cross, at least nine but usually 25 F1 females were used for the egg collection assay (Figure 5).

**Creation of the temperature-sensitive Idgf3 overexpression**

I crossed the *w*$^{1118}$*; CY2-GAL4/+/-CyO; UAS-Idgf3/TM3, Sb* to *w*$^{1118}$ *; CY2-GAL4/CyO; gal80[ts]/gal80* to obtain *w1118; CY2-GAL4; UAS-Idgf3 gal80[ts]/TM3, Sb* in the F2 generation. The F1 generation and F2 generation were tested with the following primers for the presence of GAL80: F: 5'CTG GAA ATG GCG GTT GGT AC 3' and R: 5'TTG CCA CCT TTG AAA CTG CA 3'; and to detect the *Idgf3* construct: F: 5'GCG CGC TTA TTT TCA CGA AG 3' and R: 5'CGC ACA CAA CCT TTC CTC TC 3'. Crosses were done at 22$^{o}$C.

**Dorsal-appendage analyses:**

One-day-old to four-day-old females of the desired genotypes were transferred to 30$^{o}$C in nutrient rich vials with males. 30$^{o}$C was chosen as the optimal temperature for the Gal4p driver because Gal4p is a yeast transcription factor and past work in the lab has shown that the Gal4p driver's optimal temperature is 30$^{o}$C (Peter *et al.,* 2013). Flies were transferred every day to fresh nutrient-rich vials for three days. On day four, flies were transferred to collection tubes that contained apple juice agar plates with fresh yeast where flies laid eggs. On day five, laid eggs were collected, alternately rinsed with water and embryo wash (0.7% NaCl, 0.05% Triton X-100), mounted on slides in 70 uL of Hoyer's medium (van der Meer 1977), and incubated overnight at 65$^{o}$C. Dorsal appendages were scored by using dark-field optics on a Nikon Labophot microscope at 10X magnification; n>100 unless specified in Table 1.

We grouped dorsal appendage phenotypes into three categories (Figure 2A). Eggs with DAs closely resembling wild type were classified as Normal/Mild: the dorsal appendages were positioned just lateral to the dorsal midline, extended anteriorly ~ 30% of egg length, and exhibited an oar-like shape with paddles that occupied about half the length of the entire dorsal

appendage. These DAs had smooth edges. We classified eggs as Moderate when two of the wild-type features looked mildly defective, such as slightly shorter DAs with wavy paddles. Some eggs exhibited stronger defects, such as DAs that were triangular in shape. For others, the DAs were of normal size, but there was no clear separation of the paddles with the bases, as if the paddles were missing. In some instances, the edges of the dorsal appendages looked jagged or serrated. This category also contained proportionally normal-looking dorsal appendages but of increased size relative to the entire egg, which was of normal size. We scored eggs as Severe when the DAs were short (half the normal length) and wide, or when they exhibited defects in three or more of the normal features. In some eggs, the two dorsal appendages were linked by chorion protein in between them. In other instances, there was a small quantity of chorion protein extending out of the egg, but there was not a specific shape. In other eggs, the DAs were merged at their bases, or chorion protein accumulated on the dorsal side of the egg instead of forming DAs.

**Immunostaining**

On the third day at 30°C, F1 females from the desired genotypes were anesthetized on a $CO_2$ pad and their ovaries dissected. To limit variability between samples, dissections were performed simultaneously by three people in the lab and completed within fifteen minutes. Dissected ovaries were placed in phosphate-buffered saline (PBS) on ice and fixed in 4% EM-grade formaldehyde [Thermo Fisher Scientific, Catalog# 43368] in PBS with 0.1% Tween 20 for twenty minutes. Ovaries were then washed three times in PBS with 0.1% Tween 20. To ensure even staining, single egg chambers of stages S10B and S12 were then dissected out, permeabilized with 1% Triton X-100 in PBS followed by three washes in PBS with 0.1% Tween

20. Eggs were then blocked in 10% Western Blocking Reagent (WBR, Roche) in PBS with 0.1% Tween 20 and incubated with gentle shaking overnight at 4ºC with mouse anti-Broad-core (1:250 uL, 25E9.D7 concentrate, Developmental Studies Hybridoma Bank, DHSB; Oda *et al.,* 1994) and rat anti-E-cadherin (1:50 uL, DCAD2-concentrate, DHSB; Dubreuil *et al.,* 1987). Egg chambers were then washed four times in PBS with 0.1% Tween 20 and 10% WBR and incubated for three hours at room temperature with Alexafluor 488-conjugated goat anti-mouse (1:200), Alexafluor 568-conjugated goat anti-rat (1:200), 4', 6-Diamidino-2-phenylindole (DAPI) (1 ug/mL) in PBS with 0.1% Tween 20 and 10% WBR. The egg chambers were then washed three times in PBS with 0.1% Tween 20 and 10% WBR, once in PBS 0.1% Tween 20, and mounted in Aqua polymount [Polysciences, Catalog# 18606] for imaging.

**Confocal image acquisition**

Imaging and scoring of egg chambers were done blind by covering the genotype labels with tape and assigning letters A, B, C, and D. Their names were revealed after all data analyses. We used the Leica SP8X confocal microscope, with the 20X objective and then with a zoom of $_X$2 focusing on the DA-forming patches. Wavelength emissions 488nm, 461nm, and 568nm were used with a PMT detector at 30%, 5% and 30% intensity power, respectively. The format of the acquired images was 1024 x 1024 at a speed of 600, with Z slices separated by 0.25 μm. We captured images moving basally (facing outward in this tissue) to apically (facing the oocyte), starting from where the Br-positive nuclei were visible and ending below the apical E-Cadherin staining, just after reaching the oocyte's cytoplasm.

**Image analysis**

Images were processed using ImageJ Version 2.0.0-rc-59/1.51n (FIJI) (Schindelin *et al.,* 2012). To identify DA patches, we created a Z projection using all images captured in the Br-positive channel for each egg chamber. To uniformly distinguish high-Broad staining (DA cells) from low-Broad staining (posterior and lateral cells) among different S10B egg chambers, the images were smoothed and made binary using the method Max Entropy or Momentum. We only used egg chambers in which the entire DA patch was visible, that is, those egg chambers mounted with a dorsal or partially dorsal view of the patches. To measure aspect ratios, we traced the exterior boundary of the high-Br cells to create a shape that enclosed the entire patch. Measurements were set up to calculate shape descriptors: aspect ratio, circularity and roundedness of the basal side of the cells. For apical surface measurements, we used single slices in the E-Cadherin channel at the apical-most region of the tube. We calculated length by tracing and recording a straight line from the base of the dorsal appendage tube to its tip.

**Statistical analysis**

For the modifier screen, we used a Chi-squared test for consistency to compare control and test samples. Although we categorized DAs into three groups (normal/mild, moderate, or severe), some samples lacked sufficient severe eggs to conduct the test properly; we therefore combined the moderate and severe groups into a single "defective" class for all comparisons. We used the R statistical package (R Core Team 2017) to generate a list of *p*-values using the function chisq.test() with one degree of freedom. We calculated a threshold of significance using the Bonferroni correction test by dividing the 0.05 significance value by 72 (the number of samples we compared), resulting in a $6.9 \times 10^{-4}$ cutoff. To calculate *p*-values for image analyses in figure

2.7, the R function for two-sided unpaired t-testings, t.test(), was used with a confidence interval of 95% (R Core Team 2020).

**Mical translation experimental set up.**

The *UAS-5'UTRMical-GFP* construct and a UAS-nuclear GFP stock were crossed to a CY2-GAL4 or CY2-GAL4 Idgf3 overexpression stock. Females from the F1 generation were incubated at 30oC for four days. On day four, ovaries and S10B egg chambers were dissected and stained with anti-GFP, anti-Broad and DAPI following the immunostaining protocol. We were planning to obtain dorsal view images of the S10B egg chambers with visible patches. We were pursuing to measure levels of GFP among egg chambers, controlling for exposure time and using similar settings during image acquisition. We were planning to use the changes of GFP signal from the UAS-nuclear GFP stock as a control and measure and compare the changes of 5'UTRMical-GFP signal at normal and overexpressed levels of *Idgf3*.

**ACKNOWLEDGEMENTS**

Thanks to Andreas Jenny for providing us with the *cmb* alleles; to Sebastian Rumpf for providing us with the *Mical* constructs; to Ernst Hafen for providing us with the Pten allele; to Maurizio Gatti for providing us with the Lkb1 allele; Lindsay Charley for identifying the method for patch recognition of the S10B egg chambers; to Ken Jean-Baptiste for statistics discussions; to the Berg lab for helpful discussions and input on experiments; to the Bloomington and Vienna Stock Centers for providing stocks; and to the Developmental Studies Hybridoma Bank for antibodies. This work was supported by a NSF Predoctoral Fellowship # 14-590 to CE and NIH R01 GM079433 to CAB.

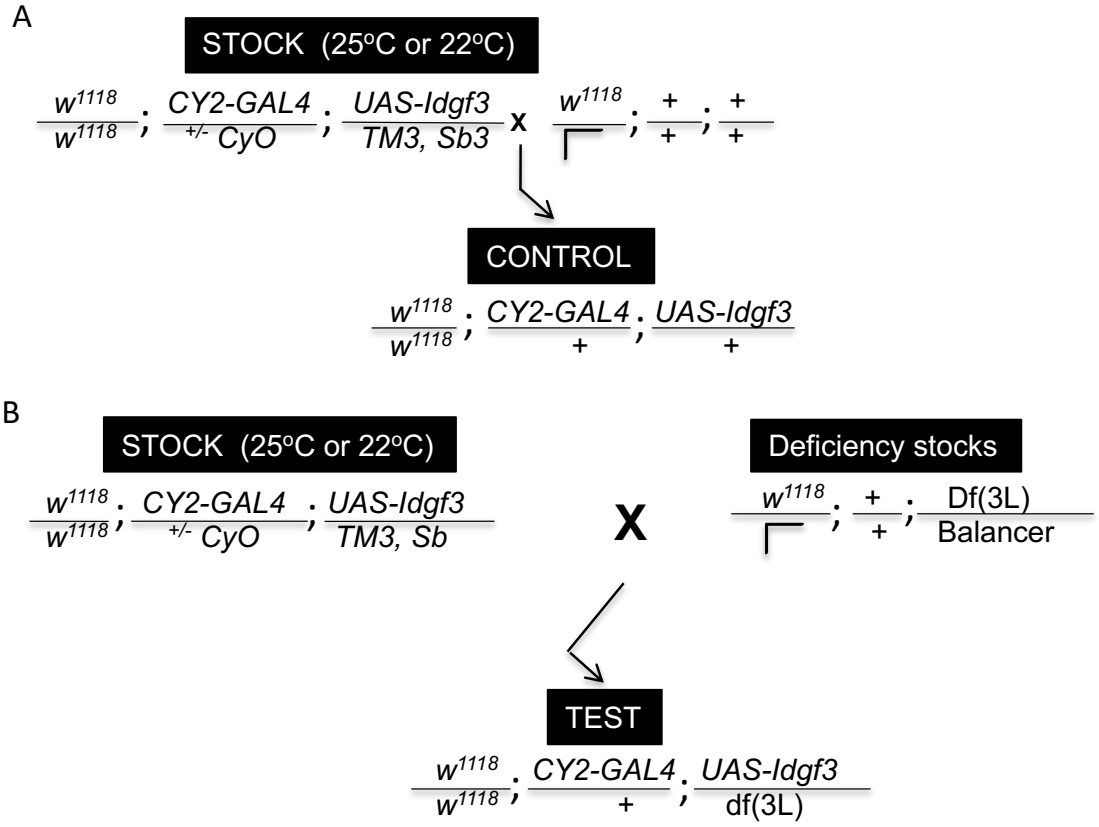


**Figure 5:** Modifier Screen crosses used to identify and narrow down regions that suppress or enhance the *Idgf3*-overexpression phenotype. A) Cross to obtain the control females. Females from the *Idgf3*-overexpression stock, which was kept at 25°C for the main modifier screen and then kept at 22°C for narrowing down regions, were crossed to $w^{1118}$ males. B) Cross to obtain the testing females. Females from the same *Idgf3*-overexpression stock from A were crossed to males from each stock of the 3L deficiency kit to obtain the females for testing, which were identified by the lack of the Balancer chromosomes (which carry a dominant marker).

**Bibliography**


1. Andrew, D. J., and A. J. Ewald, 2010 Morphogenesis of epithelial tubes: Insights into tube formation, elongation, and elaboration. *Dev. Biology* **341**: 34-55.
2. Avagliano, L., Massa, V., George, T. M., Qureshy, S., G.P.Bulfamante, et al., 2019 Overview on neural tube defects: From development to physical characteristics. *Birth Defects Research* **111**: 1455-1467.
3. Asano, K., Merrick, W. C., and J. W. Hershey, 1997 The translation initiation factor eIF3-p48 subunit is encoded by int-6, a site of frequent integration by the mouse mammary tumor virus genome. *J Biol Chem* **272**: 23477–23480.
4. Ayoob, J. C., Terman, J. R., and A. L. Kolodkin, 2006 Drosophila Plexin B is a Sema-2a receptor required for axon guidance. *Development* **133**(11): 2125-2135. doi:10.1242/dev.02380
5. Baer, M. M., Chanut-Delalande, H., and M. Affolter 2009 Cellular and Molecular Mechanisms Underlying the Formation of Biological Tubes. *Current Topics in Developmental Biology* **89**: 137-162.
6. Bamer, A. M., Connell, F. A., B. J. Dudgeon, and K. L. Johnson, 2010 Frequency of purchase and associated costs of assistive technology for Washington State Medicaid program enrollees with spina bifida by age. *Disabil Health J* **3**: 155–161.
7. Berg, C. A., 2005 The Drosophilashell game: patterning genes and morphological change. *Trends in Genetics* **21**: 346-355.
8. Berg C. A 2008 Tube formation in Drosophila egg chambers. *Tissue Eng.* Part A **14**: 1479-1488.
9. Berry, R. J., Li, Z., Erickson, J. D., Li, S., et al. 1999 Prevention of neural-tube defects with folic acid in China. *N Engl J Med* **341**: 1485–90
10. Boyle, M. J., and C. A. Berg, 2009 Control in time and space: Tramtrack69 cooperates with Notch and Ecdyson to repress ectopic fate and shape changes during Drosophila egg chamber maturation. *Development* **136**: 4187-4197.
11. Boyle, M.J., French, R. L., Cosand, K. A., Dorman, J. B., D. P. Kiehart, and C. A. Berg, 2010 Division of labor: subsets of dorsal-appendage-forming cells control the shape of the entire tube. *Developmental Biology* **346**: 68-79.
12. Boyles, A. L., Hammock, P., and M. C. Speer, 2005 Candidate Gene Analysis in Human Neural Tube Defects. *American Journal of Medical Genetics* Part C (Semin. Med. Genet.) **135C**: 9-23.
13. Brand, A.H., and N. Perrimon, 1993 Targeted gene expression as a means of altering cell fates and generating dominant phenotypes. *Development* **118:** 401–415.
14. Bridges, C. B., 1916 Non-Disjunction as Proof of the Chromosome Theory of Heredity. *Genetics* **1**(1): 1-52.
15. Broz, V., Kucerova, L., Rouhova, L., Fleischmannova, J., Strnad, H., Bryant P. J., and M. Zurovec, 2017 Drosophila imaginal disc growth factor 2 is a trophic factor involved in energy balance, detoxification, and innate immunity. *Scientific Reports* **7**: 1-15.
16. Buechner, M., Hall, D. H., Bhatt, H. and E. M. Hedghock 1999 Cystic Canal Mutants in Caenorhabditis elegans Are Defective in the Apical Membrane Domain of the Renal (Excretory). *Cell. Dev. Biol*. **214**: 227-241.
17. Butler, M. T., and J. B. Wallingford, 2017 Planar cell polarity in developmentand disease. *Nature Reviews Molecular Cell Biology* **18**(6): 375–388.

http://doi.org/10.1038/nrm.2017.11.
18. Bussink, A., Speijer, D., Aerts, J. M. F. G., and R. G. Boot, 2007 Evolution of mammalian chitinases(-like) members of family 18 glycosyl hydrolases. *Genetics* **177**(2): 959-970.
19. Cameron, M., and P. Moran 2009 Prenatal screening and diagnosis of neural tube defects.*Prenat Diagn* **29**: 402–411.
20. Catala, M., Teillet, M. A., E. M. De Robertis, and N. M. LeDouarin, 1996 Aspinal cord fate map in the avian embryo: while regressing, Hensen's node lays down the notochord and floor plate thus joining the spinal cord lateral walls. *Development* **122**: 2599-2610.
21. Chandrasekaran, V., and S. K. Beckendorf, 2005. Tec29 controls actin remodeling and endoreplication during invagination of the Drosophila embryonic salivary glands. *Development* **132**(15): 3515—3524.
22. Chen, B., Mao, H. H., Chen, L., Zhang, F. L., K. Li, et al., 2013 Loop-tail phenotype in heterozygous mice and neural tube defects in homozygous mice result from a nonsense mutation in the Vangl2 gene. *Genetics and Molecular Research* **12**(3): 3157-3165.
23. Coffman, F. D. 2008 Chitinase 3-Like-1 (CHI3L1): a putative disease marker at the interface of proteomics and glycomics. *Crit Rev Clin Lab Sci*. **45**: 531–562.
24. Colas, J.F., and G. C. Schoenwolf, 2001 Towards a cellular and molecular understanding of neurulation. *Dev. Dyn.* **221**: 117–145.
25. Cook, K. R., Parks, A. L., Jacobus, L. M., Kaufman, T. C., and K. A. Matthews, 2010 New research resources at the Bloomington Drosophila Stock Center. *Fly (Austinn)* **4**(1): 88-91.
26. Copp, A., and N. D. E. Greene, 2013 Neural tube defects- disorders of neurulation and related embryonic processes. *WIREs Dev Biol*. **2**: 213–227. doi: 10.1002/wdev.71
27. Copp, A. J., and N., DEGreene, 2010 Genetics and development of neural tube defects. *Journal of Pathology* **220**: 217-230.
28. Copp, A. J., Adzick, N. S., Chitty, L. S., Fletcher, J. M., G. N. Holmbeck, et al., 2015 Spina bifida. *Nat. Rev. Dis. Primers* **1**: 15007. doi:10.1038/nrdp.2015.7.
29. Czeizel AE, Dudás I. 1992 Prevention of the first occurrence of neuraltube defects by periconceptional vitamin supplementation. *N Engl J Med* **327**: 1832–35.
30. Czeizel, A. E., Dudás, I., Vereczkey, A., and F. Bánhidy, F 2013 Folate deficiency and folic acid supplementation: the prevention of neural-tube defects and congenital heart defects. *Nutrients* **5**(11):4760-4775. doi:10.3390/nu5114760
31. Darken, R. S., Scola, A. M., Rakeman, A. S., Das, G., M. Mlodzik, and P. A. Wilson, 2002 The planar polarity gene strabismus regulates convergence extension movements in Xenopus. *EMBO J* **21**: 976-985.
32. Dewan, M. C., and J. C. Wellons III, 2019 Fetal surgery for spina bifida. *J Neurosurg Pediatr* **24**: 105-114.
33. Diaz-de-la-Loza, M.C., Ray, R. P., Ganguly, P. S., Alt, S., J. R. Davis et al., 2018 Apical and Basal Matrix Remodeling Control Epithelial Morphogenesis. *Developmental Cell* **46**: 23-39.
34. Dietzl, G., Chen, D., Schnorrer, F., Su, K.-C., Y., Barinova, et al. 2007. A genome-wide transgenic RNAi library for conditional gene inactivation in Drosophila. *Nature* **448**(7150): 151–156. http://doi.org/10.1038/nature05954
35. Dorman, J. B., James, K. E., Fraser, S. E., D. P. Kiehart, and C. A. Berg, 2004 bullwinkle is required for epithelial morphogenesis during Drosophila oogenesis. *Developmental*

*Biology* **267**: 320-341.
36. Drosophila Genomics Resource Center. Indiana University, "S2 Stocks in the DGRC Collection," https://dgrc.bio.indiana.edu/cells/S2Isolates. Accessed 29 July 29 2020.
37. Dubreuil, R., Byers, T. J., Branton, D., L. S. Goldstein, and D. P. Kiehart, 1987 Drosophila spectrin I. Characterization of purified protein. *J. Cell Biol*. **105**: 2095- 2102.
38. Duhart, J. C., Parson, T. T., and L. A. Raftery, 2017 The repertoire of epithelial morphogenesis on display: Progressive elaboration of *Drosophila* egg structure. *Mechanisms of Development* **148:** 18-39.
39. Erdman, L. K., Petes, C., Lu, Z., Dhabangi, A., C. Musoke, et al., 2014 Chitinase 3-like 1 is induced by Plasmodium falciparum malaria and predicts outcome of cerebral malaria and severe malaria anaemia in a case-control study of African children. *Malaria Journal* **13**: 279-290.
40. Fagan, J., Dollar, G., Lu, Q., Barnett, A., J. P. Jorge, et al., 2014 Combover/CG10732, a Novel PCP Effector for Drosophila Wing Hair Formation. *Plos One*. **9**: 1-14.
41. Feinberg, E. H., VanHoven, M. K., Bendesky, A., Wang, G., and R. D. Fetter, 2008 GFP Reconstitution Across Synaptic Partners (GRASP) Defines Cell Contacts and Synapses in Living Nervous Systems. *Neuron* **57**(3) 353-363.
42. French, R. L., Cosand, K. A., and C. A. Berg, 2003 The Drosophila female sterile mutation twin peaks is a novel allele of tramtrack and reveals a requirement for Ttk69 in epithelial morphogenesis. *Developmental Biology* **253**(1): 18–35.
43. Fox, A. J. S., Bedi, A., and S.A. Rodeo. 2009. The Basic Science of Articular Cartilage: Structure, Composition, and Function. *Sports Health*. **1**(6): 461-468.
44. Funkhouser, J. D., and N. N. Aronson Jr. 2007 Chitinase family GH18: evolutionary insights from the genomic history of a diverse protein family. *BMC Evolutionary Biology*. **7**:96 doi:10.1186/1471-2148-7-96.
45. Greene, N. D. E, Stanier, P., and A. J. Copp, 2009 Genetics of human neural tube defects. *Hum Mol Genet* **18**: R113–29.
46. Greene, N. D. E., and A. J. Copp, 2014 Neural Tube Defects. Annu Rev Neurosci. **37:** 221-242.
47. Gutzei,t H. O., Eberhardt, W., and E. Gratwohl, 1991 Laminin and basement membrane-associated microfilaments in wild-type and mutant Drosophila ovarian follicles. *J Cell Sci*. **100**:781-788.
48. Guruharsha, K. G., Rual, J. F., Zhai, B., Minstseris, J., P. Vaidya, et al. 2011 A Protein Complex Network of Drosophila melanogaster. *Cell* **147:** 690-703.
49. Johansen, J. S., Williamson, M.K., Rice, J.S, P. A. Price, 1992 Identification of proteins secreted by human osteoblastic cells in culture. *J Bone Miner Res*. **7**(5): 501-512. doi:10.1002/jbmr.5650070506.
50. Hakala, B. E., White, C., and A. D. Recklies,1993 Human cartilage gp- 39, a major secretory product of articular chondrocytes and synovial cells, is a mammalian member of a chitinase protein family. *J. Biol. Chem*. **268**: 25803-25810
51. Hales, K. G., Korey, C. A., Larracuente, A. M., and D. M. Roberts. 2015 Genetics on the fly: a primer on the Drosophila model system. *Genetics* **201**: 815-842.
52. Harris, M. J., and D. M. Juriloff, 2007 Mouse mutants with neural tube closure defects and their role in understanding human neural tube defects. *Birth Defects Res A Clin Mol Teratol.* **79**:187–210.
53. Harvey, S., Weisman, M., O'Dell, J., Scott, T., M. Krusemeier, M., et al*.,* 1998

Chondrex: new marker of joint disease. *Clin Chem* **44**: 509–516.
54. He, C. H., Lee, C. G., Dela Cruz, C. S., Lee, C. M., Y. Zhou, et al., 2013 Chitinase 3-like 1 regulates cellular and tissue responses via IL-13 receptor α2. *Cell reports* **4**(4): 830–841. https://doi.org/10.1016/j.celrep.2013.07.032.
55. Hemminki, A., Markie, D., Tomlinson, I., Avizienyte, E., S. Roth, et al., 1998 A serine/threonine kinase gene defective in Peutz-Jeghers syndrome. *Nature* **391**(6663): 184-187. doi:10.1038/34432.
56. Hernandez, G., Miron, M., Han, H., Liu, N., Magescas, J., et al*.,* 2013 Mextli Is a Novel Eukaryotic Translation Initiation Factor 4E-Binding Protein That Promotes Translation in Drosophila melanogaster. *Molecular and Cellular Biology* **33**: 2854-2864.
57. Hinton, H. E., 1969 Respiratory systems of insect egg shells. *Annu. Rev. Entomol*. **14**: 343-368.
58. Hogan, B. L. M., and P. A., Kolodziej, 2002 Molecular Mechanisms of Tubulogenesis. *Nat. Reviews Genetics* **3**: 513-523.
59. Horne-Badovinac, S., and D. Bilder, 2005 Mass transit: epithelial morphogenesis in the Drosophila egg chamber. *Dev Dyn*. **232**(3):559-574. doi:10.1002/dvdy.20286
60. Hudson, A.M., and L. Cooley, 2014 Methods for studying oogenesis. *Methods* **68**: 207-217.
61. Hung, R., Yazdani, U., Yoon, J., Wu, H., T. Yang, et al., 2010 Mical links semaphorins to F-actin disassembly. *Nature* **463**: 823–827. https://doi.org/10.1038/nature08724
62. Jambor, H., Surendranath, V., Kalinka, A. T., Pavel, M., and S. Saalfeld, 2015 Systemic imaging reveals features and changing localization of mRNAs in Drosophila development. *eLife*. 4:e05003. DOI: 10.7554/eLife.05003
63. Junttila, I. S. 2018 Tuning the Cytokine Responses: An Update on Interleukin (IL)-4 and IL-13 Receptor Complexes. *Front Immunol.* **9:**1-6.
64. Kawamura, K., Shibata, T., Saget, O., D. Peel, and P. J. Bryant, 1999 A new family of growth factors produced by the fat body and active on Drosophila imaginal disc cells. *Development* **126**: 211-219.
65. Keller, R., Davidson, L., Edlund, A., Elul, T., Ezin, M., Shook, D., Skoglund, P., 2000 Mechanisms of convergence and extension by cell intercalation. *Philos. Trans. R. Soc. Lond. B Biol. Sci*. **355**: 897–922.
66. Kiehart, D. P., Galbraith, C. G., Edwards, K. A., Rickoll, W. L., and R. A. Montague, 2000 Multiple forces contribute to cell sheet morphogenesis for dorsal closure in Drosophila. *J Cell Biol*. **149**: 471–490
67. King, R. C., 1970 *Ovarian Development in Drosophila melanogaster.* Academic Press, New York and London.
68. Kirkpatrick, R. B., Matico, R. E., McNulty, D. E., J. E. Strickler, and M. Rosenberg, 1995 An abundantly secreted glycoprotein from *Drosophila melanogaster* is related to mammalian secretory proteins produced in rheumatoid tissues and by activated macrophages. *Gene* **153**: 147-154.
69. Krause S. W., Rehli M., Kreutz M., Schwarzfischer L., Paulauskis J. D., Andreesen R., 1996 Differential screening identifies genetic markers of monocyte to macrophage maturation. *J. Leukoc. Biol*. **60**: 540–545.
70. Krautz, R., Arefin, B., and U. Theopold 2014 Damage signals in the insect immune response. *Frontier in plant science*. **5**: 1-11.
71. Kronborg, G., Ostergaard, C., Weis, N., Nielsen, H., N. Obel, et al*.,* 2002 Serum level of

YKL-40 is elevated in patients with Streptococcus pneumoniae bacteremia and is associated with the outcome of the disease. *Scand J Infect Dis* **34:** 323–326.
72. Kucerova, L., Broz, V., Arefin, B., Maaroufi, H. O., Hurychova, J., Strnad, H., Zurovec, M., and U. Theopold. 2016 The Drosophila Chitinase-Like Protein IDGF3 Is Involved in Protection against Nematodes and in Wound Healing. *J Innate Immun* **8**:199–210.
73. Kzhyshkowska, J., Mamidi, S., Gratchev, A., Kremmer, E., C. Schmuttermaier, et al. 2006 Novel stabilin-1 interacting chitinase-like protein (SI-CLP) is up-regulated in alternatively activated macrophages and secreted via lysosomal pathway. *Immunobiology* **107(**8) 3221-3228.
74. Lee, C. G., Da Silva, C. A., Dela Cruz, C. S., Ahangari, F., B. Ma, et al. 2011 Role of chitin and chitinase/chitinase-like proteins in inflammation, tissue remodeling, and injury. *Annu Rev Physiol*. **73**: 479-501. doi:10.1146/annurev-physiol-012110-142250.
75. Lei, Y. P., Zhang, T., Li, H., Wu, B. L., L. Jin, et al*.,* 2010 VANGL2 mutations in human cranial neural tube defects. *N Engl J Med* **362**: 2232–35.
76. Libreros, S., R. Garcia-Areas, and V. Iragavarapu-Charyulu, 2013 CHI3L1 plays a role in cancer through enhanced production of pro-inflammatory/pro- tumorigenic and angiogenic factors. *Immunol. Res*. **57**(0): 99-105.
77. Low, D., Subramaniam, R., Lin, L., Aomatsu, T., Mizoguchi, A., A. Ng, et al*.* 2015 Chitinase 3-like 1 induces survival and proliferation of intestinal epithelial cells during chronic inflammation and colitis-associated cancer by regulating S100A9. *Oncotarget* **6**: 36535–36550.
78. Lubarsky, B., and M. A., Krasnow, 2003 Tube Morphogenesis: Making and Shaping Biological Tubes. *Cell*. **112**: 19-28.
79. Mahajan-Miklos, S. and L. Cooley 1994 Intercellular Cytoplasm Transport during Drosophila oogenesis. *Developmental Biology* **165**: 336-351.
80. Marchetti, A., Buttitta, F., Miyazaki, S., Gallahan, D., G. H. Smith, et al. 1995 Int-6, a highly conserved, widely expressed gene, is mutated by mouse mammary tumor virus in mammary preneoplasia. *J. Virol.* **69**: 1932–1938.
81. Merkle, J. A., Wittes, J., and T. Schupbach, 2020 Signaling between somatic follicle cells and the germline patterns the egg and embryo of *Drosophila. Current Topics in Developmental Biology.* **140:** 55- 86.
82. Merzendorfer, H., and L. Zimoch 2003 Chitin metabolism in insects: structure, function and regulation of chitin synthases and chitinases. The Journal of Experimental Biology **206**: 4393-4412.
83. Miyazaki, S., Rasmussen, S., Imatani, A., Diella, F., D. T. Sullivan, et al., 1999 Characterization of the Drosophila ortholog of mouse eIF-3p48/INT-6. Gene **233**: 241-247.
84. Mitchell, L. E., 2005 Epidemiology of neural tube defects. *Am J Med Genet C Semin Med Genet*. **135**: 88–94.
85. Molloy, A. M., Brody, L. C., Mills, J. L., Scott, J. M., and P. N. Kirke, 2009 The search for genetic polymorphisms in the homocysteine/folate pathway that contribute to the etiology of human neural tube defects. *Birth Defects Research (Part A)* **85**: 285-294.
86. Montell, D., Yoon, W. and M. Starz-Gaiano, Group choreography: mechanisms orchestrating the collective movement of border cells. *Nat Rev Mol Cell Biol* **13,** 631–645 (2012). https://doi.org/10.1038/nrm3433
87. Morgan, T. H., 1910 Chance or purpose in the origin and evolution of adaptation.

*Science* **31**: 301-310
88. Munjal, A., Philippe, J. M., E. Munro, and T. Lecuit, 2015 A self-organized biomechanical network drives changes during tissue morphogenesis. *Nature* **524**: 351-355.
89. Nezis, I. P., Stravopodis, D. J., Papassideri, I., M. Robert-Nicoud, and L. H. Margaritis, 2002 Dynamics of apoptosis in the ovarian follicle cells during late stages of Drosophila oogenesis. *Cell Tissue Res.* **307**: 401-409.
90. Ni, J.-Q., Zhou, R., Czech, B., Liu, L.-P., L. Holderbaum, et al. 2011 A genome- scale shRNA resource for transgenic RNAi in Drosophila. *Nature Methods* **8**(5): 405–407. http://doi.org/10.1038/nmeth.1592.
91. Neufeld, S. Q., Hibbert, A. D., and B. E. Chen, 2011 Opposing roles of PlexinA and PlexinB in axonal branch and varicosity formation. *Molecular brain*, **4**: 15. https://doi.org/10.1186/1756-6606-4-15.
92. Nievelstein, R. A. J., Hartwig, N. G., C. Vermeij-Keers, and J. Valk, 1993 Embryonic Development of the Mammalian Caudal Neural Tube. *Teratology* **48**: 21-31.
93. Nikolopoulou, E., Galea, G.L., Rolo, A., N.D.E, Greene, and A.J., Copp, 2017 Neural tube closure: cellular, molecular and biochemical mechanisms. *Development* **144**(4): 552-566. doi:10.1242/dev.145904.
94. Ober, C., and G. L. Chupp, 2009 The Chitinase and Chitinase-Like Proteins: A Review of Genetic and Functional Studies in Asthma and Immune-Mediated Disease. *Curr Opin Allergy Clin Immunol.* **9**(5): 401-408.
95. Oda, H., Uemura, T., Harada, Y., Y. Iwai, and M. Takeichi, 1994 A Drosophila homolog of Cadherin associated with Armadillo and essential for embryonic cell- cell adhesion. Dev. Biol. 165: 716-726.
96. Ospelt C., 2017 Synovial fibroblasts *RMD Open* 3:e000471. doi:10.1136/ rmdopen-2017-000471.
97. Osterfield, M., Du, X., Schüpbach, T., E. Wieschaus, and S. Y. Shvartsman, 2013 Three-dimensional epithelial morphogenesis in the developing Drosophila egg. *Dev. Cell* **24**: 400–410.
98. Osterfield, M., C.A., Berg, and S.Y., Shvartsman, 2017 Epithelia Patterning, Morphogenesis, and Evolution: Drosophila Eggshell as a Model. *Dev. Cell* **41**(4): 337-348. doi:10.1016/j.devcel.2017.02.018.
99. Park, M., and R. T. Moon, 2001 The planar cell polarity gene stbm regulates cell behaviour and cell fate in vertebrate embryos. Nat. Cell. Biol. 4: 20-25.
100. Parks, A. L., Cook, K.R., Belvin, M., Dompe, N. A., Fawcett, R., K. Huppert, et. al., 2004 Systematic generation of high-resolution deletion coverage of the Drosophila melanogaster genome. *Nat. Genet.* **36**: 288-292.
101. Peters, N. A., and C. A. Berg, 2016A In Vitro Culturing and Live Imaging of Drosophila Egg Chambers: A History and Adaptable Method. Oogenesis: Methods and Protocols, *Methods in Molecular Biology* **1457**: 35-68.
102. Peters, N. C., and Berg, C. A. 2016B. Dynamin-mediated endocytosis is required for tube closure, cell intercalation, and biased apical expansion during epithelial tubulogenesis in the Drosophila ovary. *Developmental Biology* **409**(1), 39–54. http://doi.org/10.1016/j.ydbio.2015.10.034
103. Peters, N. C., Thayer N. H., Kerr, S. A., M. Tompa, and C. A., Berg, 2013 Following the 'tracks': Tramtrack69 regulates epithelial tube expansion in the Drosophila ovary through

Paxillin, Dynamin, and the homeobox protein Mirror. *Dev. Biol*. **378**: 154-169.
104. Queenan, A. M., Ghabrial, A., and T. Schupbach, 1997, Ectopic activation of torpedo/Egfr, a Drosophila receptor tyrosine kinase, dorsalizes both the eggshell and the embryo. *Development* **124**: 3871-3880.
105. Qiu, Q., Wang, L., Jin, S. et al*.,* 2018 CHI3L1 promotes tumor progression by activating TGF-β signaling pathway in hepatocellular carcinoma. *Sci Rep* **8:** 15029 https://doi.org/10.1038/s41598-018-33239-8.
106. R Core Team (2017). R: A language and environment for statistical computing. R Foundation for statistical Computing, Vienna. Austria. URL https://www.R- project.org/. R version 3.3.3 (2017-03-06) – "Another Canoe" Copyright © 2017 The R Foundation for Statistical Computing Platform:x86_64-apple-darwin13.4.0 (64-bit).
107. R Core Team (2020). R: A language and environment for statistical computing. R Foundation for Statistical Computing, Vienna, Austria. URL https://www.R-project.org/
108. Rämet, M., Pearson, A., Manfruelli, P., Li, X., Koziel, H., V. Gobel, et al., 2001 Drosophila Scavenger Receptor CI Is a Pattern Recognition Receptor for Bacteria. *Immunity* **15:** 1027-1038.
109. Rampersaud, E., Melvin, E. C., and M. C. Speer, Nonsyndromic neural tube defects: genetic basis and genetic investigations. In: Wyszynski DF, ed. Neural tube defects: from origin to treatment. Oxford: Oxford University Press, 2006: 165–75.
110. Ratheesh, A., Gomez, G. A., Priya, R., Verma, S., E. M. Kovacs et al*.*, 2012 Centralspindlin and α-catenin regulate Rho signalling at the epithelial zonula adherens*.* *Nature Cell Biol*. **14**(8): 818-828.
111. Richardson, 2015.3.11, Int6 constructs and insertions from Helena Richardson. [FBrf0227844]
112. Riento, K., and A. J. Ridley, 2003 Rocks: Multifunctional kinases in cell behaviour. *Nature* **4**: 446-456.
113. Rittenhouse, K. R., and C. A. Berg, 1995 Mutations in the Drosophila gene Bullwinkle cause the formation of abnormal eggshell structures and bicaudal embryos. *Development* **121**: 3023-3033.
114. Rittenhouse, K. R., 1996 BULLWINKLE, AN HMG BOX PROTEIN, IS REQUIRED FOR PROPER DEVELOPMENT DURING OOGENESIS, EMBRYOGENESIS AND METAMOPRHOSIS IN DROSOPHILA MELANOGASTER. A dissertation submitted in partial fulfillment of the requirements for the degree of Doctor of Philosophy.
115. Ryder, E., Ashburner, M., Bautista-Llacer, R., Drummond, J., Webster, J., G. Johnson et al*.*, 2007 The DrosDel deletion collection: a Drosophila genomewide chromosomal deficiency resources. *Genetics* **177**: 615-629.
116. Rode, S., Ohm, H., Anha, L., Wagner, M., M. Mechthild, et al., 2018 Differential Requirement for Translation Initiation Factor Pathways during Ecdysone-Dependent Neuronal Remodeling in Drosophila*. Cell Reports* **24**: 2287-2299.
117. Saadin, A., and M. Starz-Gaiano 2016 Identification of Novel Regulators of the JAK/STAT Signaling Pathway that Control Border Cell Migration in the Drosophila Ovary. *G3 (Bethesda, Md.)* **6**(7): 1991–2002. https://doi.org/10.1534/g3.116.028100
118. Sadato, D., Ono, T., Gotoh-Saito, S., Kajiwara, N., N. Nomura et al*.*, 2018 Eukaryotic Translation initiation factor 3 (eIF3) subunit e is essential for embryonic development and cell proliferation. *FEBS Open Bio*. **8**(8): 1188-1201.
119. Sanfilippo, C., Malaguarnera, L., and M. Di Rosa, 2016 Chitinase expression in

Alzheimer's disease and non-demented brains regions. *J Neurol Sci*. **369**: 242-249. doi:10.1016/j.jns.2016.08.029
120. Sanfilippo, C., Nunnari, G., Calcagno, A., et al. 2017a The chitinases expression is related to Simian Immunodeficiency Virus Encephalitis (SIVE) and in HIV encephalitis (HIVE). *Virus Res*. **2**) **227):** 220-230. doi:10.1016/j.virusres.2016.10.012.
121. Sanfilippo, C., Longo, A., Lazzara, F., et al. 2017b CHI3L1 and CHI3L2 overexpression in motor cortex and spinal cord of sALS patients. *Mol Cell Neurosci* **85**:162-169. doi:10.1016/j.mcn.2017.10.001
122. Schindelin, J., Arganda-Carreras, I., E. Frise et al., 2012 Fiji: an open-source platform for biological-image analysis. *Nature methods* **9**(7): 676-682.
123. Schittny, J. C., 2017 Development of the lung. *Cell Tissue Res*. **367**: 427-444.
124. Spradling, A. C., Stern, D., Beaton, A., Rhem, E.J., Laverty, T., et al., 1999 The Berkeley Drosophila genome project gene disruption project. Single P-element insertions mutating 25% of vital Drosophila genes. Genetics 153(1): 135-177.
125. Smith J L. and G. C. Schoenwolf, 1997 Neurulation: Coming to closure. *Trends Neurosci.* **11**: 510–517
126. Steinhauer, J., Statman, B., Fagan, J. K., Borck, J., Surabhi, S., Yarikipati, P., et al. 2019 Combover interacts with the axonemal component Rsp3 and is required for Drosophila sperm individualization. *Development* **146**(17): dev179275. http://doi.org/10.1242/dev.179275
127. Tateno, M., Nishida, Y., and T. Adachi-Yamada, 2000. Regulation of JNK by Src During Drosophila Development. *Science* **287**(5451): 324-327.
128. Terman, J., Mao, T., Pasterkamp, R. J., Yu, H., and A. Kolodkin, 2002 MICALs, a Family of Conserved Flavoprotein Oxidoreductases, function in Plexin-Mediated Axonal Repulsion. *Cell* **109**: 887-900.
129. Torban, E., Patenaude, A. M., Leclerc, S., Rakowiecki, S., S. Gauthier, et al. 2008 Genetic interaction between members of the Vangl family causes neural tube defects in mice. *Proc Natl Acad Sci U S A* **105**:3449-3454.
130. Tran, D. H., and C. A. Berg, 2003 *bullwinkle* and *shark* regulate dorsal- appendage morphogenesis in Drosophila oogenesis. *Development* **130**: 6273- 6282.
131. Tzolovsky, G., Deng, W. M., Schlitt, T., and M. Bownes, 1999 The function of the broad-complex during Drosophila melanogaster oogenesis. *Genetics* **153**(3): 1371–1383.
132. Ulvila, J., Vanha-aho, L. M. and M. Rämet, 2011 Drosophila phagocytosis – still many unkonwns under the surface. *APMIS* **119:** 651-662.
133. van der Meer, J. M., 1977 Optical clean and permanent whole mount preparation for phase-contrast microscopy of cuticular structures of insect larvae. *Drosoph. Inf. Serv*. **52**: 160.
134. Varela, P. F., Llera, A. S., R. A. Mariuzza and J. Tormo, 2002 Crystal Structure of Imaginal Disc Growth Factor-2 A MEMBER OF A NEW FAMILY OF GROWTH-PROMOTING GLYCOPROTEINS FROM DROSOPHILA MELANOGASTER*. *The Journal of Biological Chemistry* **277**: 13229-13236.
135. Verboon, J. M., and S. M. Parkhurst, 2015 Rho family GTPase functions in Drosophila epithelial wound repair. *Small GTPases.* **6**(1): 28-35.
136. Vinayagam, A., Kulkarni, M.M., Sopko, R., Sun, X., Hu, Y. et al., 2016. An Integrative Analysis of the InR/PI3K/Akt Network Identifies the Dynamic Response to Insulin Signaling. *Cell Reports*. **16**(11): 3062-3074.

137. Wallingford, J. B., and R. M. Harland, 2001 Xenopus Dishevelled signaling regulates both neural and mesodermal convergent extension: parallel forces elongating the body axis. *Development* **128**: 2581-2592.
138. Wang, M., Marco, P. de, V. Capra, and Z. Kibar, 2019 Update on the Role of the Non-Canonical Wnt/Planar Cell Polarity Pathway in Neural Tube Defects. *Cells* **8**(10): 1198. doi.org/10.3390/cells8101198
139. Ward, E. J., and C. A. Berg, 2005. Juxtaposition between two cell types is necessary for dorsal appendage tube formation. *Mechanisms of Development* **122**(2): 241–255. http://doi.org/10.1016/j.mod.2004.10.006
140. Waring, G. L. 2000. Morphogenesis of the eggshell in Drosophila. *Int. Rev. Cytol*. **198**: 67-108.
141. Warn, R.M., Gutzeit, H.O., Sminth, L., and A. Warn 1985 F-actin rings are associated with the ring canals of the *Drosophila* egg chamber. *Experimental Cell Research* **157**:355-363.
142. Winberg M. L., Noordermeer, J. N., Tamagnone, L., Comoglio, P. M., M.K. Spriggs, et al., 1998 Plexin A is a neuronal semaphorin receptor that controls axon guidance. *Cell* **95**: 903-916
143. Wright, V.M., Vogt, K.L., Smythe, E., and M. P. Zeidler, 2011 Differential activities of the Drosophila JAK/STAT pathway ligands Upd, Upd2 and Upd3. Cell. Signal. **23**(5): 920-927.
144. Yakoby N., Lembong J., Schüpbach T., S. Y. Shvartsman, 2008 Drosophila eggshell is patterned by sequential action of feedforward and feedback loops. *Development* **135**: 343–351.
145. Yi, Y., M. Lindemann, and A., Colligs, 2011 Economic burden of neural tube defects and impact with folic acid: a literature review. *Eur J Pediatr* **170**: 1391- 1400.
146. Zimmerman, S. G., Merrihew, G. E., M. J. MacCoss, and C. A. Berg, 2017 Proteomic Analysis Identifies Orthologs of Human Chitinase-Like Proteins as Inducers of Tube Morphogenesis Defects in Drosophila Melanogaster. *Genetics* **206**: 973-984.
147. Zhu, Q., Deng, Y., Vanka, P., Brown, S. J., S. Muthukrishnan, et al. 2004 Computational identification of novel chitinases-like proteins in the Drosophila melanogaster genome. *Bioinformatics*. **20**(2): 161-169.
148. Zhu, Q., Arakane, Y., Banerjee, D., Beeman, R. W., K. J. Kramer, and S. Muthukrishnan, 2008 Domain organization and phylogenetic analysis of the chitinases-like family of proteins in three species of insects. *Insect Biochemistry and Molecular Biology* **38**: 452-466.

**Table 1**

| Deficiency | Bloomington Stock # | Number of genes | P-values | Effect | n=eggs counted | Starting coordinate | Ending coordinate |
|---|---|---|---|---|---|---|---|
| Df(3L)ED4674 | 8098 | 64 | 1.35737E-34 | Enhancer | 219 | 16661284 | 17049418 |
| Df(3L)BSC449 | 24953 | 49 | 5.01692E-31 | Enhancer | 137 | 20856915 | 21202930 |
| Df(3L)BSC371 | 24395 | 71 | 8.60277E-31 | Enhancer | 167 | 4868210 | 5634506 |
| Df(3L)BSC289 | 23674 | 59 | 3.31059E-30 | Enhancer | 174 | 1332329 | 1628101 |
| Df(3L)BSC223 | 9700 | 24 | 4.55299E-24 | Enhancer | 143 | 21916420 | 22085436 |
| Df(3L)BSC23 | 6755 | 85 | 6.03024E-20 | Suppressor | 138 | 2631116 | 3148292 |
| Df(3L)ED208 | 8059 | 75 | 4.96069E-18 | Enhancer | 127 | 3249148 | 3893148 |
| Df(3L)BSC553 | 25116 | 33 | 5.47378E-18 | Enhancer | 124 | 20991631 | 21225992 |
| Df(3L)BSC375 | 24399 | 33 | 1.01853E-16 | Enhancer | 229 | 7517780 | 7911080 |
| Df(3L)BSC368 | 24392 | 52 | 8.74998E-16 | Enhancer | 122 | 3759821 | 4040635 |
| Df(3L)BSC774 | 27346 | 90 | 1.53993E-14 | Enhancer | 182 | 15699903 | 16240280 |
| Df(3L)BSC730 | 26828 | 90 | 1.32143E-10 | Enhancer | 123 | 12162977 | 12843324 |
| Df(3L)BSC224 | 9701 | 30 | 7.06048E-10 | Enhancer | 206 | 6964457 | 7157009 |
| Df(3L)Exel8104 | 7929 | 37 | 9.19205E-10 | Enhancer | 127 | 7359986 | 7529263 |
| Df(3L)BSC451 | 24955 | 58 | 2.46519E-08 | Enhancer | 102 | 22076095 | 22691731 |
| Df(3L)ED230 | 8089 | 76 | 3.24761E-08 | Suppressor | 201 | 22134651 | 22834371 |
| Df(3L)ED4475 | 8069 | 56 | 3.79791E-08 | Enhancer | 147 | 11587040 | 12408601 |
| Df(3L)ED4457 | 9355 | 99 | 4.04774E-07 | Suppressor | 172 | 10363951 | 11125809 |
| Df(3L)ED229 | 8087 | 145 | 8.18082E-07 | Enhancer | 159 | 19170706 | 20002711 |
| Df(3L)BSC27 | 6867 | 35 | 3.22727E-06 | Enhancer | 187 | 6953872 | 7177349 |
| Df(3L)BSC414 | 24918 | 61 | 3.33494E-06 | Suppressor | 130 | 16969873 | 17476126 |
| Df(3L)ED4287 | 8096 | 94 | 4.12357E-06 | Enhancer | 142 | 1795442 | 2551761 |
| Df(3L)ED4483 | 8070 | 54 | 4.4193E-06 | Enhancer | 114 | 12277220 | 12693214 |
| Df(3L)ED4502 | 8097 | 84 | 6.42658E-06 | Enhancer | 125 | 13227765 | 13993551 |
| Df(3L)BSC362 | 24386 | 36 | 6.98476E-06 | Suppressor | 142 | 306169 | 628171 |
| Df(3L)BSC118 | 8975 | 24 | 1.98657E-05 | Enhancer | 110 | 9515672 | 9697191 |
| Df(3L)ED4341 | 8060 | 127 | 2.59977E-05 | Enhancer | 145 | 3905091 | 4542236 |
| Df(3L)ED4978 | 8101 | 68 | 6.2439E-05 | Enhancer | 141 | 21533807 | 21880685 |
| Df(3L)ED201 | 8047 | 55 | 0.000102382 | Enhancer | 147 | 123924 | 347941 |
| Df(3L)BSC389 | 24413 | 21 | 0.000134242 | Enhancer | 145 | 8422185 | 8589597 |
| Df(3L)ED210 | 8061 | 72 | 0.000187458 | Enhancer | 134 | 4544234 | 5355342 |
| Df(3L)BSC220 | 9697 | 24 | 0.000386351 | Enhancer | 197 | 18972562 | 19171268 |
| Df(3L)BSC33 | 6964 | 23 | 0.000457097 | Suppressor | 139 | 7262736 | 7357537 |
| Df(3L)BSC672 | 26524 | 42 | 0.001238689 | No effect | 111 | 3081311 | 3206906 |
| Df(3L)ED4606 | 8078 | 64 | 0.002024939 | No effect | 160 | 16087484 | 16780123 |
| Df(3L)6B-29+Df(3R)6B-29 | 2596 | 26 | 0.002053551 | No effect | 138 | 25679473 | 28110227 |
| Df(3L)ED4196 | 8050 | 117 | 0.002176122 | No effect | 109 | 639583 | 1478937 |
| Df(3L)BSC419 | 24923 | 70 | 0.002274787 | No effect | 85 | 21224932 | 21604778 |
| Df(3L)ED4470 | 8068 | 159 | 0.00236479 | No effect | 110 | 11096989 | 11833230 |
| Df(3L)AC1 | 997 | 34 | 0.002536881 | No effect | 82 | 9190597 | 10316395 |
| Df(3L)Exel6132 | 7611 | 25 | 0.003351204 | No effect | 168 | 17421582 | 17533027 |
| Df(3L)ED4543 | 8073 | 84 | 0.012687283 | No effect | 144 | 13935225 | 14758040 |
| Df(3L)ED50002 | 24627 | 12 | 0.022171773 | No effect | 142 | 1 | 128631 |
| Df(3L)ED4421 | 8066 | 87 | 0.034005531 | No effect | 101 | 8745326 | 9384075 |
| Df(3L)ED217 | 8074 | 118 | 0.034005531 | No effect | 101 | 14758070 | 15589096 |
| Df(3L)Exel6109 | 7588 | 16 | 0.035132113 | No effect | 194 | 6743113 | 6943539 |
| Df(3L)BSC181 | 9693 | 33 | 0.038986463 | No effect | 171 | 1688724 | 1841694 |
| Df(3L)BSC845 | 27888 | 58 | 0.052217093 | No effect | 69 | 15511028 | 15825923 |
| Df(3L)ED4293 | 8058 | 6 | 0.052456976 | No effect | 177 | 3226338 | 3250564 |
| Df(3L)BSC673 | 26525 | 45 | 0.064535107 | No effect | 118 | 9763614 | 10180958 |
| Df(3L)BSC884 | 30589 | 22 | 0.065343829 | No effect | 125 | 5608275 | 5777085 |
| Df(3L)Exel6085 | 7564 | 35 | 0.086847385 | No effect | 104 | 548528 | 749303 |
| Df(3L)BSC411 | 24915 | 100 | 0.090561587 | No effect | 136 | 5975960 | 6625629 |
| Df(3L)Exel6112 | 7591 | 64 | 0.11120687 | No effect | 110 | 8096473 | 8358824 |
| Df(3L)ED4858 | 8088 | 100 | 0.116637564 | No effect | 137 | 19895373 | 20401820 |
| Df(3L)BSC410 | 24914 | 118 | 0.172248155 | No effect | 106 | 5770673 | 6490185 |
| Df(3L)BSC392 | 24416 | 48 | 0.217555917 | No effect | 155 | 9678703 | 9899255 |
| Df(3L)Exel6092 | 7571 | 19 | 0.22659207 | No effect | 145 | 2821245 | 3047162 |
| Df(3L)BSC816 | 27577 | 15 | 0.330421072 | No effect | 144 | 8639081 | 8745362 |
| Df(3L)BSC119 | 8976 | 25 | 0.332900668 | No effect | 109 | 2600282 | 2823614 |
| Df(3L)ED4486 | 8072 | 70 | 0.390172144 | No effect | 157 | 12514419 | 13032485 |
| Df(3L)BSC117 | 8974 | 12 | 0.494203996 | No effect | 112 | 7249475 | 7334986 |
| Df(3L)BSC839 | 27917 | 50 | 0.619627548 | No effect | 349 | 20320147 | 20493208 |
| Df(3L)BSC815 | 27576 | 41 | 0.646112624 | No effect | 44 | 8263064 | 8506640 |
| Df(3L)BSC671 | 26523 | 49 | 0.816379333 | No effect | 122 | 2982129 | 3193143 |
| Df(3L)BSC797 | 27369 | 81 | 0.824412022 | No effect | 159 | 20452823 | 20949733 |
| Df(3L)Aprt-32 | 5411 | 120 | 0.895192941 | No effect | 124 | 1710811 | 2491352 |
| Df(3L)BSC12 | 6457 | 21 | 0.918404036 | No effect | 128 | 13028303 | 13227621 |
| Df(3L)ED5017 | 8102 | 32 | 0.949429044 | No effect | 117 | 22835497 | 22998301 |
| Df(3L)BSC800 | 27372 | 8 | 0.96411627 | No effect | 111 | 1628101 | 1647451 |
| Df(3L)BSC391 | 24415 | 46 | 1 | No effect | 159 | 9446770 | 9697191 |
| Df(3L)1-16 | 7002 | 40 | 1 | No effect | 163 | 23302668 | 23856407 |

**Table 2**

| Original deficiency | Effect with *Idgf3* overexpression | Partially overlapping deficiencies | Effect with *Idgf3* | Candidate genes | Source | Allele | Genotype | Effect |
|---|---|---|---|---|---|---|---|---|
| Df(3L)ED4674 | Enhancer | Df(3L) ED223 | Enhancer | | | | | |
| | | Df(3L) Exel6130 | Enhancer | CG9705 | B31901 | UAS-RNAi | *y[1] v[1]; P{y[+t7.7] v[+t1.8]=TRiP.JF02190}attP2* | No effect |
| | | | | CG9706 | B51908 | UAS-RNAi | *y[1] v[1]; P{y[+t7.7] v[+t1.8]=TRiP.HMC03483}attP40* | No effect |
| | | | | | V100567 | UAS-RNAi | *P{KK108219} VIE-260B* | No effect |
| | | | | eIF3e | V103559 | UAS-RNAi | *P{KK101123} VIE-260B* | N/A |
| | | | | CG9674 | B57483 | UAS-RNAi | *y[1] sc[*] v[1] sev[21]; P{y[+t7.7] v[+t1.8]=TRiP.HMC04796}attP40* | No effect |
| | | | | NudC | B33382 | UAS-RNAi | *y[1] sc[*] v[1] sev[21]; P{y[+t7.7] v[+t1.8]=TRiP.HMS00258}attP2/TM3, Sb[1]* | No effect |
| | | | | | B52980 | UAS-RNAi | *y[1] v[1]; P{y[+t7.7] v[+t1.8]=TRiP.HMJ21667}attP40/CyO* | No effect |
| | | Df(3L) ED4685 | No effect | | | | | |
| | | Df(3L) 4606 | No effect | | | | | |
| | | Df(3L) Exel9002 | No effect | | | | | |
| | | Df(3L) Exel9004 | No effect | | | | | |
| | | *Df(3L) BSC414 | Suppressor | | | | | |
| Df(3L)BSC289 | Enhancer | Df(3L)BSC426 | Enhancer | ABCBC7 | | | | |
| | | | | GC | | | | |
| | | | | CG13928 | | | | |
| | | | | CG33230 | | | | |
| | | | | CG13926 | | | | |
| | | Df(3L)ED4246 | No effect | | | | | |
| | | Df(3L)Exel6087 | No effect | | | | | |
| Df(3L)ED230 | Suppressor | *Df(3L)BSC451 | Enhancer | | | | | |
| | | Df(3L)TO2 | Suppressor | | | | | |
| | | Df(3L)ED554 | Suppressor | *Maelstrom* | | | | |
| | | | | *CG14450* | | | | |
| | | | | *CG11367* | | | | |
| | | | | *CG32454* | | | | |
| | | | | *CG11241* | | | | |
| | | | | *Lt(3)04053* | | | | |
| | | | | *CG7369* | | | | |
| Df(3L)BSC23 | Suppressor | *Df(3L)BSC671 | No effect | | | | | |
| | | *Df(3L)Exel6092 | Enhancing | | | | | |
| | | *Df(3L)BSC119 | No effect | | | | | |
| | | | | dos | | | | |
| | | | | CG16985 | | | | |
| | | | | CG16984 | | | | |
| | | | | CG12182 | | | | |
| Df(3L)ED4502 | Enhancer | *Df(3L)ED4543 | No effect | | | | | |
| | | Df(3L)Exel6119 | (Enhancer) | | | | | |
| | | Df(3L)BSC614 | Enhancer | *Caps* | B28020 | UAS-RNAi | *y[1] v[1]; P{y[+t7.7] v[+t1.8]=TRiP.JF02854}attP2* | No effect |
| | | | | *Tgi* | B34394 | UAS-RNAi | *y[1] sc[*] v[1] sev[21]; P{y[+t7.7] v[+t1.8]=TRiP.HMS00981}attP2* | (Suppressor) |
| | | | | **cmb** | V109767 | UAS-RNAi | *P{KK103563}VIE-260B* | Enhancer |
| | | | | | Andreas Jenny | cmbKO | *w[1118 ]; +/+ ; cmb[KO]/TM6B, Hu* | Enhancer |
| | | | | | Andreas Jenny | UAS-cmbRB | *w[1118] P{UAS-cmb.RB} ; +/+ ; +/+* | Suppressor |
| | | | | CG17687 | | | | |
| | | | | Nplp2 | | | | |
| | | | | CG14111 | | | | |
| | | | | CG10717 | | | | |
| | | | | SNCF | | | | |
| | | | | CG14107 | | | | |
| | | | | CG14110 | | | | |
| | | | | CG10171 | | | | |
| | | | | Poc1 | | | | |
| | | | | sens | | | | |
| | | | | CG10222 | | | | |
| | | | | flr | | | | |
| | | | | CG32121 | | | | |
| | | | | CG33263 | | | | |
| | | | | CG14106 | | | | |
| | | | | CG14105 | | | | |
| | | | | CG10713 | | | | |
| | | | | CG10154 | | | | |
| | | | | CG10725 | | | | |
| | | | | CG10140 | | | | |
| | | | | CG14109 | | | | |
| | | | | JMJD7 | | | | |
| | | | | CG10738 | | | | |
| | | | | CG10116 | | | | |
| | | | | CG10089 | | | | |
| | | | | CG43184 | | | | |
| | | | | CG8757 | | | | |
| | | | | CG8750 | | | | |
| | | | | Tsp68C | | | | |
| | | | | Hml | | | | |
| | | | | CG8745 | | | | |
| | | | | dysc | | | | |
| | | | | CG13737 | | | | |
| | | | | Rgl | | | | |

* Indicates deficiencies tested in the original screen and reported also in Table 1

**Table 3**

| Deficiency | Bloomington Stock # | Frequency of Normal Df | Frequency of defective Df | Frequency of normal control | Frequency of defective control | *p*-value | Effect | Candidate Genes | Source | Alllele | Genotype | Effect |
|---|---|---|---|---|---|---|---|---|---|---|---|---|
| Df(3L)ED223 | 8079 | 12.3015873 | 87.6984127 | 92.10526316 | 7.894736842 | 2.20E-16 | Enhancer | | | | | |
| | | | | | | | | *CG9705* | B31901 | UAS-RNAi | *y[1] v[1]; P{y[+t7.7] v[+t1.8]=TRiP.JF02190}attP2* | No effect |
| | | | | | | | | | B51908 | UAS-RNAi | *y[1] v[1]; P{y[+t7.7] v[+t1.8]=TRiP.HMC03483}attP40* | No effect |
| | | | | | | | | *CG9706* | V100567 | UAS-RNAi | *P{KK108219}VIE-260B* | No effect |
| | | | | | | | | | B59073 | UAS-eIF3e.Frag.GFP | w[*]; Kr[If-1]/CyO; P{w+mC]=UAS-eIF3e.Frag.GFP}31 | Incogruent |
| | | | | | | | | *eIF3e* | V103559 | UAS-RNAi | *P{KK101123}VIE-260B* | N/A |
| | | | | | | | | *CG9674* | B57483 | UAS-RNAi | *y[1] sc[*] v[1] sev[21]; P{y[+t7.7] v[+t1.8]=TRiP.HMC04796}attP40* | No effect |
| | | | | | | | | | B33382 | UAS-RNAi | *y[1] sc[*] v[1] sev[21]; P{y[+t7.7] v[+t1.8]=TRiP.HMS00258}attP2/TM3, Sb[1]* | No effect |
| Df(3L)Exel6130 | 7609 | 24.11764706 | 75.88235294 | 92.10526316 | 7.894736842 | 2.20E-16 | Enhancer | *nudC* | B52980 | UAS-RNAi | *y[1] v[1]; P{y[+t7.7] v[+t1.8]=TRiP.HMJ21667}attP40/CyO* | No effect |
| Df(3L) Exel9002 | 7935 | 65.57377049 | 34.42622951 | 57.45856354 | 42.54143646 | 0.3 | No effect | | | | | |
| Df(3L)ED4685 | 64121 | 85.63218391 | 14.36781609 | 72.42990654 | 27.57009346 | 0.03 | No effect | | | | | |
| Df(3L) Exel9004 | 7937 | 74.16666667 | 25.83333333 | 57.45856354 | 42.54143646 | 0.01 | No effect | | | | | |

**Table 4**

| Gene | Genotype | Reference | Effect with DA | *p*-value |
|---|---|---|---|---|
| *Tramtrack69* | w;+;FRT ttk[1e11]/TM3, Sb | CB0539 | Strong enhancer | 3.81E-11 |
| *fs(3)02534* | +;+;ry fs(3)02534(ry[+])/TM3, Sb | CB0113 | Strong enhancer | 2.50E-07 |
| *Btk29A* | w; Btk29A[K00206] FRT/ CyO | CB0510 | Mild enhancer | 0.0006473 |
| *Gβ13F* | w Gβ13F/ TM7c, Bar | CB1326 | Mild enhancer | 0.001358 |
| *Rac1 & Rac2* | y w; +; Rac1[J11] Rac2[delta] FRT/ TM6, Hu | CB0546 | Mild enhancer | 0.002489 |
| *Gγ* | y w; FRT Gγ[K08017]/CyO | CB0575 | Suppressor | 0.0002164 |
| *l(2)01326a l(2)01326b* | + ; l(2) 01326a l(2) 01326b/CyO | CB0601 | No effect | 0.3453 |
| *l(3)AtPα* | +; + ; l(3) Atpα ry/TM3, Sb | CB0606 | No effect | 0.6473 |
| *Tramtrack69* | w;+;e twk/TM3, Sb e | CB1305 | No effect | 0.7202 |
| | Lkb1[315]/TM6, Tb | Maurizio Gatti | Strong enhancer | 5.62E-09 |
| | w[1118]; P{w[+mC]=EP}Lkb1[G5285] | B30148 | Mild enhancer | 0.0002548 |
| *lkb1* | y[1] sc[*] v[1] sev[21]; P{y[+t7.7] v[+t1.8]=TRiP.HMS01351}attP2 | B34362 | No effect | 0.4966 |
| *pten* | y[1] v[1]; P{y[+t7.7] v[+t1.8]=TRiP.HMS00044}attP2 | B33643 | No effect | 0.7894 |
| *Pten null* | yw;FRT40Pten(117.1)/CyO;MKRS/TM6B, Tb Hu | Ernst Hafen | No effect | 0.09049 |
| *mxt* | y[1] sc[*] v[1] sev[21]; P{y[+t7.7] v[+t1.8]=TRiP.HMS05462}attP40 | B66996 | Mild enhancer | 0.002846 |
| | Df(1)BSC352, w[1118]/FM7h/Dp(2;Y)G, P{w[+mC]=hs-hid}Y | B24376 | Strong enhancer | < 2.2E-16 |
| *Unpaired* | Df(1)BSC352, w[1118]/FM7h/Dp(2;Y)G, P{w[+mC]=hs-hid}Y | B24376 on its own | Strong phentoype | 3.98E-14 |
| | *UAS-Mical* | Sebastian Rumpf | Strong suppressor * | < 2.2e-16 |
| | *UAS-GFP::Mical* | Sebastian Rumpf | Strong suppressor * | < 2.2e-16 |
| | *UAS-MicaldeltaC* | Sebastian Rumpf | N/A (n<100) | 0.01 |
| | *UAS-5'UTRMical-GFP* | Sebastian Rumpf | N/A (n<100) | 0.05 |
| | *UAS-GFPdeltaCH* | Sebastian Rumpf | Strong suppressor * | 1.96E-09 |
| | *UAS-GFPdeltaRedox* | Sebastian Rumpf | N/A (n<100) | 0.800 |
| | y[1] w[*]; Mi{y[+mDint2]=MIC}Mical[MI13368] | B59124 | enhancer | 0.002 |
| Mical | y[1] w[67c23]; P{y[+mDint2] w[BR.E.BR]=SUPor-P}Mical[KG00339] ry[506] | B13094 | Mild enhancer | 0.020 |
| PlexA | y[1] sc[*] v[1] sev[21]; P{y[+t7.7] v[+t1.8]=TRiP.HM05221}attP2 | B30483 | Stronger enhancer | < 2.2e-16 |
| PlexB | y[1] v[1]; P{y[+t7.7] v[+t1.8]=TRiP.HM05122}attP2 | B28911 | Mild suppressor | 0.02 |
| **Notes:** | | | | |

*** DA look thinner and smaller than the usual phentoypes**

B#: Bloomington stocks

CB#: Berg stocks